Turkish Journal of REMOTE SENSING

Türkiye Uzaktan Algılama Dergisi

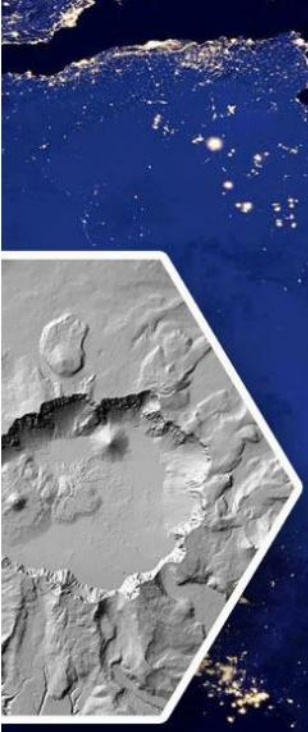

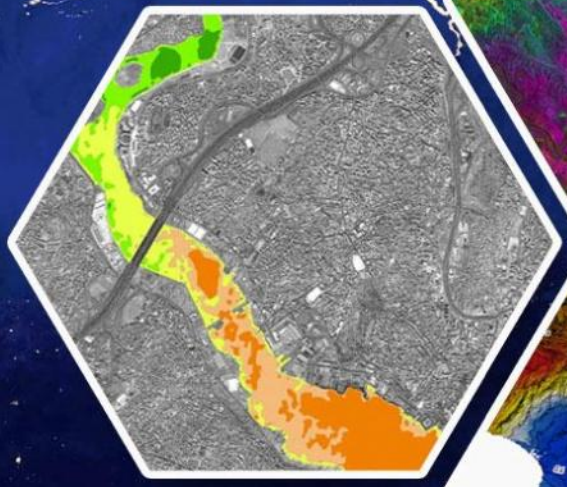

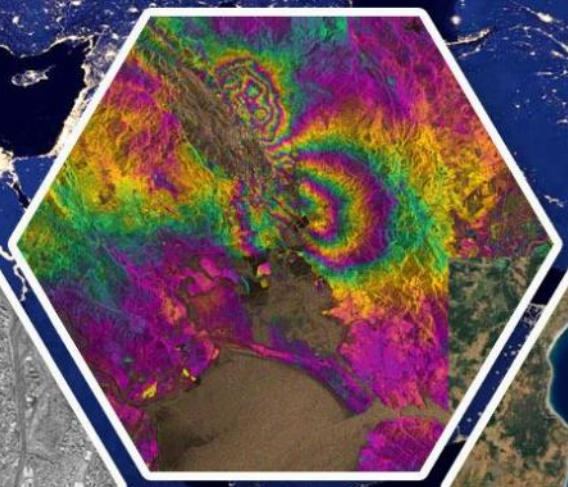

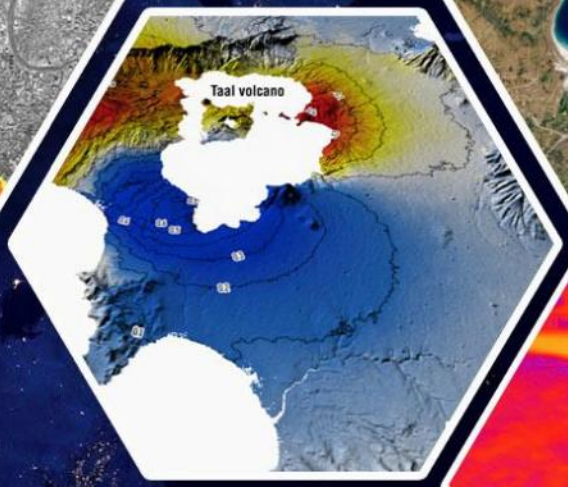

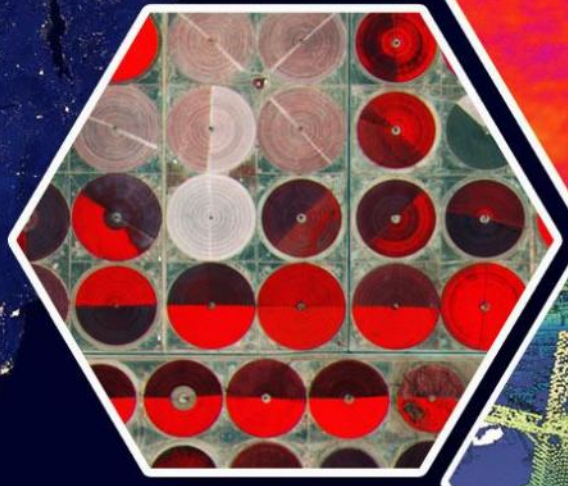

Vol/Cilt:5
Issue/Sayı:1
June/Haziran, 2023

e-ISSN: 2687-4997

Türkiye Uzaktan Algılama Dergisi

Dergi Hakkında

Türkiye Uzaktan Algılama Dergisi (TUZAL) bilim ve teknolojideki gelişmelere paralel olarak Uzaktan Algılama alanındaki yeniliklerle ilgili yapılan çalışmaları yayınlayan ve Uluslararası İndeks ve Veri tabanlarında taranan bir dergidir.

Amaç & Kapsam

TUZAL Dergisi,

- Uzaktan Algılama alanında ulusal ve uluslararası gelişmeleri Harita, jeoloji, Çevre, Elektrik ve Elektronik, Bilgisayar vb. mühendislik alanı ile ilgilenen bilim insanlarının bilgisine sunmak,
- Konu ile doğrudan veya dolaylı etkinliklerde bulunan bilim insanları, araştırmacılar, mühendisler ve diğer uygulayıcılar arasındaki bilgi ve deneyim paylaşımını güçlendirecek ve hızlandıracak, kolay erişilebilen, geniş katılımlı bir tartışma ortamı sağlamak ve bunları yayma olanağı yaratmak,
- Türkiye'nin teknolojik ve ekonomik kalkınmasında rol oynayabilecek Uzaktan Algılama teknolojisine ilişkin sorunların daha etkin bir şekilde çözüme kavuşturulması açısından büyük önem taşıyan kurumlar arası işbirliğinin başlatılmasına ve geliştirilmesine katkıda bulunmak,
- Türkçe`nin Uzaktan Algılama alanında bilim dili olarak geliştirilmesini ve yabancı sözcüklerden arındırılmasını özendirmek amaçlarına sahiptir.

Dergisinin kapsamı;

Temel Uzaktan Algılama Uygulamaları,

RADAR/SAR/LIDAR,

Hiperspektral uzaktan algılama,

Görüntü sınıflandırma ve analiz yöntemleri,

Radyometrik düzeltme için atmosferik modellemenin geliştirilmesi,

Uygu verilerinden elde edilmiş parametrelerin modellenmesi

Küresel modelleme, izleme ve sürdürülebilir kalkınma için küresel veri tabanı ve değişim göstergelerinin belirlenmesi,

Laboratuvar ve yerinde test yöntemleri kullanarak veri ve bilginin kontrolü,

Uzaktan algılama ve CBS yöntemlerinin entegrasyonu,

CBS Uygulamaları,

İnsansız Hava Araçları (İHA) ve Yersel Lazer Tarama ile gözlem uygulamaları,

Havasal ve Uzaysal Uzaktan Algılama

Afet ve risk etkilerinin azaltılması için bilgi desteği: erken uyarı sistemleri, etki değerlendirmesi, izleme, esneklik ve risk azaltma çalışmaları,

Çevre kirliliği: değerlendirme ve etki çalışmaları,

Jeoloji, Jeomorfoloji ve Pedolojide Yeryüzü Bilimi Uygulamaların ile uzaktan algılanmış girdilerin entegrasyonu,

Sürdürülebilir tarımsal üretim ve tarımın korunması için tarım ürünlerinin büyümesinin çok boyutlu izlenmesi,

İklim değişikliği çalışmaları,

Arazi kullanımı/örtüsünün küresel ve bölgesel dinamikleri, biyo-çeşitlilik, bozulma,

Çölleşme ve kuraklık çalışmaları,

Topraklar, bitki örtüsü ve iç, kıyı ve okyanus sularında karbon akıları,

Su kalitesi çalışmaları vb.

Yayınlanma Sıklığı Yılda 2 sayı(Haziran-Aralık)

ISSN 2687-4997

WEB https://dergipark.org.tr/tr/pub/tuzal

İletişim osmanorhan44@gmail.com / osmanorhan@mersin.edu.tr / tuzaldergisi@gmail.com

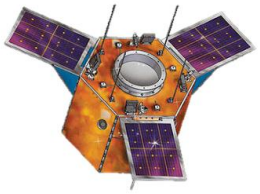

Turkish Journal of Remote Sensing

About Journal

Turkish Journal of Remote Sensing publishes studies related to innovation in the field of Remote Sensing parallel to the developments in science and technology and indexed in the International Index and database.

Aim & Scope

The Journal,

- To present to the knowledge of National and international developments in the field of Remote Sensing to scientists related with Geomatics, Geology, Environment, Electric and Electronic, Computer etc. engineering fields.
- To provide an easily accessible, broadly attended discussion environment that will strengthen and accelerate the sharing of knowledge and experience between scientists, researchers, engineers and other practitioners who engage in direct or indirect activities with the subject, and create an opportunity to disseminate them,
- Turkey's technological and economic development in the problems related to remote sensing technology that can more effectively play a role of great importance in terms of inter-agency cooperation to be initiated and resolved to contribute to the development,
- It has the aim of encouraging the development of Turkish as a scientific language in the field of Remote Sensing and to be free from foreign words.

Scope of The Journal;

- ✓ Basic remote sensing applications,
- ✓ RADAR/SAR/LIDAR,
- ✓ Hyperspectral remote sensing,
- ✓ Image classification and analysis methods,
- ✓ Development of atmospheric modelling for radiometric correction,
- ✓ Determine global database and alteration indicator for global modelling, monitoring and sustainable development,
- ✓ Data and information control using laboratory and in-situ tests,
- ✓ Integration of remote sensing and GIS methods,
- ✓ CBS Uygulamaları,
- ✓ İnsansız Hava Araçları (İHA) ve Yersel Lazer Tarama ile gözlem uygulamaları,
- ✓ Havasal ve Uzaysal Uzaktan Algılama
- ✓ Information utility for reducing disaster and risk effects: Early warning systems, impact evaluation, monitoring, flexibly and risk reducing studies,
- ✓ Environment pollution: Evaluation and effect studies,
- ✓ Integration of Earth science applications in Geology, Geomorphology and Pedology with remote sensing data
- ✓ Multidimensional monitoring of growth of agricultural goods for sustainable agricultural production and protection of agriculture
- ✓ Climate change studies,
- ✓ Land use/ Dynamics of global and regional land, biodiversity, deterioration,
- ✓ Carbon amount in Earth, plant cover and in shore, ocean waters,
- ✓ Water quality studies etc.

Publication frequency Biannual (June-December)

ISSN 2687-4997

WEB https://dergipark.org.tr/tr/pub/tuzal

Contact osmanorhan44@gmail.com / osmanorhan@mersin.edu.tr / tuzaldergisi@gmail.com

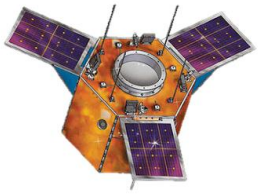

Turkish Journal of Remote Sensing

Türkiye Uzaktan Algılama Dergisi
Turkish Journal of Remote Sensing
Cilt/Volume 5
Sayı/Issue 1 *Haziran/June, 2023*

İçindekiler
Contents

Araştırma Makaleleri;
Research Articles;

Araştırma Makalesi/Research Article
https://doi.org/10.51489/tuzal.1187819

2023; 5(1); 01-13

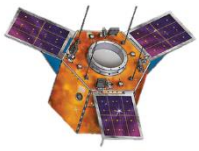

Turkish Journal of Remote Sensing

https://dergipark.org.tr/en/pub/tuzal

e-ISSN 2687-4997

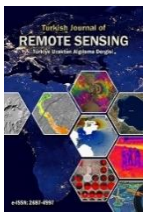

Coseismic DInSAR Analysis and Elastic Dislocation Modelling of The 24 January 2020 Elazig-Sivrice Earthquake

Şükrü Onur Karaca*[1], Gültekin Erten [1]

[1]Directorate General of Mineral Research and Exploration (MTA), Department of Geological Research, Remote Sensing and GIS Division, Ankara, Türkiye

Keywords
Remote sensing
Active Tectonics
Sivrice-Elazığ Earthquake
DInSAR
Elastic Modelling

ABSTRACT

One of Turkey's most important neotectonic structures East Anatolian Fault Zone (EAFZ), has occurred many earthquakes. One of these earthquakes, the 6.8 Mw Sivrice-Elazig earthquake dated January 24, 2020, was felt in various provinces, especially in Elazig and Malatya, and caused the death of 44 people. It is critical to investigate this earthquake, which caused significant economic damage, and to identify possible hazards on the EAFZ. One of the remote sensing methods DInSAR was used in this study. By choosing two Sentinel 1A descending datasets, 16/01/2020 and 28/01/2020 respectively (pre and post earthquake), the surface deformation and time series were determined. In addition, using the data obtained from the DInSAR results, Elastic Dislocation Modelling has been performed by applying linear and nonlinear inverse solutions to determine the slip amount of the fault structure, the fault surface slip distribution, and determine the strain area. According to the DInSAR results, while there is displacement approximately 26 cm (away from the satellite direction) on the western block of the EAF, 19 cm displacement (towards the satellite direction) are observed in the eastern block, respectively. Elastic Dislocation Modelling shows that the observed deformation pattern can be explained by the slip on a single plane fault of the Elazig earthquake. This fault plane was identified as a southwest strike-slip fault segment, which lies within the upper crustal region and extends to a depth of approximately 10 km. According to the results obtained by elastic modelling; slip ratio was calculated as 1.95 m, Mw 6.75, rupture length 34.78 km, focal depth 10 km, width 7.4 km, strike 240.27°, slope 69.19°, rake 0.19°. Overall, the study reveals the strike-slip of the Sivrice-Elazığ earthquake, shows the deformation after the earthquake, and the elastic half-space fault model.

24 Ocak 2020 Elazığ-Sivrice Depreminin Ko-sismik DINSAR Analizi ve Elastik Dislokasyon Modellemesi

Anahtar Kelimeler:
Uzaktan Algılama
Aktif Tektonik
Sivrice- Elazığ Depremi
DInSAR
Elastik Modelleme

ÖZ

Türkiye'nin en önemli neotektonik yapılarından biri olan Doğu Anadolu Fay Zonu (DAFZ) üzerinde birçok deprem meydana gelmiştir. Bu depremlerden biri olan 24 Ocak 2020 tarihli, 6.8 Mw büyüklüğündeki Sivrice-Elazığ depremi, başta Elazığ ve Malatya olmak üzere çeşitli illerde hissedilmiş ve 44 kişinin ölümüne sebep olmuştur. Önemli derecede ekonomik hasara yol açan bu depremin araştırılması ve DAFZ üzerindeki olası tehlikelerin belirlenmesi büyük önem taşımaktadır. Bu çalışmada uzaktan algılama yöntemlerinden biri olan Diferansiyel İnterferometri (DInSAR) yöntemi kullanılmıştır. 16/01/2020 ve 28/01/2020 tarihli, deprem öncesi ve sonrası olmak üzere iki adet Sentinel 1A alçalan yönlü veri seti seçilerek, deprem sonrası oluşan deformasyonu ve zaman serileri belirlenmiştir. Ayrıca DInSAR sonuçlarından elde edilen veriler kullanılarak, fay yapısına ait kayma miktarı ile fay yüzeyi kayma dağılımının belirlenmesi ve gerinim alanının tespiti için, doğrusal ve doğrusal olmayan ters çözüm işlemleri uygulanarak Elastik Dislokasyon Modellemesi uygulanmıştır. Buna göre DAF hattının batı bloğu üzerinde yaklaşık 26 cm'lik bir hareket (uydu doğrulutusundan uzaklamaşma) söz konusu iken doğu bloğu üzerinde 19 cm (uydu doğrultusuna yakınlaşma) hareket gözlemlenmiştir. Elastik Dislokasyon Modellemesi Elazığ depreminin tek bir düzlemsel fay üzerindeki kayma ile açıklanabildiğini ve fay düzlemi üst kabuk bölgesi içinde kalan ve yaklaşık 10 km'ye kadar derinliğe uzanan, güney batı doğrultu atımlı bir fay segmenti olarak tespit edilmiştir. Bu yarı uzaydaki elastik kayma modellemesiyle elde edilen sonuçlara göre; kayma miktarı (slip) 1.95 m, Mw 6.75, kırılma uzunluğu 34.78 km, odak derinliği 10 km, genişlik 7.4 km, doğrultu 240.27°, eğim 69.19°, rake 0.19° olarak hesaplanmıştır. Bu çalışma Sivrice-Elâzığ depreminin doğrultu atımını ortaya koymakta, deprem sonrası oluşan deformasyonu ve yarı uzaydaki elastik fay modelini göstermektedir.

Article Info

Received: 07/12/2022
Accepted: 28/02/2023
Published: 30/06/2023

Citation:

Karaca, Ş. O. & Erten, G. (2023). Coseismic DInSAR Analysis and Elastic Dislocation Modelling of The 24 January 2020 Elazig-Sivrice Earthquake. Turkish Journal of Remote Sensing, 5 (1) , 01-13.

***Corresponding Author:** Şükrü Onur Karaca, onurkaraca87@hotmail.com, +90 312 201 1000*

1. INTRODUCTION

Earthquakes, defined as natural disasters, can occur at any time on the earth's surface. Therefore, it is very critical to detect and monitor their effect after this rapid movement. There has been so many studies about Elazig-Sivrice Earthquake, so far. After the Elazig-Sivrice earthquake, research reports made by the General Directorate of Mineral Research and Exploration (MTA) have shown surface deformations, fault-related Riedel shear fractures, interlaced tension cracks, and surface fractures (Kürçer et al., 2020). It was stated that the Elazig-Sivrice earthquake caused surface deformation in an area of 48 km on the two lower segments of the Pötürge Segment in the northeast (Kürçer et al., 2020). It has been stated that many mass movements occur within this deformation area (Kürçer et al., 2020). According to Tatar et al. (2020) support these observations in their field studies. Tatar et al. (2020) mapped the geometry of the surface rupture and other seismic geomorphological structures in detail, and also correlated the field data with satellite images. According to these results, Differential Interferometric SAR (DInSAR) studies have shown that there is a 10 cm rise in the northwest block of the fault and a 6 cm subsidence in the southeast block (Tatar et al., 2020). Due to the difference in vertical movements between the two blocks of the fault, it has been interpreted that at least 30 km long part of the Pütürge segment between the southwest of Sivrice and Pütürge was broken during the main shock (Tatar et al., 2020). Yalvaç (2020), investigated co-seismic displacements originating from Elazığ-Sivrice earthquake in the Eastern Anatolian Fault Zone (EAFZ) on 24 January 2020 by using 11 CORS-TR stations. The results showed earthquake-induced motion of 20-60 mm at the GNSS stations located in the nearby of earthquake epicenter (Yalvaç, 2020). Pousse-Beltran et al. (2020), using DInSAR and elastic models in their studies, stated that the main shock of the earthquake spread mostly westward from the focal point with a fault slope of 10°. According to their result, the earthquake corresponding to the EAF segment boundary was only at one end of the rupture and they stated that the 1874-M~7.1 Gölcük Lake earthquake spread to the slip zone (Pousse-Beltran et al., 2020). By analyzing the Coulomb stress values, the stress levels of the main shock and aftershocks were determined and it was stated that there is still a high-stress accumulation in the area to the northeast and southwest of the fault and that aftershocks will cluster in these areas (Bayrak and Özer, 2021). It has been stated that aftershocks will decrease more rapidly in this region since the stress in the region southwest of the main shock is lower than in other regions (Bayrak and Özer, 2021).

The way to explain InSAR data and tectonic observations is to determine the faulting parameters in the deformation zones resulting from the effect of the earthquake with the help of elastic models. In this study, the basic geometry of the fault was tried to be expressed with values such as strike angle, dip angle, slip vector, and slip amount by using the elastic modelling method. Although there are many studies on the theory of half-space elastic displacement (Stekeete, 1958; Press, 1965; Wright et al., 1999, Elliott et al., 2012), Okada's (1985) studies explain this theory in the most general way. These studies are based on a formulation that will enable an efficient calculation of the slip area caused by displacement in a rectangular or triangular surface area in a spatial environment. By using this formulation, the amount of displacement that will occur on the surface due to any fault movement explained by the source parameters of the earthquake can be calculated. In addition to these, 3D results showing horizontal and vertical components were obtained with forwarding modelling. Many researchers have done various studies on the application of this theory both to the earth's crust and to its application with interferometry (Wells and Coppersmith, 1994; Wright et al., 2003; Cakir et al., 2003; Wang et al., 2004; Funning et al., 2005; Aktuğ et al., 2010; Liu Y., 2015; Demir D. Ö., 2015; Tiryakioglu I., et al., 2017; Vajedian et al., 2018; Li et al., 2018; Pousse-Beltran et al., 2020).

In this study, it was aimed to determine the surface deformations that occurred after the 24 January 2020 Elazig-Sivrice earthquake using the DInSAR method. Two Sentinel 1A complex (SLC-Single Look Complex) datasets were used, as before and after the earthquake, dated 16/01/2020 and 28/01/2020, respectively. The surface deformation information obtained from the DInSAR results and the earthquake data of the fault (geometric parameters such as length, width, depth, strike, slope) obtained from the Global Centroid Moment Tensor (GCMT) catalog used by applying linear and nonlinear inverse solutions to determine elastic dislocation model.

2. MATERIALS AND METHOD

2.1. Study Area and Tectonic

The study area is located between 38.55°N-37.90°N latitude and 38.2°E-39.5°E longitude. The area covers Sivrice which is southern part of Elazığ Province (Figure 1). The neotectonic period started in the region in the Middle Miocene and with the continent-continent collision that occurred as a result of the closure of Neotethys (Şaroğlu, 1986.) This collision created the East Anatolian Fault, which is characterized by a compressional tectonic regime and caused the largest intra-continental deformation in the region.

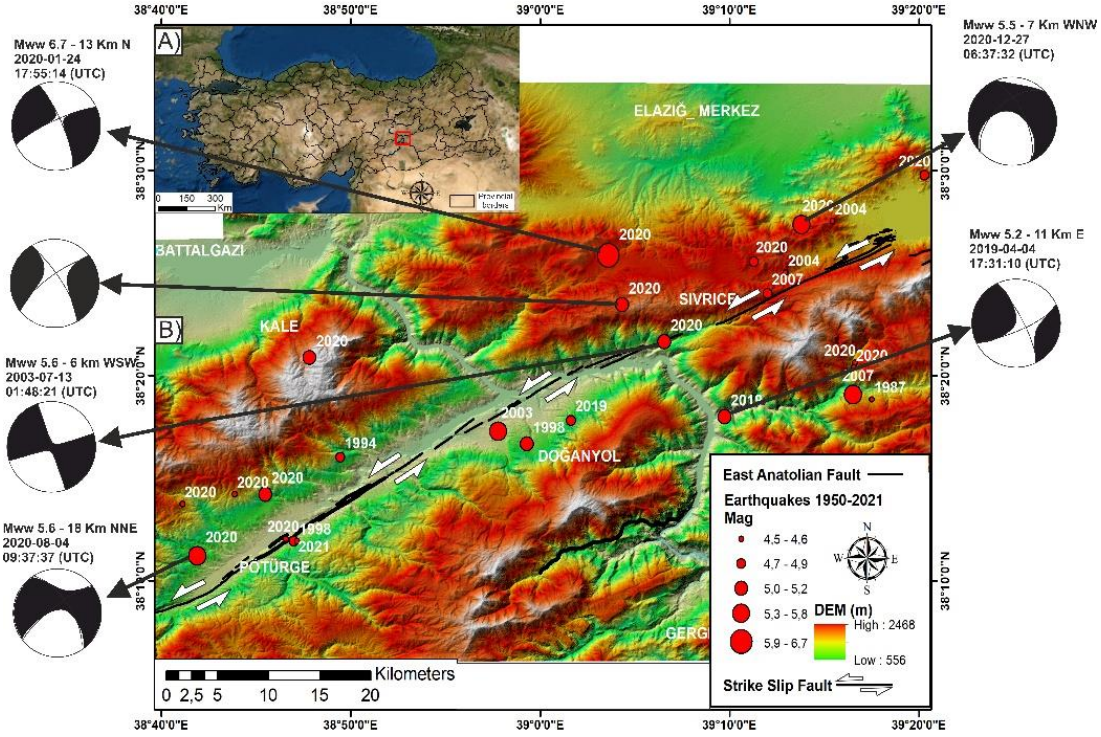

Figure 1. Digital elevation model of Elazig-Sivrice region and earthquakes with magnitude greater than 4.5 between 1950 and 2022 in this region. Some earthquakes are illustrated with focal mechanism solutions from the USGS. Active faults published by MTA are shown with black lines (Duman et al., 2012).

The dextral Eastern Anatolian Fault (EAF), which is approximately 500 km long in southeast Turkey, forms the active plate boundary between Arabia and Anatolia (Figure 1). Due to pull-apart structures, along this fault line, many expansion (releasing), compression (restraining), and stepover structures (Bozkurt, 2001) were formed. It is stated that the oblique effect of the segmentation (sloping) here is influenced by the east-west structures of the SE Anatolian Thrust Zone, which is a part of the east-west oriented Bitlis-Zagros suture (Şengör and Yılmaz, 1981; Yılmaz, 1993; Pousse-Beltran et al., 2020). When investigating past earthquakes with paleoseismic studies, by Çetin et al. (2003), they stated that the current seismic stagnation, the EAF zone may be "locked" and may accumulate elastic strain energy, but there is a possibility of movement in the near future. In these paleoseismological studies, it was stated that the left-lateral strike-slip fault had a slip rate of 11 mm/year. Aktug et al. (2016), determined the shear rate of the EAF zone to understand the kinematics of the Anatolian plate. According to these results, the EAF has an average sliding speed of 10 mm/year from the Arabian-Eurasian collision zone of Anatolia to the west. They also revealed by looking at GPS speeds that the EAF is around 10 mm/year in the northern region and this value is decreasing to around 4.5 mm/y in the southern region. (Aktuğ et al., 2016). In addition, they stated that the two known seismic cavities, Palu-Sincik and Çelikhan-Türkoğlu segments in the EAFZ, have slip gaps of 1.5 m and 5.2 m and may have the potential to produce earthquakes of magnitude Mw 7.4 and Mw 7 (Aktuğ et al., 2016). Duman and Emre (2013) showed that the shear division between the main and northern branches of the EAF covers 2/3 and 1/3 of the lateral movement between Arabian and Anatolian plates, respectively, in the Çelikhan-Adana-Antakya region. Moreover, they stated that the Pazarcık and Amanos segments in their EAF have the potential to produce devastating earthquakes in the near future.

2.2. Differential Interferometry Synthetic Aperture Radar (DInSAR)

Synthetic Aperture Radar (SAR) is an active remote sensing system operating in the microwave region of the electromagnetic spectrum. Earth deformations caused by natural disasters such as earthquakes are tried to be found by utilizing the phase differences of SAR images before and after deformation. DInSAR, one of the technique used in these systems can reveal earth surface deformations with cm-level sensitivity and wide coverage over spans of days to years (Zebker and Goldstein, 1986, Rucci et al., 2012, Aimaiti et al., 2017).

With the DInSAR technique, a new image is obtained by calculating the phase differences of the corresponding pixels from two SAR images of the same region is called an interferogram (Helz, 2005). The interferogram is measured in radians of phase difference and recorded as repeating "fringes" that each represent a full 2π cycle (Torres et al., 2012).

Surface deformation can create fringe interference texture. (Sarychikhina and Glowacka, 2015).

Interferograms are expressed by the following formula (Yague-Martinez et al., 2016);

$$\Delta\phi_{int} = \Delta\phi_{deformation} + \Delta\phi_{topo} + \Delta\phi_{orbit} + \Delta\phi_{atm} + \Delta\phi_{noise} \quad (1)$$

In formula 1, the phase difference between the DInSAR pair; $\Delta\phi_{int}$, surface deformation; $\Delta\phi_{deformation}$, the effect of residual earth topography from the Digital Elevation Model (DEM); $\Delta\phi_{topo}$, residual phase due to orbital error; $\Delta\phi_{orbit}$, atmospheric noises; $\Delta\phi_{atm}$ (such as humidity, temperature, pressure), random noises; $\Delta\phi_{noise}$, are expressed with formulas. The aim here is to try to obtain the $\Delta\phi_{deformation}$ by using $\Delta\phi_{int}$ information. In this study, the open source SNAP (The Sentinel Application Platform) software affiliated to the European Space Agency was applied for interferometric data processing (Yague-Martinez et al., 2016) (ESA, 2021) and these data processing steps are shown in figure 2A.

In the pre-processing phase, since the epicenter of the earthquake is between two swaths, area selection is made by splitting. Precise satellite orbits were obtained from ESA. The back-geocoding process is applied to the registration of the slave image to the master image. After estimating the base distance between master and slave images, interferograms are generated. At this stage, 1 arc-sec Shuttle Radar Topography Mission Height (SRTM HGT) (30 m x 30 m) was used as the digital elevation model. In the next step, the flat earth phase is calculated and extracted. Calculation and extraction of the reference DEM (topophase removal) and coherence estimation were applied. Calculation of heights after phase filtering (Goldstein phase filtering to reduce noise) (Goldstein and Werner, 1998) and unwrapping phase is performed by switching from radians to meters. Finally, terrain correction is performed for the map projection (Figure 2A).

DInSAR can only measure displacement, which is a component of radars' line of sight (LOS). When interpreting LOS, positive values should be interpreted toward satellite, and negative values should be interpreted away from the satellite.

In this study, we used two VV polarization Sentinel 1A descending datasets, 16/01/2020 and 28/01/2020, respectively. The epicenter of the eartquake was middle of two different sub-swats, therefore, we processed each sub-swath seperatley, then, we merged them. Total process covering area was almost 12 km^2.

2.3. Elastic Dislocation Modelling

In geophysical modelling processes, two main methods are used: forward and inverse modellings. Forward modelling is to produce theoretical data by creating mathematical relations within the framework of the physical conditions predicted for an existing model. The inversion method is the process of calculating the physical parameters of the geological model from measured geophysical data. Theories that will form the basis of the inversion method in geophysical modelling are given in detail by Backus and Gilbert (1967), Jackson (1972), and Wiggins (1972).

In this study, DInSAR result and geometric parameters the earthquake obtained from the GCMT catalog used for to calculate elastic parameters in half-space. The data processing steps are shown in Figure 2B.

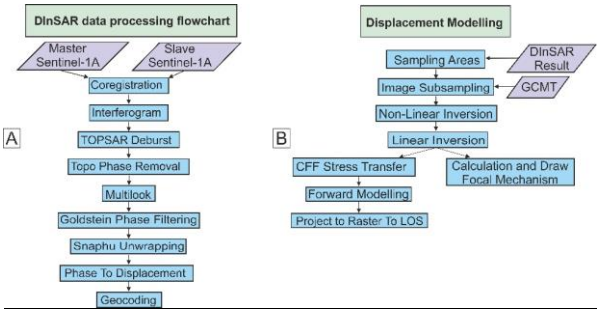

Figure 2. A) DInSAR data processing flowchart used in SNAP software. B) Elastic dislocation modelling data processing flow used in Envi-SarScape software.

In the data processing stages, firstly area selection and image sampling are formed. Here, image sampling is required to reduce the number of points to be modeled. For this, the amount of data was tried to be sparse without causing signal loss with the "Quadtree Algorithm", which is a two-dimensional data reduction algorithm (Welstad, 1999).

By using DInSAR reults in the sampled image, vertical and lateral slip amounts and geometry parameters (length, width, depth, strike, slope) of the fault planes that cause surface displacements are calculated. This process is done with linear and non-linear inverse solutions. If the parameters of the structure are determined directly in the inversion process, this process is called linear inversion (Yas and Asci 2017). Starting from an initial model, the process of determining the underground structure, whose parameters can be changed until the harmony between the theoretical anomaly and the observational anomalies reached the optimum level, is called the nonlinear inversion process (Yas and Asci 2017). After the inversion, Coulomb stress changes (CFF) is calculated, which simulates the presence of another fault close to the one modeled.

3. RESULTS

3.1. DInSAR Results

DInSAR results illustrate fringe structures related to the surface deformation (Figure 3A). Using the Sentinel 1A dataset and depending on the

C band (approximately 5.46 cm wavelength), each fringe structure (red → yellow → turquoise → blue → red) can be interpreted as 2.77 cm. The formation of the right and left sections of this fringe structure shows the place where the EAF passes, and the visible linear region between these two blocks corresponds to the area where surface rupture can occur (Figure 3A). In Figure 3B, the deformation of the earth is shown. Accordingly, while the area (blue colours) in the NW block of the DAF can be interpreted as the movement away from the satellite (westward or subsidence); the area in the SE block (red colours) can be interpreted as towards the satellite direction (eastward or uplift) (Figure 3B). The profiles shown as the A-A` and B-B` profiles in figure 3C.

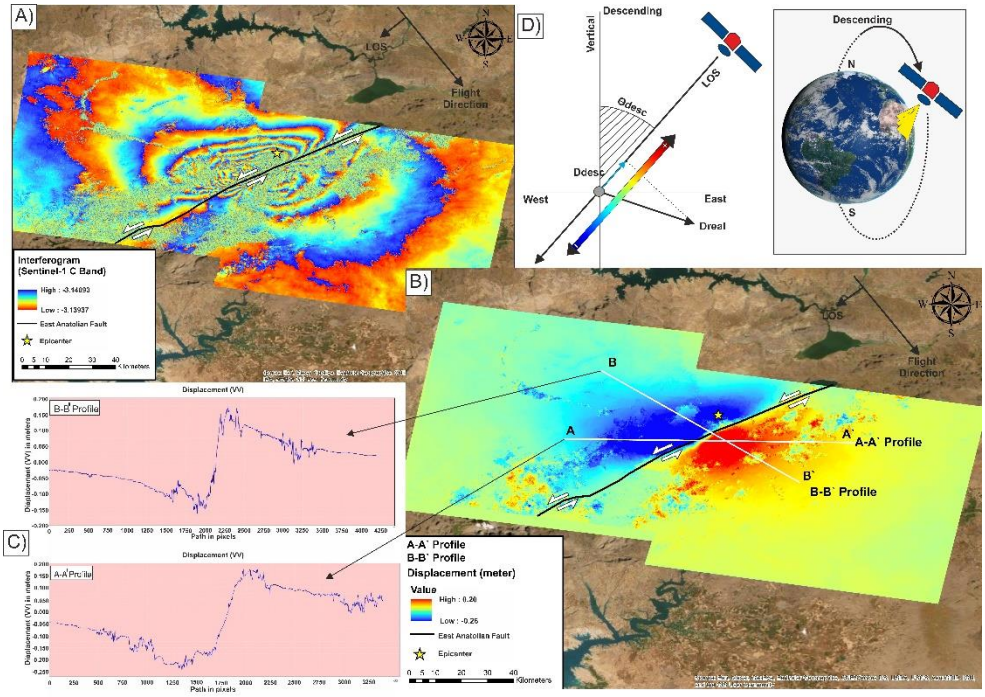

Figure 3. A) Unwrapped phase images, the 16/01/2020 and 28/01/2020 Sentinel 1A datasets were used. Active faults published by MTA are shown with black lines (Duman et al., 2012). The star shape shows the earthquake center taken from the USGS. B) LOS surface deformation. While the blue colours can be interpreted as the movement away from the satellite or subsidence, the red colours can be interpreted as towards the satellite direction or uplift movement. C) Profiles show displacement corresponding to the lines in figure 3B D) Descending satellite direction and LOS movement. While the red colours might be interpreted as either east or vertical movement, the blue colours might be interpreted as either west or subsidence movement.

These profiles show the movement on the DAF. On the A-A` profile, a maximum of roughly 23 cm subsidence or movement away from the satellite is observed in the NW block. On the same profile, on the SE block, there is a towards satellite direction or uplift movement with an approximately maximum of 17.5 cm. On the B-B` profile, approximately a maximum of 16 cm collapse or movement away from the satellite is observed on the NW block. On the same profile, in the SE block, there is a towards satellite direction or uplift movement with an approximately maximum of 17 cm.

3.2. Elastic Dislocation Modelling Results

To understand the fault mechanism and to estimate the source parameters of the earthquake, the displacements obtained from the InSAR data were and GMCT earthquake source parameters modeled. Figures 4A-4D show the surface deformation of the DInSAR observed results; figures 4B-4E represent the models created by the nonlinear inversion process based on figure 4A-4D. Figures 4C-4F show the residuals and RMS values generated according to the shear dislocation. These residues have lower RMS values than before; which means that the corrected solution decreases the error rate.

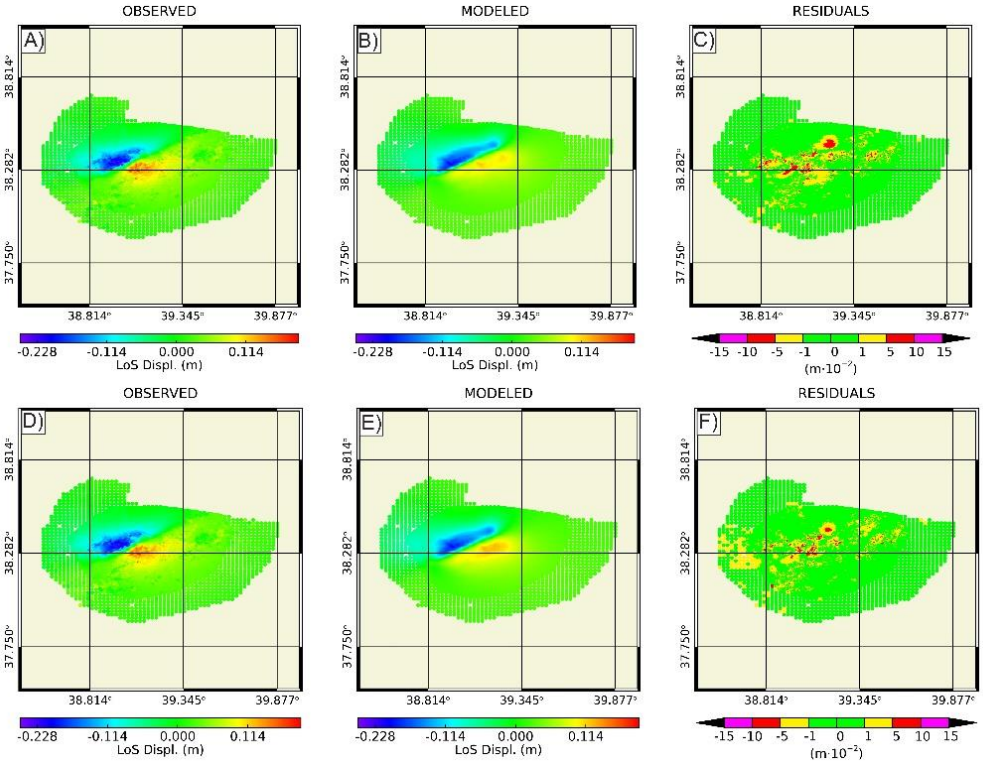

Figure 4. Nonlinear Inversion process. A) first observed data generated from the descending DInSAR dataset B) first generated model C) first residuals generated from the shear dislocation (RMS: 0.019 m (overall RMS: 0.067 m)). D) corrected observed data E) corrected generated model F) corrected residuals generated from share dislocation (RMS: 0.017 m (overall RMS: 0.067 m)).

To find the statistical mean ranges of the obtained results; Monte Carlo Analysis was used . The nonlinear inversion statistics showing the uncertainties and changes of the model parameters. In figure 5, each points represents the ranges of variation for finding the optimal inversion for a statistically different set of parameters such as length, width, depth, slope, position information, and, and amount of slip rate.

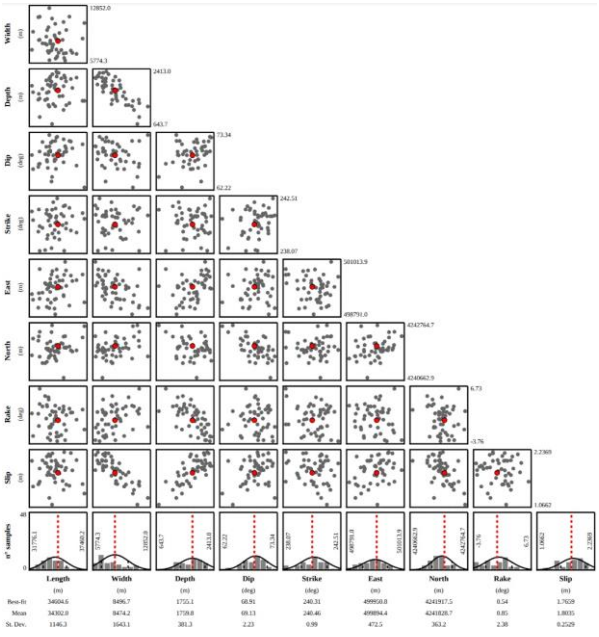

Figure 5. Non-Linear inversion Statistic showing the uncertainties and changes of the model parameters of a single fault using Monte Carlo analysis. It belongs to the UTM 37N coordinate system; length, width and depth in m. Each of the 50 points in the drawings used for different parameters represents the value for finding the most suitable solution for the selected parameter set.

Figure 6 has 2D and 3D dimensional views of the slip distribution for the fault plane sampled with equal rectangles. According to figure 6C, while the rupture distance is approximately 36 km from NE to the SW direction with approximately 24 rectangles, the maksimum slip rate is almost 1.8 m with a red colour bar on the scale. Depth is around 10 km and strike is 240.27°.

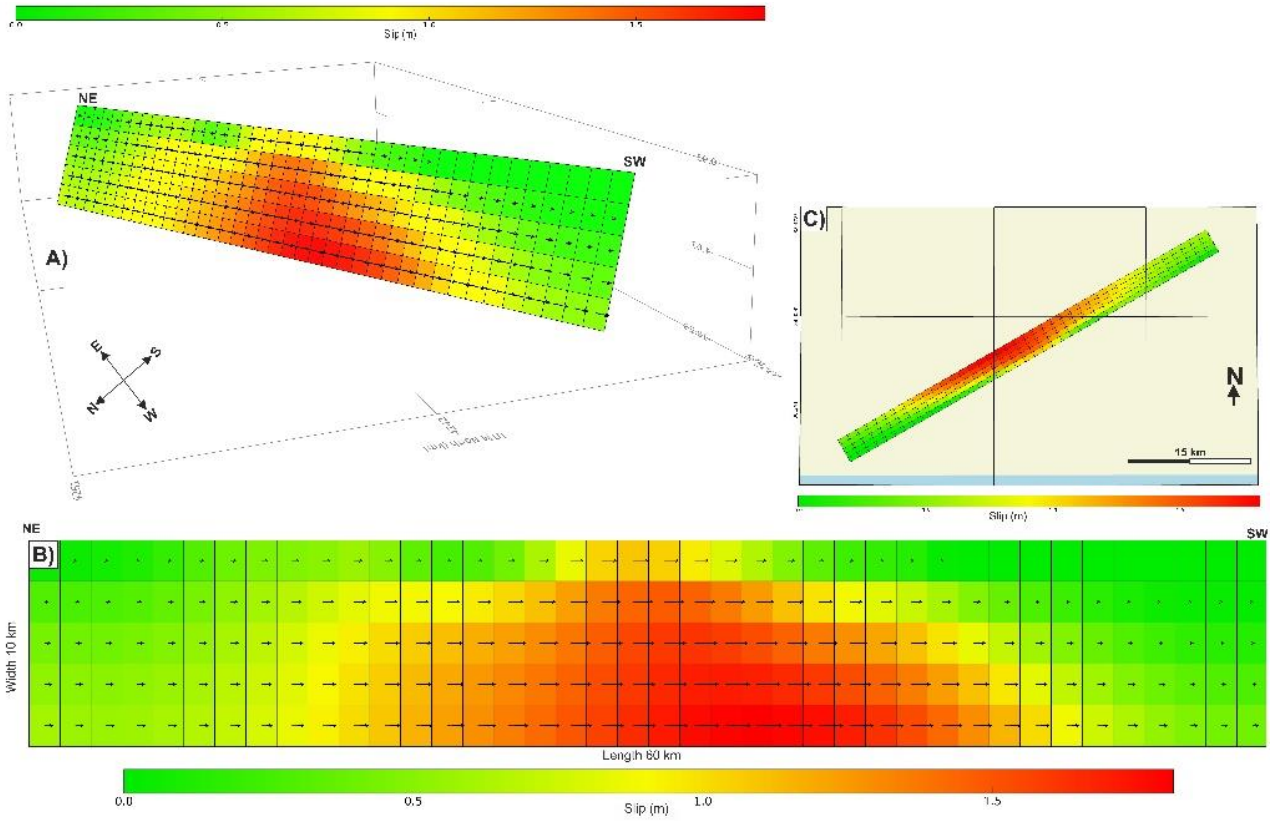

Figure 6. Slip distributions on the single fault model obtained by linear inverse solution for the 2020 Elâzığ-Sivrice earthquake. A) 3D view of the shear distribution and B) 2D view of the shear distribution. The black arrows in the figures represent the slip direction. The colour bar shows the magnitude of the shift amount.

By calculating the CFF, either increase or decreases of the stress areas due to aftershocks and main earthquakes can be determined. Stress accumulation occurs due to movements on the surface and these stresses are reduced by earthquakes. After this stress reduction, the earthquake hazard decreases until a new stress accumulation occurs (Chinery 1963). The increase in the tension due to the earthquake causes the nearby faults to be triggered. The decrease or accumulation of tension is possible by observing the CFF. By determining the CFF, the earthquake and fault relationship can be established and the earthquake hazard in the region can be calculated. Thus, the locations of earthquakes that may occur in the future can be determined (Toda et al., 1998).

The CFF caused by the Elazig-Sivrice 2020 earthquake is shown in Figure 7. Since there is only one source, the stress variation caused by the East Anatolian Fault itself is calculated from approximately 4 km south of the source point (Figure 7). In figure 7, the colour bar represents the magnitude of the shift amount and purple colour show maximum stress with 0.8 MPa.

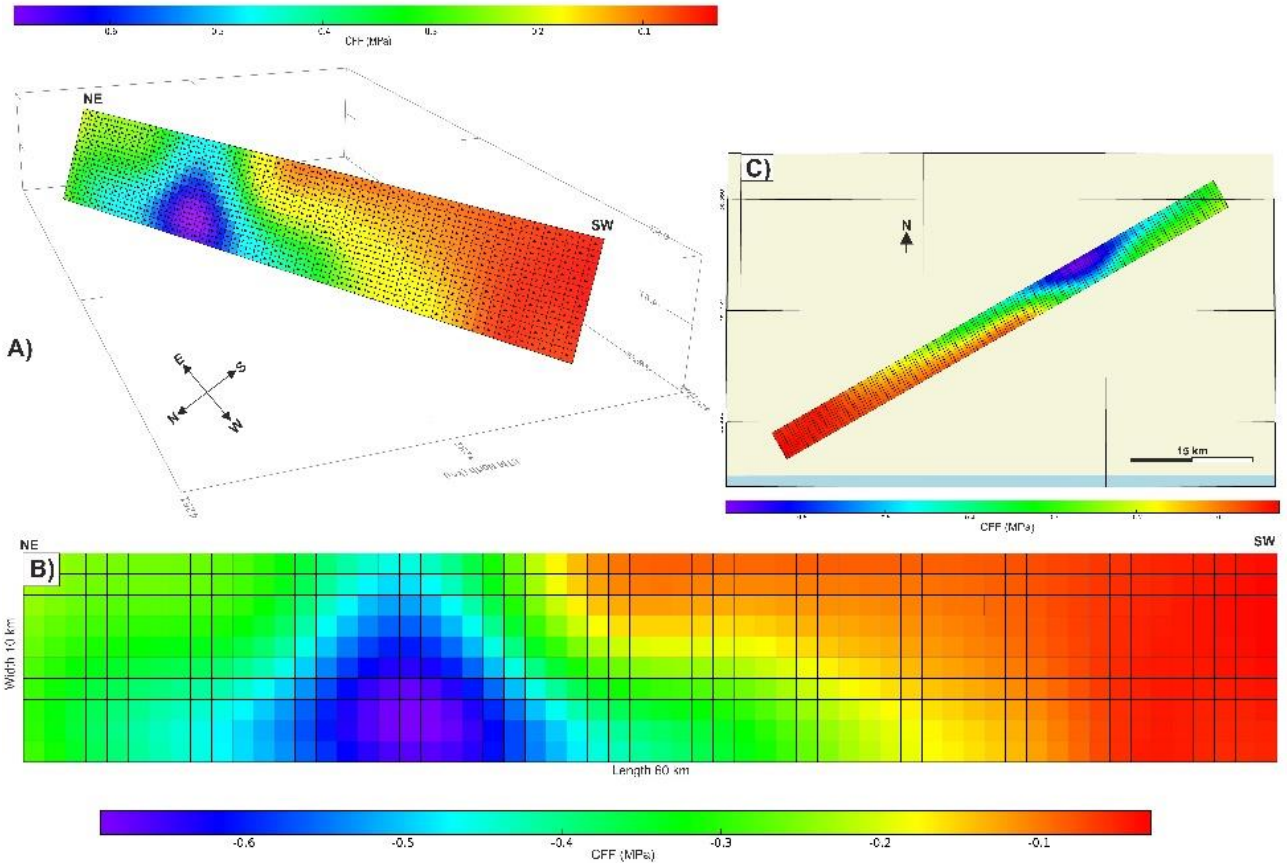

Figure 7. CFF is caused by the slip rate in Figure 6. The colour bar indicates the magnitude of the shift amount.

As known, the disadvantage of the DInSAR method is known that movement can only be detected towards or away from the satellite direction from DInSAR data. By using forward modelling tools, the components of the movement towards the satellite in the InSAR data can be decomposed to its directions. In the forward modelling process, three datasets are created, including east-west, north-south, and up-down components (Figure 8). The results show the displacements of the movement in east-west and north-south, and up-down directions of the movement. In addition, in figures 8D and 8E illustrate the model unwrape phase and LOS surface displacement.

A kinematic fault diagram with left-lateral strike-slip and normal components was created based on DInSAR and elastic modelling results.

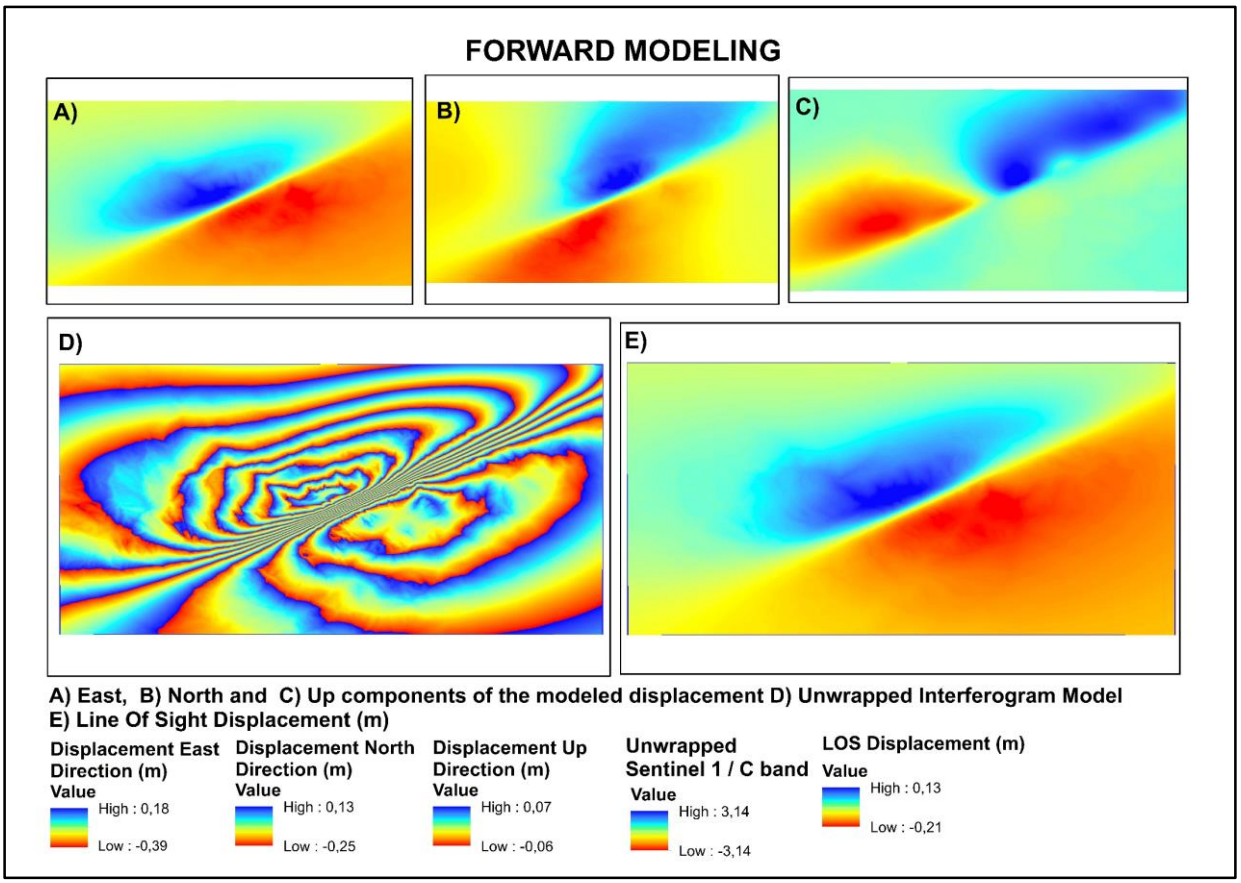

Figure 8. Components of the displacement produced by the shear distribution obtained through linear inversion: A) east-west, B) north-south and C) up-down components D) unexpanded model interferogram in the LOS direction E) model displacement data in the LOS direction

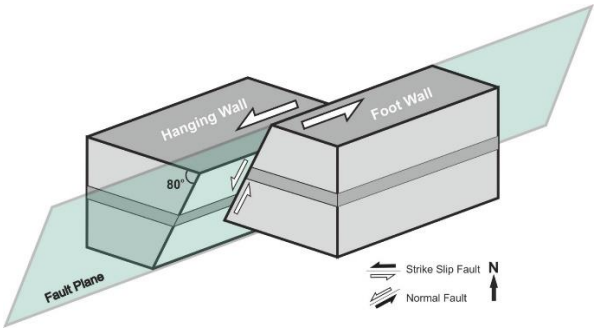

Figure 9. Left-lateral and normal component kinematic fault diagram created in accordance with DInSAR and modelling results.

4. DISCUSSION

- DInSAR analyzes showed that the 2020 Elazig-Sivrice main shock has a predominantly left-lateral strike-slip oblique fault mechanism according to the characteristic of the EAF line (Figure 3, figure 6, figure 7, and figure 8). In the left block of the fault, a displacement of approximately 26 cm away from the satellite is observed in the LOS direction, and a movement in the right block of the fault with a maximum towards to the satellite direction of 19 cm in the LOS direction. This was interpreted as the EAF being a left-lateral strike-slip oblique fault (Figure 3 and 9). These surface LOS displacement results are showing similiraites with studies (Tatar et al., 2020; Pousse-Beltran et al., 2020; Bayik C. et al., 2022).
- DInSAR result also illustrate 36 km east-west direction, 41 km southwest-northeast direction, and approximately 1558 km2 surface rupture occurred during the earthquake (Figure 3). This result is approximately 30 km in the direction of earthquake movement as surface deformation by Tatar et al., 2020; approximately 48 km in MTA reports (Kürçer et al. 2020); 36 km in Pousse-Beltran et al., 2020 study; approximately 37 km in Bayik C. et al., 2022 study, and approximately 38 km in Melgar, D. et al., (2020) study. There is a consistency in the results between the results found in this study and other studies in the literature.
- Elastic shear modelling in half-space results: slip amount (slip) 1.95 m, Mw 6.75, refraction length 34.78 km, focal depth 10 km, width 7.4 km, strike 240.27° (strike), slope 69.19° (dip), rake 0.19°. The results are consistent with the data obtained from institutions such as USGS, AFAD, and KOERI (Table 1). It is considered that the DInSAR results (Figure 3) and the modelling results are consistent with each other (Figure 6 and Figure 7) and that the fault movement and rupture spread mostly south-west from the focal point. It is observed that at approximately 10 km depth, the amount of slip reaches 1.95 m and the length of this slip is effective in an area of 38 km (Figure 6).

Table 1. USGS (United States Geological Survey Comprehensive Earthquake Catalog), GCMT (Global Centroid Moment Tensor Project), AFAD (Disaster and Emergency Management Authority of Turkey), KOERI (Kandilli Observatory and Earthquake Research Institute) Elazığ-Sivrice, 2020 earthquake informations. (modified from Bayik, C. et., all 2022).

Reference	Method	Data	Latitude°	Longitude°	Strike°	Dip°	Rake°	Depth (km)	Length (km)	Width (km)	Slip (m)	Duration (s)	Mw
This Study	Teleseismic	INSAR	38.41	39.07	240.27	69.19	0.19	10	34.78	10	7.4	-	6.75
USGS	Finete Fault	Teleseismic	38.3	39.1	246	67	-12	10	40	10	1.7	20	6.8
USGS	Moment Tensor	Teleseismic	38.39	39.1	245	80	-12	21	-	-	-	11.5	6.7
GCMT	Moment Tensor	Teleseismic	39	39.1	246	67	-9	12	-	-	-	11.8	6.8
AFAD	Moment Tensor	Regional	38.35	39.06	248	76	1	15.1	-	-	-	-	6.8
KOERI	Moment Tensor	Regional	38.52	39.29	248	87	-4	10	-	-	-	-	6.7

- The uncertainties and variations of the model parameters of a single fault calculated using Monte Carlo Analysis are shown (Figure 3). Histograms show uncertainties in individual model parameters, while scatter plots show the degrees of equilibrium between pairs of model parameters; Positive and negative correlations between pairs of parameters express tradeoffs between these parameters (Funning et al., 2005). Accordingly, most of the fault parameters (length, depth, strike, dip, and fault location) are resolved consistently, while scatter plots determine value ranges as tight clusters and narrow peaks in histograms (Figure 3) (Funning et al., 2005).
- CFF is very important for the assessment of seismic hazards, the interaction of earthquakes, and the prediction of future earthquakes. Self-induced voltage variation can be used to verify whether the aftershock distribution on a fault plane is in line with what is expected, in other words, whether the voltage variation is found where it has the highest values (SarMap, 2018). According to the results obtained from the CFF model, the stress change caused by the earthquake was calculated from approximately 4 km south of the source point in Figure 7, the maximum stress was observed as 0.8 MPa at a depth of approximately 10 km and it was observed that the strike direction was in the SW direction.

5. CONCLUSION

In this study, the coseismic surface displacements of the 24 January 2020 Elazig-Sivrice (Mw 6.8) earthquake and the source parameters of the related earthquake were analyzed using the DInSAR method, and the amount of slip and CFF at the time of the earthquake were calculated. Two Sentinel 1A complex (SLC-Single Look Complex) descending directional data sets were used before and after the earthquake, dated 16/01/2020 and 28/01/2020. While there is a maximum of 26 cm away from the satellite in the left block of the DAF, a maximum movement towards the satellite direction of 19 cm is observed in the right block, and the DAF is explained by the left-lateral strike-slip oblique fault movement. To estimate the source parameters of the earthquake, in the results obtained from elastic slip modeling in half-space, it is seen that the slip amount reaches up to 1.95 m at a depth of about 10 km and the length of this slip is effective in an area of 38 km on earth. According to the results obtained from the CFF model calculated from approximately 4 km south of the earthquake source point according to the CFF; the maximum stress was calculated as 0.8 Mpa.

Acknowledment

This study was supported by the General Directorate of Mineral Research and Exploration (MTA). The authors would also like to special thank Prof. Derman Dondurur for insightful constructive comments and suggestions.

Author contributions

S. O. Karaca: Conceptualization and writing of original draft preparation. Collected the datasets and analyzed the data, Methodology, Validation. Writing the manuscript–review and editing;
G. Erten: Elastic Dislocation Modelling process.

Conflicts of Interest

The authors declare no conflict of interest.

Research and publication ethics statement

In the study, the authors declare that there is no violation of research and publication ethics and that the study does not require ethics committee approval.

REFERENCES

Aimaiti, Y., Yamazaki, F., Liu, W., & Kasimu, A. (2017). Monitoring of land-surface deformation in the Karamay oilfield, Xinjiang, China, using SAR interferometry. *Applied Sciences (Switzerland)*, *7*(8). https://doi.org/10.3390/app7080772

Aktuğ, B., Kaypak, B., & Çelik, R. N. (2010). Source parameters for the Mw = 6.6, 03 February 2002, Çay Earthquake (Turkey) and aftershocks from GPS, Southwestern Turkey. *Journal of Seismology*, *14*(3), 445–456. https://doi.org/10.1007/s10950-009-9174-y

Aşçı, M., & Yas, T. (2017). Doğal Kaynakli Potansiyel Alanlarin Birleşik Ters Çözümü. Uygulamalı Yerbilimleri Dergisi 16:27-50

Backus, G. E., & Gilbert, J. F. (1967). Numerical Applications of a Formalism for Geophysical Inverse Problems. Geophysical Journal of the Royal Astronomical Society, 13(1–3), 247–276. https://doi.org/10.1111/j.1365-246X.1967.tb02159.x

Bayrak, E., & Ozer, C. (2021). The 24 January 2020 (Mw 6.8) Sivrice (Elazig, Turkey) earthquake: a first look at spatiotemporal distribution and triggering of aftershocks. *Arabian Journal of Geosciences*, *14*(22). https://doi.org/10.1007/s12517-021-08756-y

Bayik, C., Gurbuz, G., Abdikan, S., Gormus, K. S., & Kutoglu, S. H. (2022). Investigation of Source Parameters of the 2020 Elazig-Sivrice Earthquake (Mw 6.8) in the East Anatolian Fault Zone. *Pure and Applied Geophysics*. https://doi.org/10.1007/s00024-022-02944-x

Bozkurt, E. (2001). Neotectonics of turkey–a synthesis. *Geodinamica Acta*, *14*(1–3), 3–30. https://doi.org/10.1080/09853111.2001.11432432

Cakir Z., Barka A., Akyuz S., (2003), Coulomb Gerilme Etkileşimleri ve 1999 Marmara Depremleri Itü dergisi Mühendislik Cilt:2, Sayı:4, 99-111.

Çetin, H., Güneyli, H., & Mayer, L. (2003). Paleoseismology of the Palu-Lake Hazar segment of the East Anatolian Fault Zone, Turkey. *Tectonophysics*, *374*(3–4), 163–197. https://doi.org/10.1016/j.tecto.2003.08.003

Chinery, M.A.,1963. The stress changes that accompany strike slip faulting. Bull. Seismol. Soc. Am., 53, 921-932.

Demir, D. O. (2015). 3 Ekim 2011 (Mw=7.2) Van Depreminden Kaynaklanan Kabuk Deformasyonlarinin Jeodezik Yöntemlerle Araştirilmasi, Doktora Tezi, Harita Mühendisliği Anabilim Dali Geomatik Programi, Yildiz Teknik Üniversitesi Fen Bilimleri Enstitüsü.

Duman, T. Y., & Emre, Öm. (2013). The east Anatolian fault: Geometry, segmentation and jog characteristics. *Geological Society Special Publication*, *372*(1), 495–529. https://doi.org/10.1144/SP372.14

Duman, T.Y., Emre, Ö., Özalp, S.,Elmacı, H. ve Olgun, Ş., (2012). 1:250.000 Ölçekli Türkiye Diri Fay Haritası Serisi, Elazığ (NJ 37-7) Paftası, Seri No:45, Maden Tetkik ve Arama Genel Müdürlüğü, Ankara - Türkiye (https://www.mta.gov.tr/v3.0/hizmetler/yenilenmis-diri-fay-haritalari)

Helz, R. L. (2005). *Monitoring Ground Deformation from Space*. US Department of the Interior, US Geological Survey.

Elliott, J. R., Nissen, E. K., England, P. C., Jackson, J. A., Lamb, S., Li, Z., Oehlers, M., & Parsons, B. (2012). Slip in the 2010-2011 Canterbury earthquakes, New Zealand. *Journal of Geophysical Research: Solid Earth*, *117*(3). https://doi.org/10.1029/2011JB008868

Emre, Ö., Duman, T.Y., Özalp, S., Elmacı, H., Olgun, Ş. and Şaroğlu, F., (2013). Açıklamalı Türkiye Diri Fay Haritası. Ölçek 1:1.250.000, Maden Tetkik ve Arama Genel Müdürlüğü, Özel Yayın Serisi-30, Ankara-Türkiye.

Funning, G. J., Parsons, B., Wright, T. J., Jackson, J. A., & Fielding, E. J. (2005). Surface displacements and source parameters of the 2003 Bam (Iran) earthquake from Envisat advanced synthetic aperture radar imagery. Journal of Geophysical Research: Solid Earth, 110(9), 1–23. https://doi.org/10.1029/2004JB003338

Goldstein RM, Werner CL (1998). Radar interferogram fltering for geophysical applications. Geophys Res Lett 25(21):4035–4038

Jackson, D. D. (1972). Interpretation of Inaccurate, Insufficient and Inconsistent Data. Geophysical Journal of the Royal Astronomical Society, 28(2), 97–109. https://doi.org/10.1111/j.1365-246X.1972.tb06115.x

Kürçer A, Elmacı H, Yıldırım N, Özalp S (2020). 24 Ocak 2020 Sivrice (Elazığ) Depremi (Mw=6,8)

Saha Gözlemleri ve Değerlendirme Raporu. MTA Jeoloji Etütleri Dairesi, p 41

Li, Y., Shan, X., Qu, C., Liu, Y., & Han, N. (2018). Crustal Deformation of the Altyn Tagh Fault Based on GPS. *Journal of Geophysical Research: Solid Earth*, *123*(11), 10309–10322. https://doi.org/10.1029/2018JB015814

Liu, Y., (2015). InSAR Technique for Earthquake Studies, Master Thesis, Geoscience and Earth Observing Systems Group (GEOS) School of Civil and Environmental Engineering Faculty of Engineering, The University of New South Wales

Melgar, D., Ganas, A., Taymaz, T., Valkaniotis, S., Crowell, B. W., Kapetanidis, V., Tsironi, V., Yolsal-Çevikbilen, S., & Öcalan, T. (2020). *Earthquake on the East Anatolian Fault Zone Imaged by Space Geodesy Abbreviated title: The Mw6.7 Doğanyol-Sivrice Earthquake*. https://doi.org/10.1093/gji/ggaa345/5872486

Okada, Y., (1985). "Surface Deformation Due to Shear and Tensile Faults in a Half-space", Bulletin of the Seismological Society of America, 75: 1135-1154.

Pousse-Beltran, L., Nissen, E., Bergman, E. A., Cambaz, M. D., Gaudreau, É., Karasözen, E., & Tan, F. (2020). The 2020 Mw 6.8 Elazığ (Turkey) Earthquake Reveals Rupture Behavior of the East Anatolian Fault. *Geophysical Research Letters*, *47*(13). https://doi.org/10.1029/2020GL088136

Press, F. (1965). Displacements, strains, and tilts at teleseismic distances, J. Geophys. Res., 70(10), 2395–2412, https://doi:10.1029/JZ070i010p02395

Rucci, A., Ferretti, A., Monti Guarnieri, A., & Rocca, F. (2012). Sentinel 1 SAR interferometry applications: The outlook for sub millimeter measurements. *Remote Sensing of Environment*, *120*, 156–163. https://doi.org/10.1016/j.rse.2011.09.030

Sarychikhina, O., & Glowacka, E. (2015). Spatio-Temporal evolution of aseismic ground deformation in the Mexicali Valley (Baja California, Mexico) from 1993 to 2010, using differential SAR interferometry. *Proceedings of the International Association of Hydrological Sciences*, *372*, 335–341. https://doi.org/10.5194/piahs-372-335-2015

Stekeete, J. A., (1958). "On Volterra's Dislocations in a Semi-infinite Elastic Medium, Canadian Journal of Physics, 36 (2): 192-205.

SARMAP (2018). ENVI SarScape v5.5.0: Geophysical Modeling Tutorial. Available at: https://www.sarmap.ch/tutorials/GeophysicalModelingTutorial_55.pdf (Accessed: 02/03/2022).

Şaroğlu, F. (1986). Doğu Anadolu'nun Neotektonik Dönemde Jeolojik Ve Yapısal Evrimi. Rapor No: 7857. Maden Tetkik Arama Genel Müdürlüğü, Ankara.

Şengör C, A. M., Yilmaz, Y., Bijliimii, J., & Fakiiltesi, Y. (1981). *Tethyan Evolutıon of Turkey: a Plate Tectonic Approach* (Vol. 75).

Tatar, O., Sözbilir, H., Koçbulut, F., Bozkurt, E., Aksoy, E., Eski, S., Özmen, B., Alan, H., & Metin, Y. (2020). Surface deformations of 24 January 2020 Sivrice (Elazığ)–Doğanyol (Malatya) earthquake (Mw = 6.8) along the Pütürge segment of the East Anatolian Fault Zone and its comparison with Turkey's 100-year-surface ruptures. *Mediterranean Geoscience Reviews*, *2*(3), 385–410. https://doi.org/10.1007/s42990-020-00037-2

Tiryakioğlu, Aktuğ, B., Yiğit, C., Yavaşoğlu, H. H., Sozbilir, H., Özkaymak, Poyraz, F., Taneli, E., Bulut, F., Doğru, A., & Özener, H. (2018). Slip distribution and source parameters of the 20 July 2017 Bodrum-Kos earthquake (Mw6.6) from GPS observations. *Geodinamica Acta*, *30*(1), 1–14. https://doi.org/10.1080/09853111.2017.1408264

Torres, R., Snoeij, P., Geudtner, D., Bibby, D., Davidson, M., Attema, E., Potin, P., Rommen, B. Ö., Floury, N., Brown, M., Traver, I. N., Deghaye, P., Duesmann, B., Rosich, B., Miranda, N., Bruno, C., L'Abbate, M., Croci, R., Pietropaolo, A., Rostan, F. (2012). GMES Sentinel-1 mission. Remote Sensing of Environment, 120, 9–24. https://doi.org/10.1016/j.rse.2011.05.028

Vajedian, S., Motagh, M., Mousavi, Z., Motaghi, K., Fielding, E. J., Akbari, B., Wetzel, H. U., & Darabi, A. (2018). Coseismic deformation field of the Mw 7.3 12 November 2017 Sarpol-e Zahab (Iran) earthquake: A decoupling horizon in the Northern Zagros Mountains inferred from InSAR observations. *Remote Sensing*, *10*(10). https://doi.org/10.3390/rs10101589

Yague-Martinez, N., Prats-Iraola, P., Gonzalez, F. R., Brcic, R., Shau, R., Geudtner, D., Eineder, M., & Bamler, R. (2016). Interferometric Processing of Sentinel-1 TOPS Data. IEEE Transactions on Geoscience and Remote Sensing, 54(4), 2220–2234.

Yalvaç, S. (2020). Determining the Effects of the 2020 Elazığ-Sivrice/Turkey (Mw 6.7) Earthquake from the Surrounding CORS-TR GNSS Stations. In Turkish Journal of Geosciences (Vol. 1, Issue 1). Retrieved from : https://dergipark.org.tr/tr/pub/turkgeo/issue/54166/731709

Yilmaz, Y. (1993). New evidence and model on the evolution of the southeast Anatolian orogen. *Geological Society of America Bulletin*, *105*(2), 251–271. https://doi.org/10.1130/0016-7606(1993)105<0251:NEAMOT>2.3.CO;2

Zebker, H.A. & Goldstein, R.M. (1986). Topographic mapping from interferometry synthetic aperture radar observations. – Journal of Geophysical Research, 91/B5, 4993–4999.

Wang, J., Xu, C., Freymueller, J. T., Li, Z., & Shen, W. (2014). Sensitivity of Coulomb stress change to the parameters of the Coulomb failure model: A case study using the 2008 Mw 7.9 Wenchuan earthquake. *Journal of Geophysical Research: Solid Earth*, *119*(4), 3371–3392. https://doi.org/10.1002/2012JB009860

Wang, R., Xia, Y., Grosser, H., Wetzel, H. U., Kaufmann, H., & Zschau, J. (2004). The 2003 Bam (SE Iran) earthquake: Precise source parameters from satellite radar interferometry. *Geophysical Journal International*, *159*(3), 917–922. https://doi.org/10.1111/j.1365-246X.2004.02476.x

Wells, D. L., & Coppersmith, K. J. (1994). New Empirical Relationships among Magnitude, Rupture Length, Rupture Width, Rupture Area, and Surface Displacement. In *Bulletin of the Seismological Society of America* (Vol. 84, Issue 4).

Welstead, S. T., (1999). Fractal and wavelet image compression techniques, SPIE Optical Engineering Press, Bellingham, Washington, 232 pp

Wiggins, R. A. (1972). The General Linear Inverse Problem: Implication of Surface Waves and Free Oscillations for Earth Structure. in reviews of geophysics and space physics (Vol. 10, Issue 1).

Wright, T. J., Parsons, B. E., Jackson, J. A., Haynes, M., Fielding, E. J., England, P. C., & Clarke, P. J. (1999). Source parameters of the 1 October 1995 Dinar (Turkey) earthquake from SAR interferometry and seismic bodywave modelling. In *Earth and Planetary Science Letters* (Vol. 172).

Wright, T. J., Lu, Z., & Wicks, C. (2003). Source model for the Mw 6.7, 23 October 2002, Nenana Mountain Earthquake (Alaska) from InSAR. *Geophysical Research Letters*, *30*(18). https://doi.org/10.1029/2003GL01

Araştırma Makalesi/Research Article
https://doi.org/10.51489/tuzal.1268275

2023; 5(1); 14-26

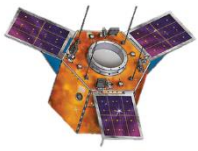

Turkish Journal of Remote Sensing

https://dergipark.org.tr/en/pub/tuzal

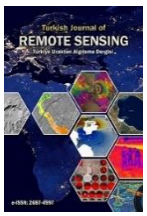

e-ISSN 2687-4997

Suitability Analysis based on GIS and AHP for Urban Development Projects

Sinan Levend*[1], Mehmet Akif Sağ [1]

[1]Konya Technical University, Architecture and Design Faculty, Urban and Regional Planning Department, Konya, Türkiye

Keywords
Urban Development Projects
Suitability Analysis
GIS
AHP
Konya

ABSTRACT

As urban areas grow, natural areas around the city become more vulnerable to degradation. Therefore, adopting an approach that balances protection and usage without harming the natural environment is essential to ensure that urban development projects are produced sustainably. For this reason, it is crucial that the suitability analysis, in which the factors related to the planning area are systematically evaluated and integrated, is decisive in determining the urban development areas. In this study, suitability analysis based on Geographic Information System (GIS) and Analytical Hierarchy Process (AHP) was produced for the "Bizim Şehir Project" in Konya. Within the scope of the suitability analysis, six factors were evaluated: soil characteristics, geological conditions, natural disasters, aspect analysis, slope analysis, and property analysis. First, thematic maps were produced and standardized for each factor using GIS. Then, using the AHP method, the percentages of factors affecting the suitability analysis were determined. Finally, by using the spatial analysis capability of GIS, the factors were integrated according to the determined percentage weights and the suitability analysis was produced. The results showed that 54.9% of the case area was suitable for development. This study proposes a method for designing sustainable living areas using suitability analysis.

Kentsel Gelişim Projeleri için CBS ve AHP Tabanlı Uygunluk Analizi

Anahtar Kelimeler:
Kentsel Gelişim Projeleri
Uygunluk Analizi
CBS
AHP
Konya

ÖZ

Kentsel alanlar büyüdükçe, kentin çevresindeki doğal alanlar bozulmaya karşı daha savunmasız hale gelmektedir. Doğal çevreye zarar vermeden koruma ve kullanma arasında denge kuran bir yaklaşımın benimsenmesi, kentsel gelişim projelerinin sürdürülebilir bir şekilde üretilmesini sağlamak için gereklidir. Bu nedenle kentsel gelişim alanlarının belirlenmesinde, planlama alanına ilişkin faktörlerin sistematik olarak değerlendirilip, bütünleştirildiği uygunluk analizinin tercih edilmesi kritik öneme sahiptir. Bu çalışmada Konya'da "Bizim Şehir Projesi" için Coğrafi Bilgi Sistemi (CBS) ve Analitik Hiyerarşi Sürecine (AHP) dayalı uygunluk analizi üretilmiştir. Uygunluk analizi kapsamında toprak özellikleri, jeoloji yapı, doğal afetler, bakı, eğim ve mülkiyet durumu olmak üzere altı faktör değerlendirilmiştir. CBS kullanılarak her bir faktör için tematik haritalar üretilmiş ve standardize edilmiştir. Daha sonra AHP yöntemi kullanılarak uygunluk analizini etkileyen faktörlerin analizi etkileme yüzdelikleri belirlenmiştir. Son olarak, CBS'nin mekânsal analiz kabiliyeti kullanılarak faktörler belirlenen yüzde ağırlıklarına göre bütünleştirilmiş ve uygunluk analizi üretilmiştir. Sonuçlar, örneklem alanın %54,9'unun gelişme/imar için uygun olduğunu gösterdi. Bu çalışma, sürdürülebilir yaşam alanları tasarlamak için uygunluk analizinin üretilmesine yönelik bir yöntem önermektedir.

Article Info

Received: 20/03/2023
Accepted: 07/06/2023
Published: 30/06/2023

Citation:

Levend, S. & Sağ, M.A. (2023). Suitability Analysis based on GIS and AHP for Urban Development Projects. Turkish Journal of Remote Sensing , 5 (1) , 14-26 .

***Corresponding Author:** Sinan Levend, sinanlevend@gmail.com, +90 332 205 11 11*

1. INTRODUCTION

Sustainability means limiting the damage to natural resources and structures caused by human activities while ensuring that we can meet our future needs in a balanced way (Brundtland & Khalid, 1987). However, unplanned urban growth and sprawl can harm the environment, putting pressure on agricultural areas, forests, and watersheds on the periphery of cities (Malczewski, 2006; Saha & Roy, 2021). That is why planning is crucial for sustainable urban development. Planning helps us find the best way to achieve a specific goal when faced with a problem or situation and involves deciding how to implement these actions (Aydemir, 1999; Ersoy, 2007; Tekel & Altıntaş, 2011; Keskinok, 2020). Urban planning is a multidisciplinary field that requires strategic decision-making at different levels to shape cities (Healey, 2006). Since the publication of the Brundtland Report in 1987, sustainability has been the guiding principle for urban planning activities.

Planning aims to make sustainable decisions for urban development. The future success of urban plans depends heavily on considering scientific data and rationality (Keskinok, 2020). The planning process typically involves research (data collection), analysis and synthesis of the current situation, and decision-making through developing alternatives and implementation (Çalışkan, 2017; Şahin, 2020). The success of the planning process relies on the first step since it determines the success of the following steps and the outcome. Therefore, it is crucial to analyze the planning area with analytic techniques for the proper execution of the planning process (Alkay, 2014).

As a scientific discipline, planning should be conducted rationally. In order to make informed decisions, planners need to analyze the current situation in the planning area holistically and in line with the purpose determined in the planning process. To determine the appropriate location for construction within the context of urban development projects and sustainability principles, planners must evaluate a large number of parameters and information, both quantitative and qualitative. Analytical techniques, such as spatial analysis, data analysis, and mathematical models, are used in the planning process to reach conclusions related to the study area (Çubukçu, 2017). By overlapping these analyses, the planner produces various analyses (maps) considering the factors and determines the appropriate construction areas. However, producing analyses can be complicated depending on the size and nature of the study area. To meet this challenge, planners use GIS's ability to process and integrate complex data. By analyzing and integrating various factors related to the planning area in the GIS environment, planners can determine the most suitable land for construction.

This study aims to develop a robust spatial decision support system for assessing suitability by integrating the AHP, a multicriteria decision analysis approach, into GIS. The study presents the suitability analysis for the Bizim Şehir Project, an urban development initiative within the Selçuklu Municipality of Konya. The spatial analysis tools and mapping capability of GIS software were used to conduct the suitability analysis for the urban development project. In this process, the AHP method was employed to establish the priorities of the factors contributing to the suitability analysis. These priorities were determined through a survey with 14 participants from the three main areas of expertise that shape the space: Architecture, Urban Planning, and Geomatics Engineering. Integrating AHP and GIS in the decision-making process for the Bizim Şehir Project facilitated the identification of suitable areas for construction in the urban development project. The findings of this study provide valuable insights into suitability analyses for urban development projects and contribute to the transparency and acceptability of the decision-making technique.

2. SUITABILITY ANALYSIS

During the planning process, data from various institutions regarding the planned area is transformed into understandable and usable information through several processes (Şahin, 2020). This information includes visual aids such as graphics, diagrams, and maps produced by collecting and analyzing data on the natural, built, and socio-economic environments. Factors such as topography, water resources, climate, geological structure, and soil quality are considered in analyzing the natural environment. In addition, factors such as land use, density, ownership, environmental problems, transportation, and infrastructure related to the existing construction in the planning area are discussed for the built environment. Finally, the socio-economic environment analysis covers the demographic, social, and economic structure, lifestyles, migration analysis, expectations, and priorities of the society (Okumuş, 2014). The diagrams and maps produced in this analysis process facilitate stakeholder involvement in decision-making, directly affecting the planning process's success.

Suitability analysis is a commonly used tool in determining suitable areas for settlement in the planning process for sustainable urban development (Özügül, 2012). Experts in the field evaluate and grade factors used in suitability analysis systematically. They provide data on factors such as land use, geology, geomorphology, slope, soil type, and land ownership, and produce maps. Integrating GIS and AHP evaluates the relevant factors holistically and produces a suitability analysis (Malczewski, 2006). Data collection and processing have become more analytical and faster thanks to developing science and technology. Therefore, GIS is an essential tool in planning to create a spatial

decision support system, make data-driven queries, analyze spatial data, and produce maps to present final products.

Factors used in suitability analysis are standardized and synthesized according to the weight values determined in line with the purpose of the study (Saha & Roy, 2021). This spatial analysis plays a crucial role in determining the most suitable areas by analyzing the spatial data related to the area to be planned, taking into account environmental sustainability. As a result, a detailed image of the most suitable areas for the determined purpose is produced, while a spatial model is generated in which the unusable or less preferred areas are filtered (Kumar & Shaikh, 2013; AlFanatseh, 2021).

An expenditure and weighting system can be applied to determine the criteria used during the suitability analysis and end product management (Kumar & Shaikh, 2013). AHP is the most widely used method among multicriteria decision-making methods as it reduces the time and effort required (AlFanatseh, 2021). It can be integrated into the suitability analysis in two ways (Malczewski, 2004). The first method uses it for the initial suitability analysis to weigh and estimate the appropriate parameters. The second method is determining how much the particles are weighted appropriately and affect the suitability analysis produced.

When designing for sustainable urban development, it is crucial to consider and analyze various criteria. In Türkiye, the Spatial Plans Construction Regulation of 2014 mandates threshold analysis when preparing zoning plans and using it as primary data in forming plan decisions (Mekânsal Planlar Yapım Yönetmeliği, 2014). This regulation emphasizes the need to superimpose maps such as topography, hydrology, geology, land use, and protection areas related to the planning area. However, the threshold analyses produced during the implementation process are insufficient to determine suitable residential areas in the urban design process. Alternatively, suitability analysis provides more accurate results in determining the suitability of a particular piece of land for the residential area (Al-Shalabi, et al., 2006; Aburas, et al., 2017). Unfortunately, there is no example of suitability analysis in Türkiye's residential area design process. The Bizim Şehir Project's conformity analysis is expected to serve as an example for future studies in Türkiye. Furthermore, the study determined the relative weights of the factors used in the suitability analysis through expert opinions from experienced urban designers and integrated GIS and AHP. The study is expected to contribute significantly to the literature on this topic.

3. METHOD

3.1. Case Study: Bizim Şehir Project

Konya's urban areas population, the seventh largest city in Türkiye by population, is around 1.3 million inhabitants. The city's population structure reflects the growth of its industrial sector. As a result, numerous urban development projects are being undertaken as the population increases. One such project is Bizim Şehir, located in the western periphery of Konya's urban area and serving as the focus of this study (see Figure 1). At around 350 hectares, Bizim Şehir Project aims to create a sustainable, livable residential area.

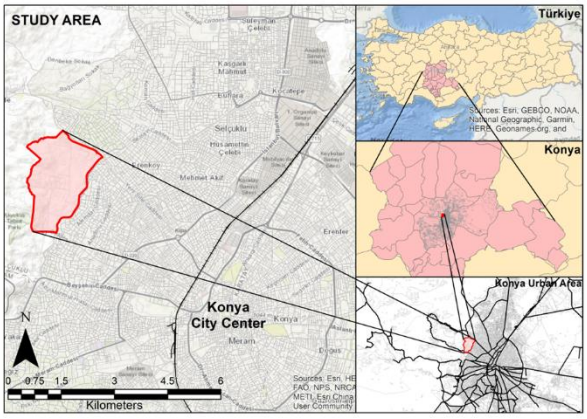

Figure 1. Location of the case study

The suitability analysis presented in the study was produced as part of the analysis and synthesis phase of the urban development project called Bizim Şehir - Konya. The Bizim Şehir Project is an initiative of the Ministry of Environment and Urbanization aimed at exploring the idea of the "*city of future & future of the city*" and the principles of urban planning that can effectively combine past and future developments. Its vision is to bring together the city's historical and contemporary dynamics for a sustainable future. In line with this vision, the Ministry of Environment and Urbanization requested the preparation of "*a plan, project and urban design guide which functions systematically, protects the local identity of the city, meets the needs of the age, is sustainable and includes spatial arrangements with a high quality of life for an area of approximately 350 hectares within Konya Province's Selçuklu District, Sarayköy Neighborhood*" from Selçuk University. A group of professionals from Selcuk University, including architects, engineers, urban planners, and sociologists, worked together on the project. After completing it, they handed it over to the Ministry in 2020.

3.2. Methodology

The Geographic Information System's analysis methods make it easy to produce a suitability analysis for urban planning decisions. This analysis is widely used to evaluate alternative areas to make sustainable decisions by determining the most suitable locations for land use decisions, such as housing, industry and solar farming (Koramaz, 2014; ArcGIS Pro, 2023; ArcGIS, 2023). The suitability analysis is prevalent in urban design because it

allows for evaluating many factors in the decision-making process. This is especially important when determining suitable areas for residential use.

When the literature is examined, different methodological approaches have been put forward for suitability analysis for different purposes (Malczewski, 2004; Dong, et al., 2008; Chandio, et al., 2014; Koramaz, 2014; Aburas, et al., 2017; Parry, et al., 2018; AlFanatseh, 2021; Johnston & Graham, 2021; Luan, et al., 2021; ArcGIS Pro, 2023; ArcGIS, 2023). By evaluating these studies, a five-step suitability method was created in this study. (see Figure 2):

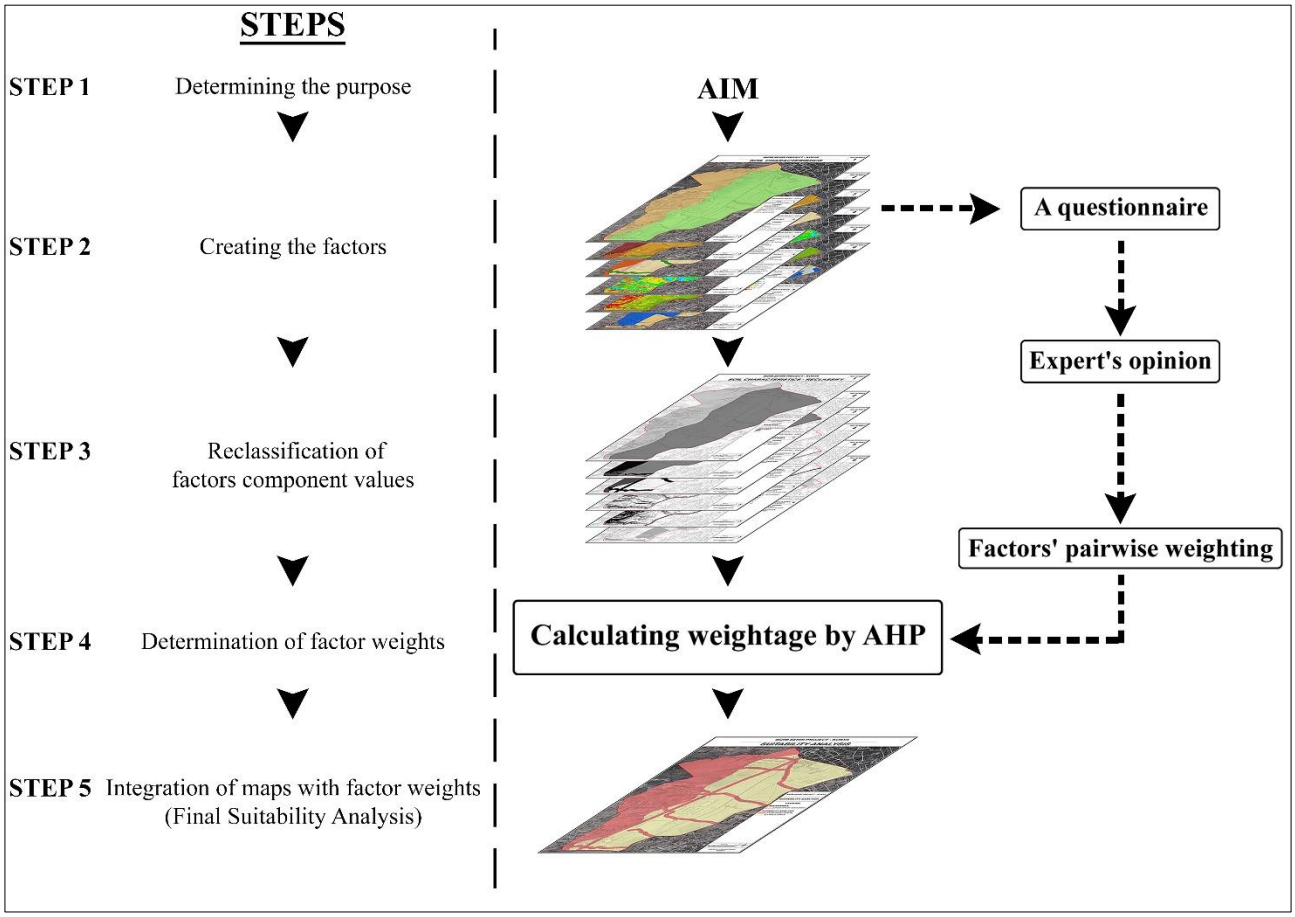

Figure 2. The AHP-Based suitability analysis methodology workflow (visualised by the authors)

Step 1. Determining the purpose:

The purpose of the decision makers (e.g., priority, philosophy) regarding the planning area forms the framework/boundaries of the analysis of suitability for settlement. The decision-makers must determine the factors (analysis) and constraints for settlement suitability analysis. The values/weights assigned to the purpose in the creation process of the analysis are decisive. For example, risk-sensitive location analysis should use detailed data showing the risk factors.

Step 2. Determine and create factors (analyses or limiting criteria):

After the aim of the suitability analysis has been established, the factors related to the analysis should be determined. Each identified factor must be effective in achieving the aim. The factors for suitability analysis are mapped and converted to raster format according to the determined purpose. First, each factor is classified according to its parameters. Then, each factor data is converted to a raster (grid) data type.

Step 3. Standardization and reclassification of parameter values for factors:

At this stage, the analyses related to the field should be reclassified according to a certain standard. Therefore, for the suitability analysis, the factor parameters are reclassified by assigning values between 10 (the most suitable value for settlement) and 0 (the value that cannot be settled) and converted into raster maps. Thus, all factors (analyses) are standardized at specific values.

Step 4. Determination of factor weights in line with the purpose:

For the suitability analysis, a percentage value (with a sum of factor weights of 100) should be assigned to each factor (analysis) to the extent that it affects the suitability analysis. Methods such as AHP can be used to determine the values in question, which allows the evaluation of the many participants' views.

Step 5. Creating a suitability analysis by integrating the analyses with factor weights:

The thematic map is created by integrating the raster data according to the percentage rate (factor weights) determined for each factor (analysis) using the spatial analysis capability of GIS. Thus, suitability analysis is obtained in line with the determined purpose.

This study utilized the Analytic Hierarchy Process (AHP) and Geographic Information System (GIS) to conduct a suitability analysis. These multicriteria decision analysis approaches help create a robust spatial decision support system by prioritizing factors. In addition, GIS enables the creation, storage, association, querying, analysis, and visualization of spatial data and attribute information related to this data in a structured manner (Dunn, 2007; Okumuş, 2014; Malczewski & Rinner, 2015). The suitability analysis for an urban development project was conducted using the GIS software's mapping capabilities and spatial analysis tools. The Konya Metropolitan Municipality provided the data used in the analysis, including property, topography, geology, soil capability, and erosion.

To determine the suitability of a region for a specific use, factors that make up the unique structure of the land are systematically analyzed. Multicriteria decision analysis approaches, such as the AHP method, provide the necessary procedures and techniques for structuring decision problems and forming, evaluating, and prioritizing factors and alternative decisions (Malczewski, 2006; Estoque, 2012). The AHP method in this study is used to objectively determine the weights of the factors that are effective on urban growth and integrated with the GIS environment. The AHP method is a frequently used multicriteria technique in GIS-based analyses for determining the priority weights of factors affecting urban growth (Saaty, 2008; Saaty & Vargas, 2012). The AHP method calculates the priority weights of the factors by comparing all the objective factors in pairwise comparison matrices. (Saaty, 1990; Bhushan & Rai, 2007; Filipović, 2007; Kumar & Shaikh, 2013). To determine the relative weight values for each factor and alternative, the AHP methodology follows the steps of establishing the decision hierarchy, making pairwise comparisons, calculating the factor priorities for each level, checking the consistency ratios, and finalizing the weight values (Saaty, 1989; Saaty, 2008; Saaty & Vargas, 2012; Ullah & Mansourian, 2016).

AHP is a robust and easy-to-understand methodology, making it an ideal tool for group and individual decision-making processes. Integrating with GIS provides an analytical framework for identifying new development areas in urban environments (Levend & Fischer, 2022). To ensure a participatory approach, expert opinions and stakeholder feedback can be integrated into the analytical structure of the suitability analysis. The weights of the factors used for suitability analysis were determined based on information gathered through questionnaires administered to 14 participants with expertise in three main fields: architecture, urban planning, and geomatics engineering.

The study identified the factors affecting the suitability for settling in the case area and created factor maps using the visualization capabilities of GIS. The factors were reclassified and standardized to ensure that the map parameters were comparable and combinable with each other. A joint scale of 0 to 10 was chosen, where higher values indicate more suitable places for urban growth. The weight of each factor affecting the suitability analysis was determined using expert opinions and pairwise comparisons according to the importance of the factors for the factor weights with the AHP method. Finally, using the weighted overlay tool of ArcGIS software, all factor maps were integrated with the line with the weights determined by expert opinions, and the final suitability map was prepared.

3.3. Factors Description

Various factors, such as physical, socio-economic, and environmental structures, influence the design and development of residential areas (Al-Shalabi, et al., 2006). In the Bizim Şehir project, these factors were considered at different stages of the design process. The City 2023 Project (Bizim Şehir - Konya) urban development/design project aims to identify sustainable and livable areas through a suitability analysis considering factors. To achieve this, relevant criteria were carefully chosen for evaluation. The selection process was based on the study's objective, a literature review, experts' opinions, and data availability in the study area. The study evaluated six factors: soil characteristics, geological condition, natural disasters, aspect analysis, slope analysis, and property analysis.

Soil Characteristics

Soil structure is one of the most critical factors in determining settlement areas because of its sensitivity to erosion, surface drainage, and soil fertility. Therefore, decisions regarding site selection for urban use should be based on the compatibility of the proposed function with the soil structure, which leads to a sustainable urban development process. For example, an area well-suited for residential use may not be appropriate for recreational activities (Aburas, et al., 2017; Parry, et al., 2018; McBride, 2019). Thus, settlement areas should be established in areas with low production capacity and soil quality to ensure sustainable urban development.

Geological Condition

The geological structure of the ground plays a crucial role in determining where urban settlements should be built. It affects the bearing capacity of the ground, the construction engineering, and the construction method. Therefore, planning settlements in the most stable geological regions is

vital to avoid disaster risks. (McBride, 2019; Deliry & Uygucgil, 2020; Luan, et al., 2021).

Natural Disasters

When choosing areas for settlement, natural disasters such as erosion, earthquakes, and floods should be considered. Areas with a high risk of disaster should not be developed. For example, erosion state maps can show an area's erosion severity (Dong, et al., 2008; Kumar, et al., 2018; Luan, et al., 2021). Geological fault lines should also be considered when planning settlements, and buffer zones should be created to ensure a safe distance from the fault lines. These zones will create conservation areas (Deliry & Uygucgil, 2020). Flooding is another critical factor to consider when choosing a location for structures. Therefore, the hydrological structure should also be considered during the planning process.

Aspect Analysis

Aspect analysis is an essential factor when selecting a site for residential areas. It determines the direction of the land slope. Aspect analysis represents the main directions in the form of north, south, east, west, and intermediate directions related to these directions with general classification. This analysis is used in many design-related issues, such as the positioning of buildings, planting, and ensuring the protection of residential areas from sunlight (Al-Shalabi, et al., 2006; Chandio, et al., 2014; Aburas, et al., 2017; McBride, 2019). Generally, South (S), Southeast (SE), Southwest (SW), East (E) and West (W) aspects in Türkiye are warmer because these aspects receive more sun than the other aspects. On the other hand, the North (N), Northwest (NW) and Northeast (NE) aspects are cooler as they receive few lights. Therefore, it is essential to choose a location compatible with the climate to reduce energy dependence and make maximum use of solar energy. Northern slopes are not preferred because of low radiation levels. In a temperate climate, the upper parts of the southeast-eastern slopes are suitable for settlement in harmony with the climate.

Slope Analysis

The slope is a crucial factor to consider in suitability analysis, as it affects both the visual and functional aspects of construction. Although the slope is primarily related to landscape design, it also significantly determines construction costs, disaster risk, and drainage (Al-Shalabi, et al., 2006; Dong, et al., 2008; Chandio, et al., 2014; Aburas, et al., 2017; Parry, et al., 2018; Akbulut, et al., 2018). To evaluate the slope for different uses and activities, it is categorized according to percentage changes. Generally, the slope classification for construction is as follows: 0-2% is suitable, 2-8% is quite suitable, 8-16% is suitable, but with an upper limit for roads and walkways, 16-24% has significant restrictions, and 24%+ is restricted for residential areas. In addition, different slope categories can be used for particular land use types and facilities (McBride, 2019; Luan, et al., 2021).

Property Analysis

Analyzing properties is crucial in making settlement decisions. When evaluating property data, it is essential to consider both opportunities and constraints related to construction (McBride, 2019). Properties with public land status (such as state and local government) tend to lead to quicker decision implementation.

4. RESULTS AND DISCUSSION

It is essential to identify suitable areas for construction in line with the sustainable urban development approach. In the context of the sample study, various data related to the natural, built and socio-economic environment were systematically evaluated. Six factors were used for suitability analysis, and suitable construction areas were determined using ArcGIS software's weighted overlay tool. Thus, a rational substrate was created for more accurate alternatives and decisions in the decision-making process.

4.1. Determining The Purpose

In the decision-making process, the purpose forms the basis of the settlement suitability analysis. In addition, the purpose determines which analyses are used in assessing the suitability and the weight given to each analysis. The Bizim Şehir Project, which serves as the study's case area, aims to create new living spaces that prioritize human-centred, identity-driven, smart, green, and safe city policies while meeting society's social, cultural, and physical needs. The project aims to design a sustainable settlement that prioritizes ecological and social sustainability, develops the spatial organization of public spaces, is adaptable to global climate changes and unexpected conditions through walkable and accessible transportation options, and integrates tradition and the future through learning and teaching. The primary objective is to use the suitability analysis produced for the Bizim Şehir Project area to determine suitable ecological settlement areas consistent with the principle of sustainability.

4.2. Creating The Factors

In the second stage of the settlement suitability analysis, the factors used for suitability analysis should be determined and mapped in line with the purpose. Then, the maps should be converted to raster format. The factor data used in the study is in vector data format, so six thematic maps were created on the GIS platform. Each factor was classified according to its parameters, resulting in maps for Soil Capability, Geological Structure, Natural Disasters, Aspect Analysis, Slope Analysis, and Property Status (see Table 1). Then, each factor data should be converted to a raster (grid) data type (see Figure 3).

Table 1. Factors, factor weights, factor parameters and standardization value of the parameter

Factors	Factor Weights	Factor Parameters	Standardization Value of Parameter
Soil Characteristics	0.210	II. degree soil lands	5
		VII. degree soil lands	8
Geology	0.228	Geologically unsuitable areas	0
		Stream beds	0
		High slope, transition floors	3
		Alluvial fan	5
Natural Disasters	0.382	II. degree erosion zone	10
		IV. degree erosion zone	2
		Fault avoidance band	0
		Stream band	0
Aspect	0.049	Flat	10
		North (0-22.5 and 337.5-360)	2
		Northeast (22.5-67.5)	4
		East (67.5-112.5)	8
		Southeast (112.5-157.5)	10
		South (157.5-202.5)	10
		Southwest (202.5-247.5)	8
		West (247.5-292.5)	6
		Northwest (292.5-337.5)	4
Slope (%)	0.075	% 0-2	8
		% 2-8	10
		% 8-16	7
		% 16-24	5
		% 24-40	3
		% 40+	0
Property Status	0.056	Public Property (central and local gov.)	10
		Public Property and Private Property	8
		Private Property	7

4.3. Standardizing Parameter Values for Factors and Reclassifying Factors

In this stage, a value ranging from 0 (least suitable for settlement) to 10 (most suitable for settlement) was assigned based on analyzing suitability to the factor parameters. Next, each factor parameter was standardized on a scale of 0 to 10 (see Table 1). These factors were then reclassified based on their standardized values and converted into raster maps (see Figure 4). This step ensures that the field analyses are reclassified based on a set standard for conformity analysis. Table 1 lists the standardization values of the parameters used in the ecologically focused settlement suitability analysis for the Bizim Şehir Project area.

The first analysis focused on the physical structure of the project area is soil capability. The site contained seventh and second-degree soil, classified as marginal agricultural land. Based on this information, a standardized soil capability analysis was conducted, with a high value of 8 assigned to the region with seventh-degree soil and a median value of 5 assigned to the area with second-degree soil.

It is crucial to thoroughly evaluate the geological structure of the ground in the project area, particularly regarding potential disaster risks during construction. As such, alluvial fans, one of the ground condition parameters in the area, were assigned a value of 5. Transition areas with high slopes were given a value of 3. Finally, to prevent settlements in areas with geological quarries (which pose a risk of rockfall) and in stream beds, a standardized value of 0, the lowest possible value, was assigned to the geological structure.

While standardizing natural disasters, the areas with very little erosion, such as secondary-degree erosion areas, are assigned the highest settlement value of 10. Conversely, the areas with severe erosion, such as fourth-degree erosion, are assigned a settlement value of 2. However, the Konya Fault line runs north-south within the study area, and construction is prohibited within the Fault Conservation Band established for this fault line. As a result, the standardization value for this field is taken as 0. Additionally, a 25-meter conservation band has been designated on both sides of the stream beds that may cause natural disasters like the flooding in the area. Since construction is not allowed within this band, the standardization value for the areas within the band lines has been set to 0.

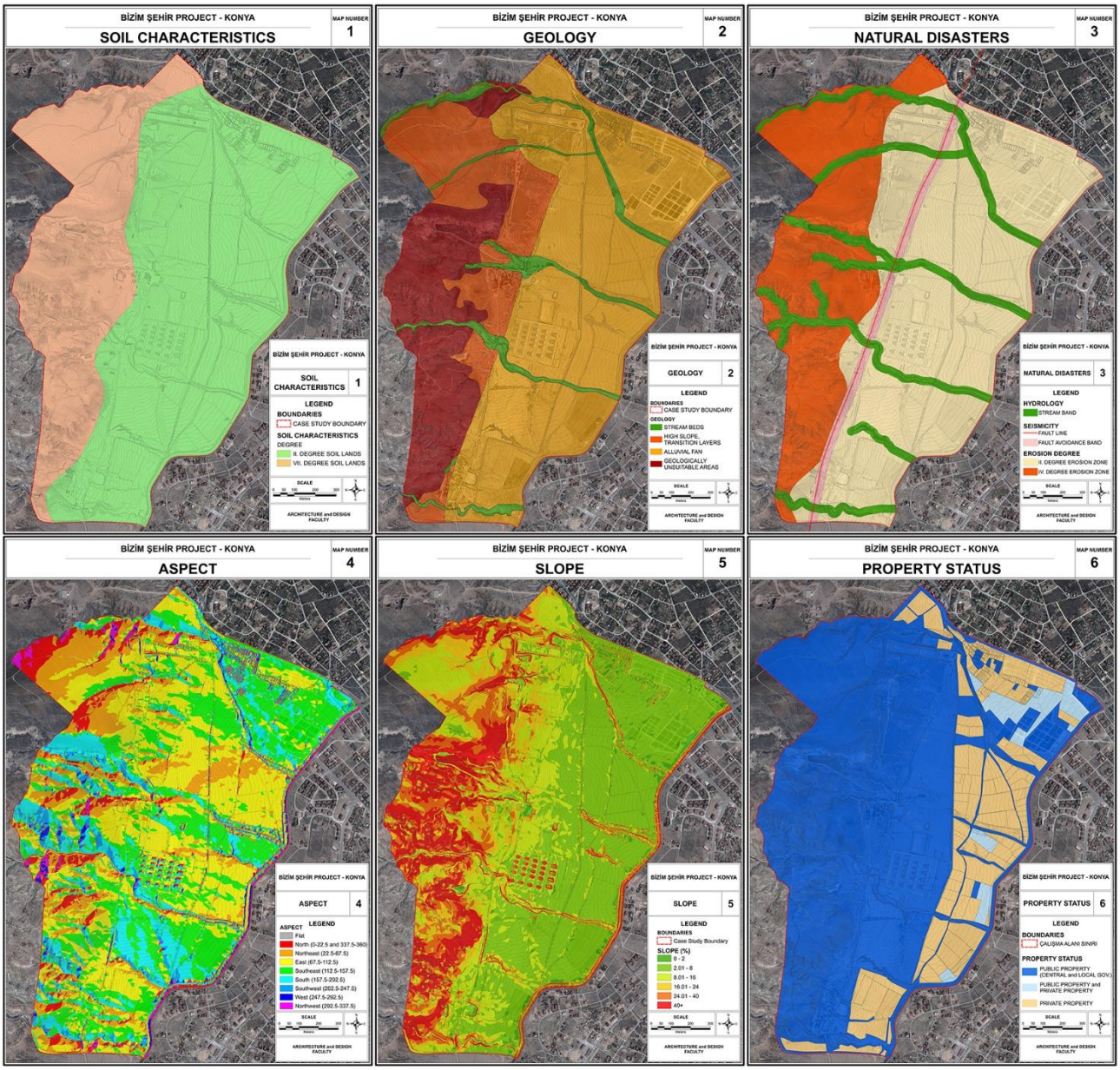

Figure 3. Factors evaluated for suitability analysis; 1) soil characteristics, 2) geology, 3) natural disasters, 4) aspect, 5) slope, 6) property status

In Türkiye, the south and southeast, southwest, east, and west directions (predominantly south and southeast) receive more sunlight and are warmer. Designing houses with these factors in mind can help reduce energy consumption and lower carbon footprint. The cooler fronts, such as the north, northwest, and northeast directions, receive less light, so it is vital to consider a location compatible with the climate to minimize energy dependence and maximize solar energy. Since the northern slopes have a low radiation level, they are not preferred. In a temperate climate, the upper parts of slopes facing southeast and east directions are suitable for settlement in harmony with the climate. To standardize the aspect analysis regarding the placement of residential areas in appropriate directions, the highest value of 10 is assigned to flat areas and areas facing south and southeast (S, SE) directions. The value of 8 is assigned to areas facing southwest and east (SW, E). The median value of 6 is assigned to areas facing the west (W) direction, and the lowest value of 4 is assigned to areas facing northwest and northeast (NW, NE). Finally, the lowest value of 2 is assigned to areas facing north (N).

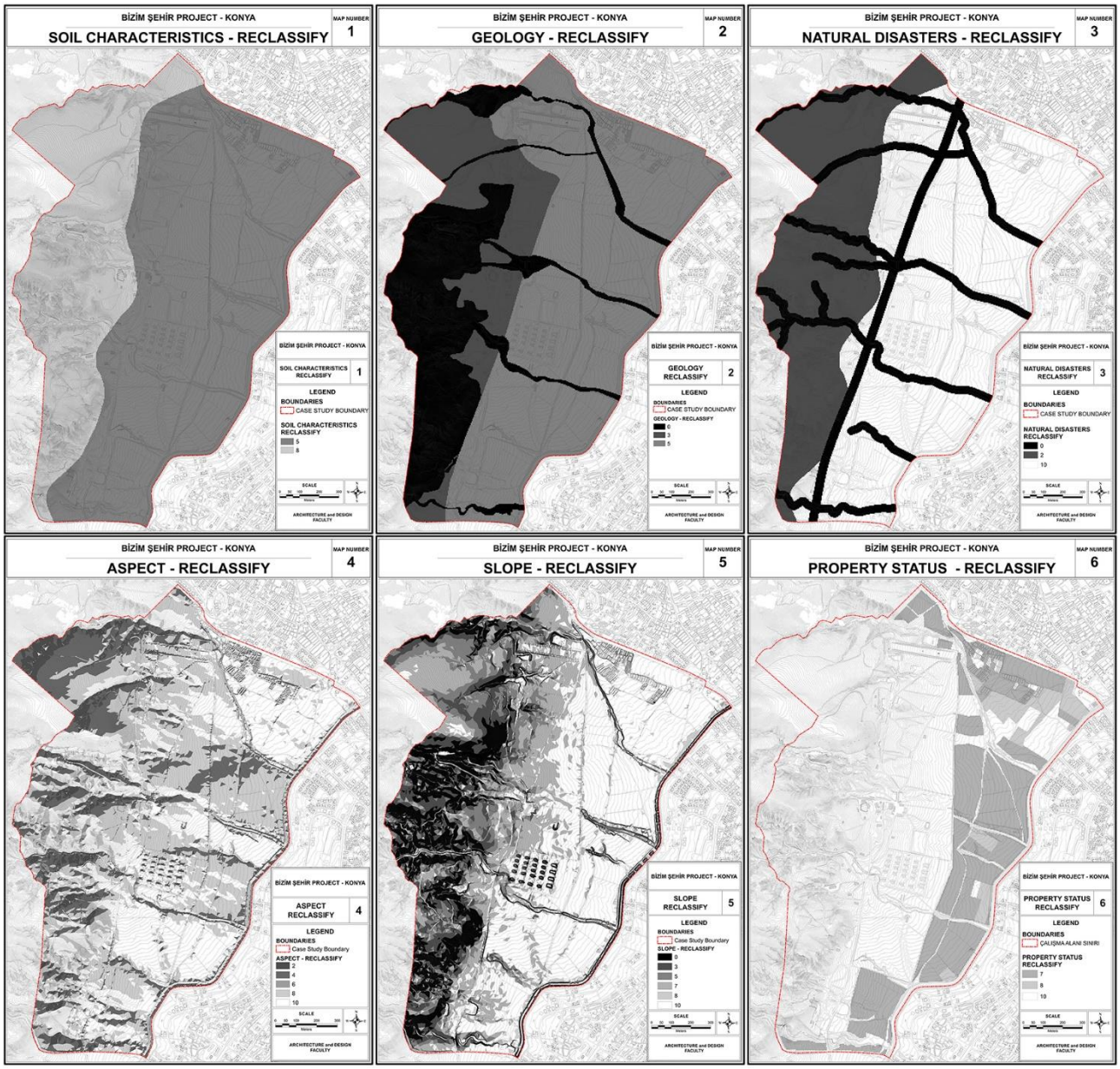

Figure 4. Reclassification of analysis parameters based on the given standardization value

When choosing locations for residential areas, it is essential to consider the slope. Therefore, a score of 8 is given to areas with a slope percentage between 0-2%, 10 for areas with a slope of 2-8%, 7 for areas with a slope of 8-16%, 5 for areas with a range of 16-24%, and 3 for fields in the range of 24-40%. For areas with a slope percentage over 40%, the score is 0. The slope analysis was standardized using these values. Finally, to standardize the property status analysis, the standardization value of public property is 10, the standardization value of public and privately owned property is 8, and the value of private property is 7, among the analysis parameters.

The standardization values of Soil Characteristics, Geology, Natural Disasters, Aspect, Slope, and Property Status analyses used within the scope of settlement suitability analysis are explained above. In addition, these analyzes were classified by the reclassification method, one of the spatial analyzes of geographic information systems. Thus, the values of the parameters of all analyzes were standardized between 0 and 10 (Figure 4).

4.4. Determination of Factor Weights in Line with the Purpose

In producing the suitability analysis, after the factor parameters are standardized, the factors should be integrated using the analysis infrastructure of the geographic information system. At this stage, in line with the suitability analysis's purpose, the factors' effects on the settlement suitability analysis were determined as percentages. These percentages were determined using the AHP method. The Bizim Şehir Project aims to determine the areas suitable for settlement with an ecological focus in line with the principle of sustainability. In

this context, the opinions of 14 experts who were informed about the purpose and vision of the project were taken. With a questionnaire prepared for the AHP method, experts were asked to compare the factors pairwise using Saaty's 1-9 ratio scale (Saaty, 1990). The pairwise comparison values of the experts for the factors were entered into a table, and the geometric average was taken (Ullah & Mansourian, 2016). Thus, a single pairwise value was obtained for each pairwise comparison of the factors, and the pairwise comparison matrix was created (Table 2). The Super Decision program was used for all calculations made within the scope of AHP.

When the weights of the factors constituting the conformity analysis with the AHP method are calculated, it is seen that natural disasters are the most critical factors, with a value of 38.2% (Table 2). After natural disasters, factor weights are listed as geological conditions (22.8%), soil characteristics (21.0%), slope analysis (7.5%), property analysis (5.6%) and aspect analysis (4.9%).

Table 2. The pairwise comparison matrix and Factors' Priorities

	Soil Characteristics	Geology	Natural Disasters	Aspect	Slope	Property Status
Soil Characteristics	1	1	1/2	4	3	4
Geology	1	1	1/2	5	3	5
Natural Disasters	2	2	1	7	5	6
Aspect	1/4	1/5	1/7	1	1/2	1
Slope	1/3	1/3	1/5	2	1	1
Property Status	1/4	1/5	1/6	1	1	1
FACTORS	**Soil Characteristics**	**Geology**	**Natural Disasters**	**Aspect**	**Slope**	**Property Status**
PRIORITIES	% 21.0	% 22.8	% 38.2	% 4.9	% 7.5	% 5.6
Consistency Ratio (CR)= % 0.8						

4.5. Creation of Suitability Analysis

The results of the suitability analysis can differ depending on the intended purpose or scenario. Therefore, the assigned values or weights of the objective-related factors play a decisive role in the analysis creation process. In the final stage of preparing the suitability analysis, standardized and reclassified factors and determined factor weights were integrated using spatial analyst tools like map algebra and raster calculator. Suitability analysis was then obtained by integrating factors based on their percentage weights (see Figure 5).

By utilizing Geographical Information Systems and the Analytic Hierarchy Process method, a multicriteria decision analysis method, the suitability values for settlement varied between 1.5 and 7.8. When evaluated in terms of sustainability, the threshold for settlement suitability was determined to be 5.5. Areas below the value of 5.5 were deemed unsuitable for settlement, while areas above 5.5 were deemed suitable (see Figure 5). These results indicated that 54.9% of the case area was suitable for development (200.9 ha), and 45.1% was unsuitable (165.1 ha). Analysis of the settlement suitability revealed that high slope areas, stream beds, and areas within the fault conservation band in the west of the project area were unsuitable for settlement. Conversely, areas to the east of the project area with a relatively low slope facing south, southeast, and east were suitable for settlement.

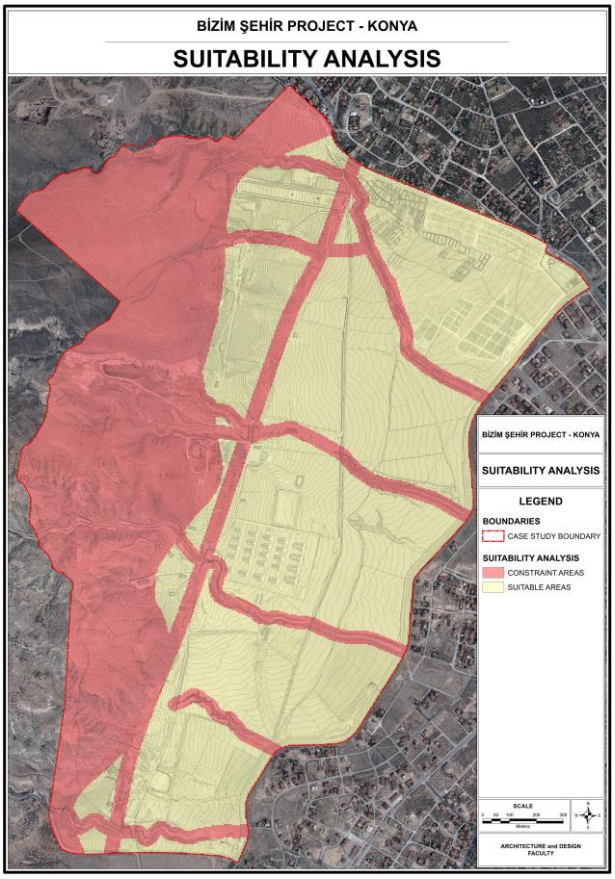

Figure 5. Suitability Analysis: reclassification of analysis parameters based on the given standardization value

5. CONCLUSIONS

Sustainable and livable human settlements can only be put forward with an objective planning approach. Therefore, analysis and synthesis studies, such as suitability analysis, play a crucial role in the success of the design process. The suitability analysis integrates multiple factors affecting construction based on specific weight values, minimizing resource waste in the urban development process. The spatial model generated by the suitability analysis provides decision-makers with a systematic integration of many factors, making each factor's effects visible. This approach enables decision-makers to make more accurate decisions. Within this framework, a suitability analysis based on GIS and AHP was conducted for the Bizim Şehir Project area. The suitability analysis showed that 54.9% of the Bizim City Project area is suitable for development/zoning.

The suitability analysis produced, based on GIS and AHP, provides insights into sustainable urban

development and highlights the limitations of the study area in terms of urban development. However, it is essential to remember that the settlement suitability analysis is not a result but a tool to increase the decision makers' capacity to make the right decision. The map obtained by the suitability analysis is not a plan but a synthesis created by integrating data that guides planning and design. Therefore, the relationship between the planned area and the rest of the city should be evaluated before making policy decisions regarding the planning area in line with the sustainability principle. Data on the socio-economic environment should also be analyzed using the correct methods. The planning process is a discipline that should include physical and technical actions and decisions with a strong social dimension. Therefore, the social dimension must not be ignored.

In the planning process of the city, a social phenomenon, it is not sufficient to analyze the physical structure of the planning area with a quantitative approach. Nevertheless, qualitative analyses are necessary to understand the lifestyles and cultures of people and society in the planning process. Also, involving the public in the planning process through participatory methods and identifying the needs and priorities of stakeholders is another critical component of making the right decision.

The suitability analysis conducted within the scope of the study was for the project area of Bizim Şehir, an urban design project. It is important as an example for future sustainable-oriented urban development projects. Additionally, the methodology used in the study can be used to identify suitable areas for different functions.

Acknowledgement

This study is based on the suitability analysis produced in the analysis and synthesis section of the urban development (urban design) project process named City 2023 Project (Bizim Şehir Konya). The project was prepared by Konya Technical University for the Ministry of Environment, Urbanization, and Climate Change.

Author contributions

S. Levend: He designed the research, collected the datasets, analyzed the data, and wrote;
M. A. Sağ: He designed and investigated the research and reviewed and edited the manuscript.

Conflicts of Interest

The authors declare no conflict of interest.

Declaration of research and publication ethics

In the study, the authors declare that there is no violation of research and publication ethics and that the ethics committee permission document of the study has been submitted to the journal.

REFERENCES

Aburas, M. M., Abdullah, S. H., Ramli, M. F., & Asha'ari, Z. H. (2017). Land suitability analysis of urban growth in Seremban Malaysia, using GIS based analytical hierarchy process. *Procedia engineering*, 198, pp. 1128-1136.

Akbulut, A., Ozcevik, O., & Carton, L. (2018). Evaluating suitability of a GIS–AHP combined method for sustainable urban and environmental planning in Beykoz district, Istanbul. *International Journal of Sustainable Development and Planning*, 13(8), pp. 1103–1115.

AlFanatseh, A. (2021). Land suitability analysis of urban development in the Aqaba area, Jordan, using a GIS-based analytic hierarchy process. *GeoJournal*, pp. 1-17.

Alkay, E. (2014). Giriş. In E. Alkay, *Şehir Planlamada Analiz ve Değerlendirme Teknikleri* (pp. 11-15). İstanbul: Literatür.

Al-Shalabi, M. A., Mansor, S. B., Ahmed, N. B., & Shiriff, R. (2006). GIS based multicriteria approaches to housing site suitability assessment. *XXIII FIG congress, shaping the change*, (pp. 8-13). Munich, Germany.

ArcGIS. (2023, 05 13). Site suitability analysis. ArcGIS: https://doc.arcgis.com/en/imagery/workflows/resources/site-suitability-analysis.htm

ArcGIS Pro. (2023, 05 13). The general suitability modeling workflow. ArcGIS Pro: https://pro.arcgis.com/en/pro-app/latest/help/analysis/spatial-analyst/suitability-modeler/the-general-suitability-modeling-workflow.htm

Aydemir, Ş. (1999). Planlama ve planlama Türleri. In Ş. Aydemir, *Kentsel Alanların Planlanması ve Tasarımı* (pp. 33-40). Trabzon: Akademi.

Bhushan, N., & Rai, K. (2007). *Strategic decision making: applying the analytic hierarchy process*. London: Springer.

Brundtland, G. H., & Khalid, M. (1987). *Our common future*. Oxford, GB: Oxford University Press.

Chandio, I. A., Matori, A. N., Yusof, K., Talpur, H. M., & Aminu, M. (2014). GIS-basedland suitability analysis of sustainable hillside development. *Procedia Engineering*, 77, pp. 87-94.

Çalışkan, O. (2017). Kentsel Tasarım. In S. S. Özdemir, Ö. B. Özdemir Sarı, & N. Uzun, *Kent Planlama* (pp. 387-428). Ankara: İmge.

Çubukçu, K. M. (2017). Kent Planlamada Nicel Teknikler. In S. S. Özdemir, Ö. B. Özdemir Sarı, & N. Uzun, *Kent planlama* (pp. 537-560). Ankara: İmge.

Deliry, S. I., & Uyguçgil, H. (2020). GIS-Based land suitability analysis for sustainable urban development: A case study in Eskisehir, Turkey. *Afyon Kocatepe Üniversitesi Fen ve Mühendislik Bilimleri Dergisi*, 20(4), pp. 634-650.

Dong, J., Zhuang, D., Xu, X., & Ying, L. (2008). Integrated evaluation of urban development suitability based on remote sensing and GIS techniques–a case study in Jingjinji Area, China. *Sensors*, 8(9), pp. 5975-5986.

Dunn, C. (2007). Participatory GIS—a people's GIS? *Progress in human geography*, 31(5), pp. 616-637.

Ersoy, M. (2007). Planlama Kuramına Giriş. In M. Ersoy, *Kentsel Planlama Kuramları* (pp. 9-34). Ankara: İmge.

Estoque, R. (2012). Analytic hierarchy process in geospatial analysis. In Y. Murayama, *Progress in geospatial analysis* (pp. 157-181). Springer: Springer.

Filipović, M. (2007). The analytic hierarchy process as a support for decision making. *Spatium*, pp. 44-59.

Healey, P. (2006). U*rban complexity and spatial strategies: Towards a relational planning for our times*. London: Routledge.

Johnston, K. M., & Graham, E. (2021). ArcGIS Spatial Analyst–Suitability Modeling. *Esri International User Conference* (pp. 1-67). California: Esri.

Keskinok, H. Ç. (2020). Farklı Kademelerde Bölge ve Kent Planlama. In M. Şenol Balaban, *Kent, Planlama ve Afet Risk Yönetimi* (pp. 28-57). Eskişehir: Anadolu Üniversitesi.

Koramaz, T. K. (2014). Uygunluk Analizi. In E. Alkay, *Şehir Planlamada Analiz ve Değerlendirme Teknikleri* (pp. 129-139). İstanbul: Literatür.

Kumar, A., Sharma, R. K., & Kuma, V. (2018). Landslide hazard zonation using analytical hierarchy process along National Highway-3 in mid Himalayas of Himachal Pradesh, India. *Environmental Earth Sciences*, 77(20), pp. 1-19.

Kumar, M., & Shaikh, V. R. (2013). Site suitability analysis for urban development using GIS based multicriteria evaluation technique. *Journal of the Indian Society of Remote Sensing*, 41(2), pp. 417-424.

Levend, S., & Fischer, T. B. (2022). Determining People's Design Priorities for Neighbourhood Units: A Study in Liverpool, Merseyside. *ICONARP International Journal of Architecture and Planning*, 10(1), pp. 21-42.

Luan, C., Liu, R., & Peng, S. (2021). Land-use suitability assessment for urban development using a GIS-based soft computing approach: A case study of Ili Valley, China. *Ecological Indicators*, 123, pp. 107333.

Malczewski, J. (2004). GIS-based land-use suitability analysis: a critical overview. *Progress in planning*, 62(1), pp. 3-65.

Malczewski, J. (2006). GIS-based multicriteria decision analysis: a survey of the literature. *International journal of geographical information science*, 20(7), pp. 703-726.

Malczewski, J., & Rinner, C. (2015). *Multicriteria decision analysis in geographic information science*. New York: Springer.

McBride, S. B. (2019). *Site Planning and Design*. West Virginia University. https://researchrepository.wvu.edu/rri-web-book/1

Mekânsal Planlar Yapım Yönetmeliği. (2014). *Mekânsal Planlar Yapım Yönetmeliği*. Ankara: Resmî Gazete (Sayı: 29030). https://www.resmigazete.gov.tr/eskiler/2014/06/20140614-2.htm

Okumuş, G. (2014). Planlamada Analiz Teknikleri ve Coğrafi Bilgi Sistemleri. In E. Alkay, *Şehir Planlamada Analiz ve Değerlendirme Teknikleri* (pp. 17-32). İstanbul: Literatür.

Özügül, M. D. (2012). Ekolojik planlama. In M. Ersoy, *Kentsel Planlama Ansiklopedik Sözlük* (pp. 107-112). İstanbul: Ninova.

Parry, J. A., Ganaie, S. A., & Bhat, S. M. (2018). GIS based land suitability analysis using AHP model for urban services planning in Srinagar and Jammu urban centers of J&K, India. *Journal of Urban Management*, 7(2), pp. 46-56.

Saaty, T. (1989). Group decision making and the AHP. In T. Saaty, *The Analytic Hierarchy Process* (pp. 59-67). Berlin: Springer.

Saaty, T. (1990). How to make a decision: the analytic hierarchy process. *European journal of operational research*, 48(1), pp. 9-26.

Saaty, T. (2008). Decision Making With The Analytic Hierarchy Process. *International Journal of Services Sciences*, 1(1), pp. 83-98.

Saaty, T., & Vargas, L. (2012). *Models, methods, concepts & applications of the analytic hierarchy process*. London: Springer Science & Business Media.

Saha, A., & Roy, R. (2021). An integrated approach to identify suitable areas for built-up development using GIS-based multi-criteria analysis and AHP in Siliguri planning area, India. *SN Applied Sciences*, 3(4), pp. 1-17.

Şahin, S. Z. (2020). Planlamada Yerel Yönetimlerin Sorumlulukları. In M. Şenol Balaban, *Kent, Planlama ve Afet Risk Yönetimi* (pp. 56-85). Eskişehir: Anadolu Üniversitesi.

Tekel, A., & Altıntaş, Y. (2011). Türk İmar Mevzuatı'nda Tanımlanan Plan Türleri ve Yetkili Kurumlar. In Ç. Varol, A. Gürel Üçer, & A. Uğurlar, *Yasal ve Yönetsel Boyutlarıyla Planlama* (pp. 79-91). Ankara: BİB.

Ullah , K. M., & Mansourian, A. (2016). Evaluation of land suitability for urban land-use planning: case study Dhaka City. *Transactions in GIS*, 20(1), pp. 20-37.

Araştırma Makalesi/Research Article
https://doi.org/10.51489/tuzal.1301462

2023; 5(1); 27-32

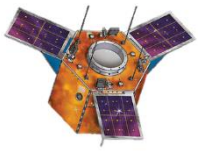

Turkish Journal of Remote Sensing

https://dergipark.org.tr/en/pub/tuzal

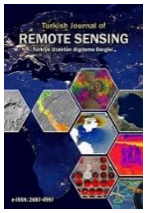

e-ISSN 2687-4997

Mühendislik Yapılarında Meydana Gelen Deformasyonların Daimi Yansıtıcı İnterferometre Tekniği ile İzlenmesi: Samsun 19 Mayıs Stadyumu Örneği

Sefa Yalvaç*[1]

[1]Gümüşhane Üniversitesi Mühendislik ve Doğa Bilimleri Fakültesi, Harita Mühendisliği Bölümü, Gümüşhane, Türkiye

Anahtar Kelimeler:
Daimi Yansıtıcı interferometre
Deformasyon analizi
Samsun 19 Mayıs Stadyumu
Yapay Açıklıklı Radar

ÖZ

Mühendislik yapılarındaki olası deformasyonların izlenmesi, yapısal bütünlük, güvenlik ve maddi kaynakların korunumu için önemli etkileri olabilecek kritik bir konudur. Bu deformasyonların zamanında, doğru ve etkili bir jeodezik yöntemle izlenmesi can ve mal kayıplarının önüne geçilmesinde hayati önem taşımaktadır. Bu kapsamda daimi yansıtıcı interferometre (PSI) tekniği geniş alansal izleme kabiliyeti, yüksek çözünürlükte santimetre altı doğruluk sunması, kısa geçiş süresi ile mühendislik yapılarındaki deformasyonların izlenmesinde güçlü bir jeodezik teknik olarak öne çıkmaktadır. Bu çalışmada, Samsun 19 Mayıs stadyumu ve yakın çevresinde meydana gelen deformasyonları araştırılmıştır. Bu amaçla, Sentinel 1 uydu misyonuna ait 2021 ile 2023 yılları arasını kapsayan 25 SAR görüntüsü elde edilerek daimi yansıtıcı interferometre (PSI) tekniğiyle analiz edilmiştir. Analizlerde, interferogramların üretilmesi aşaması için SNAP (Sentinel Application Platform) yazılımı, daimi yansıtıcı noktaların üretilerek zaman serilerinin oluşturulmasında ise açık kaynak kodlu StaMPS (Stanford Method for Persistent Scatterers) yazılımına başvurulmuştur. Analiz sonuçlarına göre, stadyum alanı üzerinde yıllık hızı 5-10 mm arasında değişkenlik gösteren çökme ve yükselme yönlü deformasyonlar tespit edilirken, stadyum yapısı dışında herhangi bir deformasyon tespit edilememiştir.

Monitoring of Deformation in Engineering Structures with PSI (Persistent Scatter Interferometry) Technique: The Example of Samsun 19 Mayıs Stadium

Keywords:
Persistent Scatter Interferometry
Deformation analyse
Samsun 19 Mayıs Stadium
Synthetic Aperture Radar

ABSTRACT

Monitoring possible deformations in engineering structures is a critical issue that can have significant implications for structural integrity, safety, and conservation of material resources. Timely, accurate, and effective monitoring of these deformations with a geodetic method is of vital importance in preventing loss of life and property. In this context, the Persistent Scatter Interferometry (PSI) technique stands out as a powerful geodetic technique for the monitoring deformations in engineering structures, offering wide-area coverage, high spatial resolution, and frequent revisits in sub-cm accuracy. In this study, the deformations of Samsun 19 Mayıs stadium and its nearest vicinity were investigated. To accomplish this, 25 SAR images of the Sentinel 1 satellite mission, covering the years 2021 to 2023 were obtained and analyzed through the Persistent Scatter Interferometry (PSI) technique. In the analysis, SNAP (Sentinel Application Platform) software was used for the creation of the interferograms, and the open source software StaMPS (Stanford Method for Persistent Scatterers) was used to generate the time series by producing the Persistent Scatter (PS) points. According to the results of the analysis, different directional deformations with annual velocity ranging between 5-10 mm were detected inside the stadium area, but no deformation was detected outside the stadium structure.

Makale Bilgileri/Article Info

Geliş /Received: 23/05/2023
Kabul/Accepted: 09/06/2023
Yayınlanma/Published: 30/06/2023

Alıntı/Citation:

Yalvaç, S. (2023). Mühendislik Yapılarında Meydana Gelen Deformasyonların Daimi Yansıtıcı İnterferometre Tekniği ile İzlenmesi: Samsun 19 Mayıs Stadyumu Örneği. Türkiye Uzaktan Algılama Dergisi , 5 (1) , 27-32 .

***Sorumlu Yazar/Corresponding Author:** Sefa Yalvaç, sefayalvac@gmail.com, +90 456 233 10 00 (1718)

1. GİRİŞ

Mühendislik yapılarındaki deformasyonların izlenmesi, insan eliyle tesisi yapılmış büyük mühendislik yapılarının güvenliğini ve stabilitesini sağlamak açısından yer bilimleri için oldukça önemli bir konudur. Mühendislik ölçmeleri ile yer kabuğunda ve mühendislik yapılarında zaman içerisinde meydana gelen değişimlerin yapılacak olan ölçümlerle belirlenip yorumlanması, ortaya çıkabilecek ciddi zararların önlenmesinde de etkin bir role sahip olacaktır. Bu amaçla, yıllar içinde teknolojinin imkan verdiği farklı noktasal ve alansal bazlı izleme tekniklerine başvurulmuştur.

Söz konusu teknikleri klasik yersel yöntemler ve uzay bazlı yöntemler olarak ikiye ayırmak mümkündür. Deformasyon ölçmeleri çalışmaları 1990'lı yıllara kadar doğrultu-kenar ağları ve nivelman gibi klasik yersel yöntemlerle yürütülmüştür (Poland, 1984). Daha sonraki yıllarda, uydu jeodezisinin etkin bir biçimde kullanılmasıyla birlikte, görece düşük hassasiyetli ve zaman, maliyet açısından oldukça büyük yükler getiren klasik yöntemler yerini her türlü hava koşulunda, 3-boyutlu ve yüksek hassasiyette nokta konum doğruluğu sunan GNSS (Global navigation Satellite Systems) yöntemine bırakmıştır (Feigl ve ark., 1993, Abidin ve ark., 2008, Ustun ve ark., 2010). GNSS yönteminin noktasal bazlı izleme kabiliyeti ve arazi çalışmaları sebebiyle, ekstra maliyet ve zaman gereksinimi kısıtlayıcı birer etki olarak göründüğünden araştırmacıları LIDAR, InSAR (Interferometric Synthetic Aperture Radar) gibi uzaktan algılama yöntemlerini kullanmaya yöneltmiştir (Baer ve ark., 2002, Schmidt ve Bürgmann, 2003). Bu yöntemlerden InSAR yöntemi ücretsiz veri erişimi, arazi çalışması gerektir-memesi, geçmişe dönük zengin arşiv verisi ile cm altı seviyelerde alansal izleme kabiliyetine sahip olması sebepleriyle son yıllarda deformasyon ölçmelerinde sıklıkla tercih edilen bir jeodezik izleme tekniği olarak karşımıza çıkmaktadır (Yalvac, 2020).

Geleneksel InSAR tekniği, iki SAR imajı arasındaki faz farklarından yararlanarak, geniş alanlarda deformasyonların belirlenmesine imkan tanıyan bir uzaktan algılama tekniğidir. Ancak, bu teknikte doğruluk ve deformasyonların izlenebilirliği geometrik ve zamansal uyuşumsuzluklar ve atmosferik etkilere bağlı olarak değişkendir (Bürgmann vd., 2000). Dahası, uzun zamansal süreçlere yayılan deformasyonların bu teknikle sağlıklı olarak izlenmesi de mümkün olmamaktadır. Bu kısıtlamaların ortadan kaldırılması için SBAS (en kısa baz interferometresi) ve PSI (daimi yansıtıcı interferometre) gibi ileri seviye SAR analiz tekniklerine başvurulur (Ferretti vd., 2001; Berardino vd., 2002; Hooper vd., 2004). Bu teknikler sayesinde yüzey deformasyonlarının izlenmesinde doğruluk birkaç mm seviyelerine kadar düşmekte ve uzun zamansal süreçlere yayılan deformasyonların davranışı zaman serileri ile belirlenebilmektedir.

PSI tekniği, mühendislik yapılarının doğal bir reflektör ve daimi yansıtıcı nokta (PS noktaları) özelliği göstermesinden dolayı, özellikle mühendislik yapılarındaki deformasyonların belirlenmesinde sıklıkla tercih edildiği görülmektedir. Literatür incelendiğinde, Ezquerro vd., (2020) tarafından zemin deformasyonu görülen bölgelerdeki yapılarda deformasyon analizlerinin PSI tekniği ile ortaya konulduğu, Bayik ve Abdikan (2021) tarafından Ordu-Giresun havaalanındaki deformasyonların yine PSI tekniği ile kestirildiği ve cm altı seviyelerdeki deformasyonların varlığının tespit edildiği ve Othman vd., (2019) tarafından Musul baraj kretindeki deformasyonların yine PSI tekniği ile başarıyla izlenebildiği görülmektedir.

Bu çalışmada, son günlerde yerel medyada Samsun 19 Mayıs stadı yapısında oluşan deformasyonlara ilişkin haberler üzerine söz konusu yapıdaki deformasyonların araştırılması gerekliliği ortaya çıkmıştır (URL-1). Bu kapsamda, izleme bölgesinin Avrupa Uzay Ajansına (ESA) ait Sentinel 1 uydu misyonunu verileri, Ocak 2021 ile Ocak 2023 yılları aralığında her ay için SAR görüntüsü (toplam 25 adet) elde edilerek PSI tekniğiyle analiz edilmiş ve yapıdaki deformasyonların varlığı araştırılmıştır.

2. YÖNTEM

Bu bölümde, çalışma bölgesi olan Samsun 19 Mayıs Stadyumu ve bölgenin izlenmesindekullanılanacak olan veri seti ve PSI yöntemiyle yapılacak analizler hakkında detaylı bilgi verilecektir.

2.1. Çalışma Bölgesi

Çalışma alanı olarak seçilen, Samsun 19 Mayıs stadyumu Samsun ilinin Tekkeköy ilçesine konumlanmaktadır. 2017 yılında Toplu Konut İdaresi tarafından yaptırılan stadyum, 137.700 m^2 alan üzerinde kurulu olup, 50.000 m^2'lik kısmı tribünleri oluşturmakta ve geri kalan kısmı otopark, yeşil alan ve alışveriş merkezlerinden oluşmaktadır (URL-2). Stadyumun bulunduğu alanı gösteren harita ve Google Earth yazılımından elde edilen uydu görüntüsü Şekil 1'de sunulmuştur. Yerel gazetelerde yayınlanan, yapı içerisinde oluşan çeşitli çatlak ve açılmaları gösteren fotoğraflar ise Şekil 2'de sunulmaktadır.

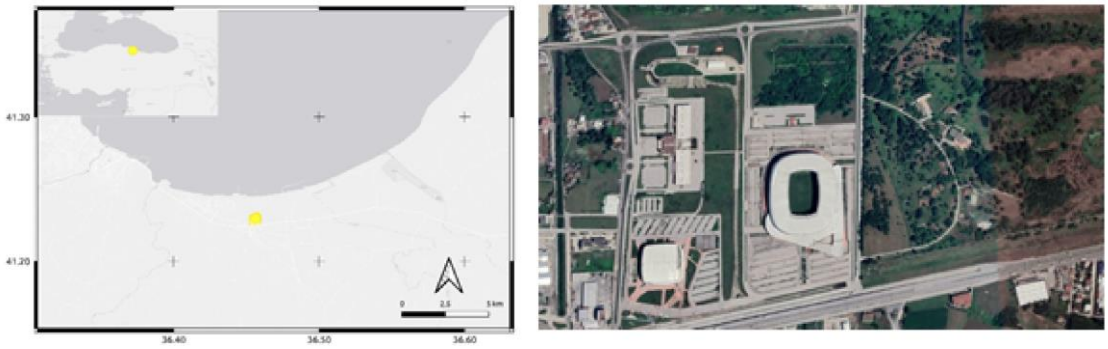

Şekil 1. Çalışma bölgesi ve uydu görüntüsü

2.2. Veri Seti ve Daimi Yansıtıcı İnterferometre (PSI) Analizleri

Söz konusu alandaki olası deformasyonların incelenmesi için yapılan görüntü arşivi çalışmalarında, ücretsiz olması, kısa tekrarlılık süresi ve cm altı hassasiyette izleme yeteneğine sahip, Avrupa Uzay Ajansı (ESA) tarafından yürütülen Sentinel 1 uydu misyonuna ait görüntülerden yararlanılmıştır. Sentinel uydu misyonunun görüntülerine ilişkin özellikler Tablo 1'de verilmiştir.

Şekil 2. Yerel gazetede yayınlanan, Samsun 19 Mayıs stadyumu yapısında oluşan çatlaklar ve açılmaları gösteren fotoğraflar (URL-1)

Tablo 1. İzleme çalışmasında kullanılacak Sentinel-1 uydu görüntülerine ait bilgiler

Özellik	Değer
Gözlem modu	IW
Yörünge yüksekliği	698 km
Tekrar geçiş süresi	12 gün
Frekans	5.3 GHz
Bant	C
Dalga boyu	5.7
Polarizasyon	HH+HV, VV, VH
Bakış açısı	20°-45°
Tarama genişliği	250 km x 250 km
Çözünürlük	5 m x 20 m

Çalışma bölgesini izlemek amacıyla, Ocak 2021 ile Ocak 2023 tarihleri arasında (2 yıl) birer ay aralıklarla seçilen 25 SAR imajı Sentinel SciHub'dan elde edilmiştir (URL-3). Bu görüntüler, SLC (Single Look Complex) modunda, alçalan modda ve 116 numaralı rölatif uydu yörüngesine aittir. Bilgisayar donanımından ve zamandan tasarruf etmek amacıyla, görüntüler çalışma alanı olan stadyum ve yakın çevresini kapsayacak şekilde kırpılmıştır. Bu kapsamda 116 numaralı çerçevenin, VV polarizasyonlu IW2 alt çerçevesine ait 5 ve 6 numaralı yanal şeritler (burst) analizlerde kullanılmıştır. 116 yörünge numaralı çerçevenin kapsama alanı ve analizlerin gerçekleştirileceği kırpılma alanı Şekil 3'de gösterilmektedir.

Şekil 3. Çalışma bölgesini kapsayan ana çerçeve (1) ve çalışma çerçevesi (2)

Daimi yansıtıcı interferometre analizleri iki temel aşamada gerçekleştirilmiştir. Bu aşamalardan ilki master imaj seçimi sonrası, SNAP (The Sentinel Application Platform) yazılımı yardımıyla interferogramların üretilmesidir. Bu aşamada, yapılan zamansal ve bazsal uzunluk parametreleri göz önünde bulundurularak 10.04.2022 tarihinde algılanan görüntü birincil (master) olarak seçilmiştir. Diğer 24 görüntü ise ikincil (slave) görüntü olarak kabul edilerek SNAP yazılımında interferogramların üretilmesi sağlanmıştır. İkincil görüntülerin, birincil görüntüye göre zamansal ve baz uzunluğu olarak dağılımı Şekil 4'de gösterilmektedir.

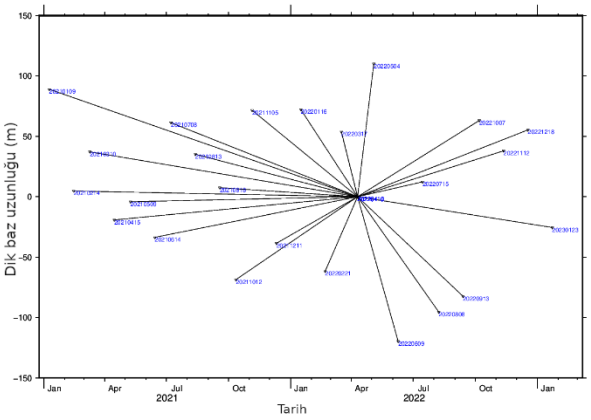

Şekil 4. Yardımcı görüntülerin, master görüntüye göre zamansal ve bazsal durumunu gösteren grafik

İkinci aşamada ise, SNAP yazılımında üretilen interferogramlar StaMPS (Stanford Method for Persistent Scatterers) yazılımı için dışa aktarılmış ve açık kaynak kodlu StaMPS V4.1b1 yazılımı yardımıyla analiz edilmiştir. Analizlerde DEM (Digital Elevation Model) hataları düzeltilerek unwrap işlemi gerçekleştirilmiştir. PS noktaları ve her PS noktasına ait uydunun bakış doğrultusundaki uzunluk değişimleri esas alınarak, noktalarına ait her görüntü tarihi için deformasyon zaman serileri üretilmiştir.

3. ANALİZ SONUÇLARI VE TARTIŞMA

Daimi yansıtıcı interferometre analizleri kapsamında çalışma alanı olan Samsun 19 Mayıs stadyumu yapısı ve yakın çevresinde çok sayıda PS noktası (daimi yansıtıcı noktalar) üretilmiştir. PSI tekniğinin doğasına uygun olarak söz konusu noktalar insan yapımı yansıtıcılığı yüksek objeler üzerinde konumlanmış olup, stadyumun doğu bölgesindeki ağaçlık alanda PS noktası üretilememiştir. PS noktaların çalışma bölgesi ve yakın çevresine dağılımı Şekil 5'de gösterilmektedir.

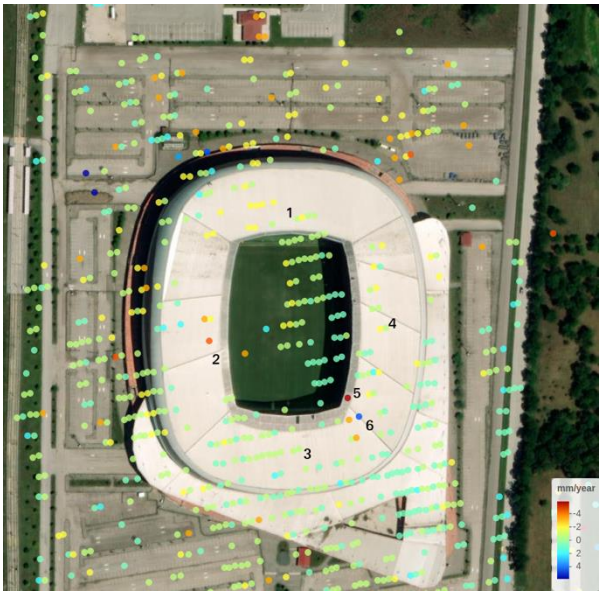

Şekil 5. PS noktalarının çalışma bölgesine dağılımı ve zaman serisi üretilen PS noktaları (1-6)

Şekil 5'de verilen deformasyon hız ölçeğinden, bölgedeki deformasyonların yıllık hızının -5 mm/yıl ile +5 mm/yıl arasında değişiklik gösterdiği anlaşılmaktadır. PS noktalarındaki deformasyon değerlerine ait standart sapmalar, StaMPS yazılımından elde edilmiş ve 0.35 mm ile 1 mm arasında değişiklik gösterdiği görülmüştür.

Yapı üzerindeki deformasyonlar detaylı incelendiğinde, stadyum alanı dışında herhangi bir deformasyon olmadığı görülmektedir. Stadyum üzerindeki noktalar incelendiğinde, yapının Kuzey, Güney ve Doğu bölümünde (1, 3 ve 4 numaralı PS noktaları) yaklaşık olarak sabit olduğu görülmektedir. Stadyumun Batı bölümünde (2 numaralı PS noktası) ise -3 ila -5 mm/yıl seviyelerinde çökme hareketi olduğu görülmüştür. Son olarak yapının Güneydoğu bölgesinde (5 ve 6 numaralı PS noktaları) ise yıllık hızı 5 mm'ye varan yükselme ve çökme hareketleri birlikte görülmektedir. Söz konusu bölgelerdeki radarın bakış doğrultusundaki yer değiştirmelerin zamanla değişimini incelemek üzere, izleme zamanı boyunca zaman serileri üretilmiş ve Şekil 6'da sunulmuştur.

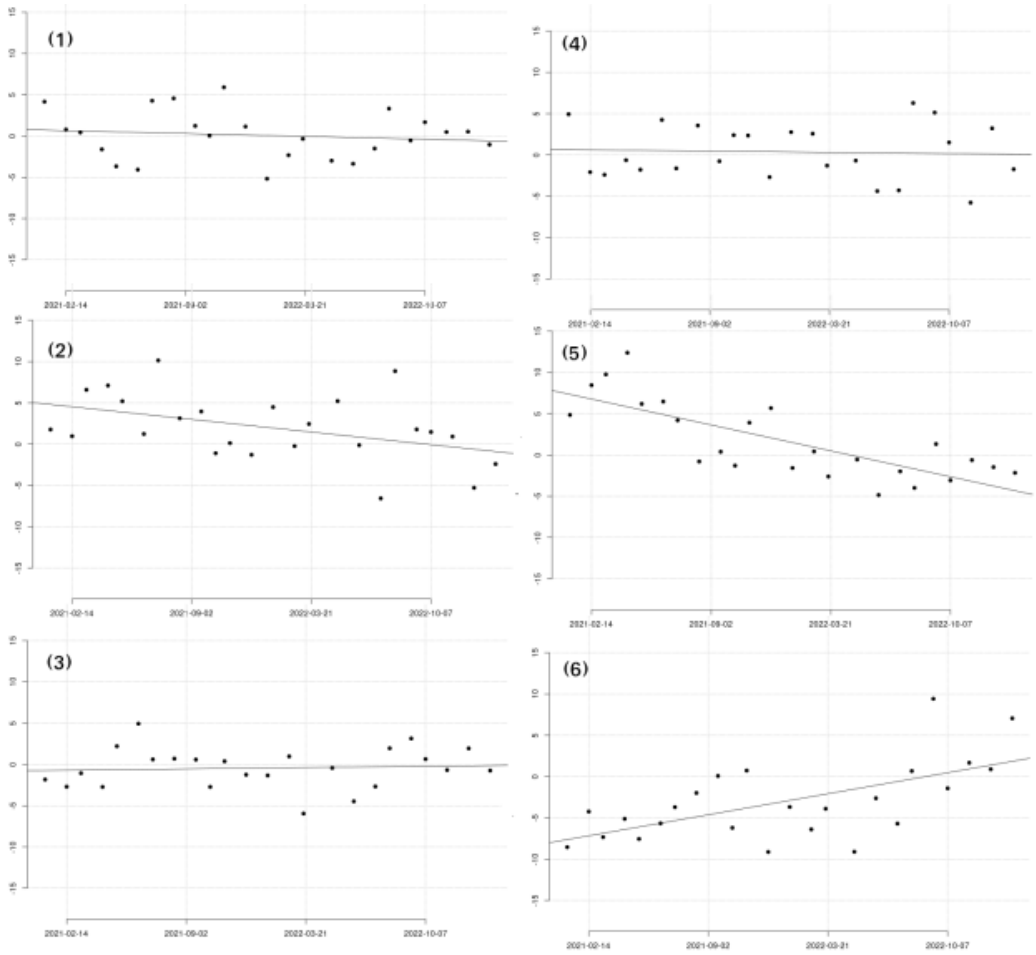

Şekil 6. Şekil 5'de gösterilen 1-6 numaralı bölgelerde yer alan PS noktalarına ait zaman serileri

Şekil 6 incelendiğinde, 1, 3 ve 4 numaralı PS noktalarında doğrusal eğilim olmadığı ve uydunun bakış doğrultusundaki değişimlerin yaklaşık sıfır mm etrafına rastgele saçıldığı görülmektedir. Diğer taraftan, 2, 5 ve 6 numaralı PS noktalarında izleme süresi boyunca negatif ya da pozitif yönlü eğilim oluştuğu, yani deformasyona maruz kaldığı görülmektedir. Ayrıca, söz konusu deformasyonların izleme süresi boyunca doğrusal olarak oluştuğu, ani olarak gelişmediği anlaşılmaktadır.

4. SONUÇ VE ÖNERİLER

Bu çalışmada, Samsun 19 Mayıs stadyumu yapısı üzerinde oluşan deformasyonlar ilk defa daimi yansıtıcı interferometre tekniğiyle izlenmiş ve çalışma bölgesinin farklı noktalarında deformasyon zaman serileri üretilmiştir. Analiz sonuçları değerlendirildiğinde, stadyum yapısı dışında yer alan yapılarda deformasyon tespit edilmezken, stadyum yapısı üzerinde yıllık hızı -5 mm ile +5 mm seviyelerinde değişen deformasyonlar olduğu görülmüştür. Söz konusu deformasyonlara ait standart sapmaların 0.35 mm ile 1 mm arasında olduğu göz önünde bulundurulduğunda anlamlı yer değiştirmeler olduğu düşünülmektedir. Deformasyon gözlenen noktalardaki zaman serilerinden anlaşılacağı üzere deformasyonların gelişimi, izleme süresine yayılmış bir biçimde kademeli olarak gelişmiştir. Bu kapsamda, deformasyonların söz konusu bölgedeki, zemin özelliklerinden kaynaklanabileceği düşünülmektedir.

Mühendislik yapıları üzerinde böylesi düzensiz yer değiştirmeler yapı ömrünü kısaltmakla birlikte, zamana bağlı olarak yapının zarar görmesine neden olabilmektedir. Bu kapsamda, stadyum yapısı üzerinde özellikle Güneydoğu bölgesinde tespit edilen düzensiz yönlü deformasyonlar uzun zamansal ölçekte yapının zarar görmesiyle sonuçlanabilir. Bu nedenle, çalışma bölgesinin ilerleyen zamanlarda da yüzey deformasyonlarının gelişimine karşı, daha fazla sayıda uydu görüntüsü ve yersel yöntemlerle de desteklenerek daha detaylı olarak izlenmesi gerekliliğini ortaya çıkarmaktadır.

Araştırmacıların katkı oranı beyan özeti

Yazar makaleye %100 oranında katkı sağlamıştır.

Çıkar çatışması beyanı

Makale ile ilgili olarak, herhangi bir kurum, kuruluş, kişi ile mali çıkar çatışması yoktur ve yazarlar arasında çıkar çatışması bulunmamaktadır.

Araştırma ve yayın etiği beyanı

Yapılan çalışmada yazar, araştırma ve yayın etiğine aykırı bir durum olmadığını ve çalışmanın etik kurul izni gerektirmediğini beyan etmektedir.

KAYNAKÇA

Abidin, H. Z., Andreas, H., Djaja, R., Darmawan, D., & Gamal, M. (2008). Land subsidence characteristics of Jakarta between 1997 and 2005, as estimated using GPS surveys. *Gps Solutions*, *12*, 23-32.

Baer, G., Schattner, U., Wachs, D., Sandwell, D., Wdowinski, S., & Frydman, S. (2002). The lowest place on Earth is subsiding—An InSAR (interferometric synthetic aperture radar) perspective. Geological Society of America Bulletin, 114(1), 12-23.

Bayik, C., & Abdikan, S. (2021). Monitoring of small-scale deformation at sea-filled Ordu-Giresun Airport, Turkey from multi-temporal SAR data. Engineering Failure Analysis, 130, 105738.

Berardino, P., Fornaro, G., Lanari, R., & Sansosti, E. (2002). A new algorithm for surface deformation monitoring based on small baseline differential SAR interferograms. IEEE Transactions on geoscience and remote sensing, 40(11), 2375-2383.

Bürgmann, R., Rosen, P. A., & Fielding, E. J. (2000). Synthetic aperture radar interferometry to measure Earth's surface topography and its deformation. Annual review of earth and planetary sciences, 28(1), 169-209.

Ezquerro, P., Del Soldato, M., Solari, L., Tomás, R., Raspini, F., Ceccatelli, M., ... & Herrera, G. (2020). Vulnerability assessment of buildings due to land subsidence using InSAR data in the ancient historical city of Pistoia (Italy). Sensors, 20(10), 2749.

Feigl, K. L., Agnew, D. C., Bock, Y., Dong, D., Donnellan, A., Hager, B. H., ... & Webb, F. H. (1993). Space geodetic measurement of crustal deformation in central and southern California, 1984–1992. *Journal of Geophysical Research: Solid Earth*, *98*(B12), 21677-21712.

Ferretti, A., Prati, C., & Rocca, F. (2001). Permanent scatterers in SAR interferometry. IEEE Transactions on geoscience and remote sensing, 39(1), 8-20.

Hooper, A., Zebker, H., Segall, P., & Kampes, B. (2004). A new method for measuring deformation on volcanoes and other natural terrains using InSAR persistent scatterers. Geophysical research letters, 31(23).

Othman, A. A., Al-Maamar, A. F., Al-Manmi, D. A. M., Liesenberg, V., Hasan, S. E., Al-Saady, Y. I., ... & Khwedim, K. (2019). Application of DInSAR-PSI technology for deformation monitoring of the Mosul dam, Iraq. Remote Sensing, 11(22), 2632.

Poland, J. F. (1984). Guidebook to studies of land subsidence due to ground-water withdrawal.

Schmidt, D. A., & Bürgmann, R. (2003). Time-dependent land uplift and subsidence in the Santa Clara valley, California, from a large interferometric synthetic aperture radar data set. Journal of Geophysical Research: Solid Earth, 108(B9).

Ustun, A., Tusat, E., & Yalvac, S. (2010). Preliminary results of land subsidence monitoring project in Konya Closed Basin between 2006–2009 by means of GNSS observations. Natural Hazards and Earth System Sciences, 10(6), 1151-1157.

Yalvac, S. (2020). Validating InSAR-SBAS results by means of different GNSS analysis techniques in medium-and high-grade deformation areas. Environmental monitoring and assessment, 192(2), 120.

URL-1:
https://www.gazeteduvar.com.tr/samsun-19-mayis-stadyumundaki-catlaklar-sosyal-medyada-gundem-oldu-galeri-1604690
[Erişim Tarihi: 10.05.2023]

URL-2:
https://tr.wikipedia.org/wiki/Samsun_19_May%C4%B1s_Stadyumu
[Erişim Tarihi: 10.05.2023]

URL-3:
https://scihub.copernicus.eu/
[Erişim Tarihi: 01.04.2023]

Araştırma Makalesi/Research Article
https://doi.org/10.51489/tuzal.1300531

2023; 5(1); 33-49

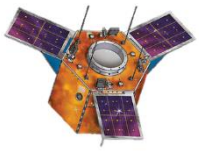

Turkish Journal of Remote Sensing

https://dergipark.org.tr/en/pub/tuzal

e-ISSN 2687-4997

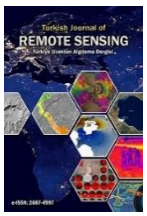

Measuring the Vulnerability of the Urban Fabric in the Face of Land Subsidence (Case Study: District 17 of Tehran)

Ramin Rezaeishahabi*[1], Alireza Arab [2], Amir Pishva[2] Vahid Hajipour[3], Marzieh Zahaki[2]

[1]Art University of Isfahan, Isfahan, Iran
[2]Kharazmi University, Tehran, Iran
[3]Islamic Azad University of Tabriz, Tabriz, Iran

Keywords
Land subsidence
Urban context
Vulnerability
Network analysis (ANP)
17th district of Tehran

ABSTRACT

The involvement of the 17th district of Tehran with the issue of land subsidence was the initial idea of the current research. The current research was conducted in the form of an analytical model in four steps. In the first step, after studying the research literature, the vulnerability indicators of the urban fabric were identified and organized into three criteria (physical and demographic, accessibility and proximity to high risk centers). In the second step, by using Delphi questionnaires and pairwise statistical comparisons, the priorities of vulnerability of the urban fabric in the face of land subsidence were determined. In the third step, the analytical model was defined based on the network analysis process (ANP). Also, the weight of each of the sub-criteria and criteria was obtained using Super Decision software. Finally, in the fourth step, these weights were applied to each of the layers related to the criteria in the ArcGIS software environment, and the final map of the vulnerability of the urban fabric was obtained as a raster in the geographic information system. The results of the model implementation showed that the urban fabric of the 17th district is prone to high vulnerability due to features such as high population and building density, the presence of worn-out fabric, buildings with low structural strength and very low construction quality. In total, about 657 hectares (80%) of the total built-up lands of Tehran's 17th district are under the influence of land subsidence.

Arazi çökmesi karşısında kentsel dokunun kırılganlığının ölçülmesi (Örnek olay: Tahran'ın 17. Bölgesi)

Anahtar Kelimeler:
Zemin çökmesi
Kentsel bağlam
Hasar görebilirlik
Ağ analizi (ANP)
Tahran'ın 17. bölgesi

ÖZ

Tahran'ın 17. bölgesinin arazi çökmesi sorununa dahil edilmesi, mevcut araştırmanın ilk fikriydi. Mevcut araştırma analitik model şeklinde dört adımda gerçekleştirilmiştir. İlk adımda, araştırma literatürü incelendikten sonra, kentsel bağlamın savunmasızlık göstergeleri belirlendi ve üç kriter (fiziksel ve demografik, erişilebilirlik ve yüksek riskli merkezlere yakınlık) halinde düzenlendi. İkinci adımda, Delphi anketleri ve ikili istatistiksel karşılaştırmalar kullanılarak, arazi çökmesi karşısında kentsel dokunun kırılganlığının öncelikleri belirlendi. Üçüncü adımda, ağ analiz sürecine (ANP) dayalı olarak analitik model tanımlanmıştır. Ayrıca Super Decision yazılımı kullanılarak her bir alt kriter ve kriterin ağırlığı elde edilmiştir. Son olarak dördüncü adımda, bu ağırlıklar ArcGIS yazılım ortamında kriterlere ilişkin katmanların her birine uygulanmış ve kentsel bağlamın nihai etkilenebilirlik haritası coğrafi bilgi sisteminde raster olarak elde edilmiştir. Model uygulamasının sonuçları, 17. bölgenin kentsel dokusunun, yüksek nüfus ve bina yoğunluğu, yıpranmış doku varlığı, düşük yapısal dayanıklılığa sahip binalar ve çok düşük inşaat kalitesi gibi özelliklerden dolayı yüksek hassasiyete eğilimli olduğunu göstermiştir. Toplamda, Tahran'ın 17. bölgesindeki meskun arazinin yaklaşık 657 hektarı (yüzde 80'i) arazi çökmesinin etkisi altındadır.

Article Info

Received: 22/05/2023
Accepted: 19/06/2023
Published: 30/06/2023

Citation:

Rezaeishahabi, R, Arab, A., Pishva, A., Hajipour, V. & Zahaki, M. (2023). Measuring the Vulnerability of the Urban Fabric in the Face of Land Subsidence (Case Study: District 17 of Tehran) . Turkish Journal of Remote Sensing , 5 (1) , 33-49 .

***Corresponding Author:** Ramin Rezaeishahabi, r.r.shahabi@gmail.com, +98 313 626 91 67

1. INTRODUCTION

Urban vulnerability analysis is the evaluation and prediction of the probability of life, material and spiritual damage to the city and its residents against possible natural and unnatural hazards (Patton & Fohnston, 2001; Recchia, 2008; Karashima et al., 2014). In general, there are different types of vulnerability that are divided into four main categories: physical, social, economic and environmental (Ahsan & Warner, 2014; Kim & Marcouiller, 2015). Vulnerability is also classified in two spectrums, natural and man-made, based on the origin of the incident (Sennewald & Bailie, 2015). In this regard, land subsidence is the slow sinking of the earth's surface as a result of natural factors or human activities (Corapcioglu, 1984). Even if described as a moderate and gradual geological process that rarely causes casualties, land subsidence can be responsible for significant economic losses in urban areas (Wu et al., 2009). This issue reaches a new level of influence in the conditions of climate change, which is characterized by severe drought and rising sea levels (IPCC, 2013; Vousdoukas et al., 2017).

Land subsidence is a phenomenon that has been identified and monitored in many countries (Baer et al., 2002; Closson et al., 2005; Fares & Rana, 2005; Paine et al., 2009; Casu, 2009; Castaneda et al., 2009; Osmanoğlu et al., 2011; Chaussard et al., 2013; Liu et al., 2014; Qu et al., 2014; Üstün et al., 2015; Yalvac, 2020; Karimzadeh & Matsuoka, 2020) and has left numerous negative effects on structures, facilities and vital arteries (Galloway & Burbey, 2011; Tung & Hu, 2012; Chaussard et al., 2013; Brown & Nicholls, 2015; Corbau et al., 2019; Orhan et al., 2021). Research results show that subsidence threatens more than 12 million square kilometers (80%) of the earth's surface in the world with a probability of more than 50%. Out of 7343 big cities in the world, about 1596 big cities (22 percent) are located in potential land subsidence areas. Also, 19% of the world's population is at risk from subsidence (Garcia et al., 2021). Many countries and cities (For example, the subsidence rate in Tehran/Iran (25 cm), Yunlin/China (10 cm), Mexico City (9 cm), California/USA (7 cm), Bologna/Italy (4 cm) and Karapinar/Turkey (7 cm)) suffer from subsidence of the earth in the amount of tens of centimeters per year.

Land subsidence is probably one of the most visible environmental effects of groundwater pumping. Globally, the demand for fresh water is the main cause of this phenomenon (Oruji et al., 2019; Poland, 1984; Amelung et al., 1999; Mayoral et al., 2019). Land subsidence caused by the drainage of the aquifer system can reach total values of up to 14.5 meters (Guzy & Malinowska, 2020). Land subsidence is characterized by slow movements that usually cover large areas and include agricultural and economic activities, as well as buildings, cultural heritage and linear infrastructure, which cause significant economic losses (Ezquerro et al., 2020). Geological disasters caused by surface deformation are common, especially in urban areas, which seriously hinder the sustainable development of urbanization. Monitoring and analysis with high spatial and temporal resolution is especially important for assessing the risk of geological disasters caused by urban transformation (Hu et al., 2022). Land subsidence has harmful consequences on the constructions on the soil and the vital arteries buried in the soil. If the process of withdrawing water from an aquifer continues, this phenomenon can cause the loss of the efficiency of structures and vital arteries, and the result will be a crisis in the region (Baum et al., 2008; Bott et al., 2021). The effect of land subsidence can be seen mainly from four aspects: 1) Damage to infrastructure, e.g. pipelines, buildings and dams; 2) Reducing the serviceability of roads and railways due to the deformation of the road surface and railway foundations (Chen et al., 2020); 3) Increased flood exposure (Du et al., 2018); and 4) It may become a channel for the penetration of ground pollution sources into underground sources and cause groundwater pollution (Hussain & Abed, 2019; Zhang, 2019). Despite the studies conducted on land subsidence issues, many studies have not been conducted on the effect of land subsidence on the urban fabric and its components (Table 1). For this reason, it is felt necessary to deal with the effect of land subsidence on the urban fabric - which can endanger the lives of millions of people - in order to better understand the effect of this phenomenon.

Due to the uncontrolled extraction of groundwater, Iran is currently one of the countries with the highest annual subsidence rate (25 cm of subsidence per year) (Garcia et al., 2021). Excessive extraction of water from underground aquifers during decades for agricultural and industrial purposes has caused severe land subsidence in many plains of Iran (such as Marand plain (Roustaei & NajafVand, 2022), Ardabil plain (Abedini et al., 2022), Kashan plain (Saqazadeh et al., 2022), central plain of Qain city (Hosseinzadeh et al., 2022), Hashtgerd plain (Mehrnour et al., 2022), Sarab plain (Asghari Saraskanroud et al., 2022), Isfahan (Azarm et al., 2022), Hamedan urban area (Ganjaian et al., 2022), Qara Balag plain of Fars Province (Yamani et al., 2009), Rafsanjan plain (Motagh et al., 2017), Neyshabour (Dehghani et al., 2009), Tehran plain (Azadnejad et al., 2020), Qazvin plain (Babaei et al., 2020) and Neishabor plain (Rezaei et al., 2020)). In the meantime, the southwest plain of Tehran is one of the areas that is facing a decrease in the level of underground water, and as a result, signs of subsidence can be seen in this area (Mahmoudpour et al., 2016; Country Mapping Organization, 2018) and this issue is a serious threat to the urban and industrial fabric and body as well as the agricultural lands of this region. In this regard, district 17 of Tehran is one of the areas where land subsidence has

occurred (SharifiKia et al., 2013) and is subsiding at a rate of 1 to 25 cm (Karimi et al., 2014; Country Mapping Organization, 2018). The possibility of simultaneous subsidence with an earthquake due to the proximity of the 17th region to the active Ray fault (as a trigger for landslides) makes this region susceptible to a severe disaster with high human casualties. Therefore, the main goal of this research is to measure the vulnerability of the urban fabric in the face of land subsidence, and to achieve this goal, the urban fabric of the 17th district of Tehran has been selected. The tools used in this research to measure the vulnerability of the urban fabric are network analysis (ANP) and GIS.

Table 1. Some studies done in relation to land subsidence

Researchers	The subject of research
Pratt and Johnson	First observation of subsidence associated with subsurface processes (Pratt and Johnson, 1926)
Terzaghi, 1923	The first milestone in the theory of aquifer consolidation due to groundwater pumping (Gambolati et al., 2015)
Gambolati and Freeze	The first mathematical modeling of subsidence (Gambolati et al., 2015)
Poland	Acceptance of concepts related to land subsidence and water harvesting thanks to the substantial contributions of Polland (Poland, 1958, 1960, 1961; Poland and Davis, 1956, 1969; Poland et al., 1959; Poland and Green, 1962)
Feth, 1949	Observation of ground ruptures related to ground subsidence (Holzer and Davis, 1976; Holzer et al., 1979)
Holzer and Pampeyan	Holzer and Pampian recognized that fissures were caused by human factors (Jachens and Holzer, 1979; Holzer and Pampeyan, 1981; Jachens and Holzer, 1982)
Baum et al.	Loss of efficiency of vital structures and arteries under the influence of land subsidence (Baum et al, 2008)
Gutierrez et al.	Investigating the impact of subsidence on a building with 100 apartments using geophysics and trenching techniques (Gutierrez et al., 2009)
Chaussard et al.	Heavy rains associated with monsoon and tropical storms, lack of coastal or river defenses, as well as limited evacuation potential, increase the vulnerability of Indonesian cities to land subsidence (Castellazzi et al., 2013)
Castellazzi et al.	Correspondence between recent changes in subsidence rate with geological data in large cities of central Mexico (Castellazzi et al, .2016)
Herrera Leon et al.	Investigating the relationship between natural factors and human factors as the causes of subsidence (Herrera Leon et al., 2018)
Oruji et al.	The most important reason for land subsidence is excessive extraction of underground water tables (Oruji et al., 2019)
Aslan et al.	Correlation between subsidence and changes in groundwater depth (Aslan et al., 2019)
Ciampalini et al.	Subsidence analysis of a recently built cargo terminal (Guasticce Terminal) in the Tuscany region (Central Italy) (Ciampalini et al., 2019)
Ezquerro et al.	Assessing the vulnerability of buildings due to ground subsidence in the historic city of Pistoia, Italy (Ezquerro et al, 2020)
Orhan et al.	Correlation between subsidence and changes in groundwater depth (Orhan et al., 2021)
Garcia et al.	Mapping the global threat of land subsidence (Garcia et al., 2021)

2. THE STUDY AREA

District 17, as one of the 22 districts in the southwest of Tehran metropolis (Figure 1), is located on the bed of its alluvial plain. With an area of 824 hectares (equivalent to 1.15% of the total land of Tehran's legal boundaries), this area is the smallest and densest area of Tehran after area 10, which has 3 districts and 14 neighborhoods (Azizzadeh et al., 2016). The population of the region in 2022 is 278,354 people with a net population density of 668 people per hectare. District 17 is referred to as the densest district of Tehran (having a population density four times that of other districts). Desolation (weariness of 70% of buildings) and severe density, unstable and irregular urban fabric, severe interference of uses, irregular street construction and nested alleys with narrow and long passages and heavy traffic of vehicles are among the distinctive features of this area (Table 2).

Table 2. Characteristics of district 17 of Tehran city

Characteristics	District 17	Percent
Area	824 hectares	100
The area of built up land	774 hectares	94
Residential area	417 hectares	54
Area of worn tissue	684 hectares	88
Population	278354	

Region 17 is affected by three faults north of Tehran, south and north of Ray, and from this point of view, it is considered one of the most vulnerable areas of Tehran in dealing with accidents caused by earthquakes. The lands of this region are located on a bed of stones resulting from the aggregation of volcanic rocks, which consists of sedimentary alluvium of Tehran lands and clay forms a major part of it (Asgari et al., 2002: Site of Region 17 of Tehran Municipality, 2002).

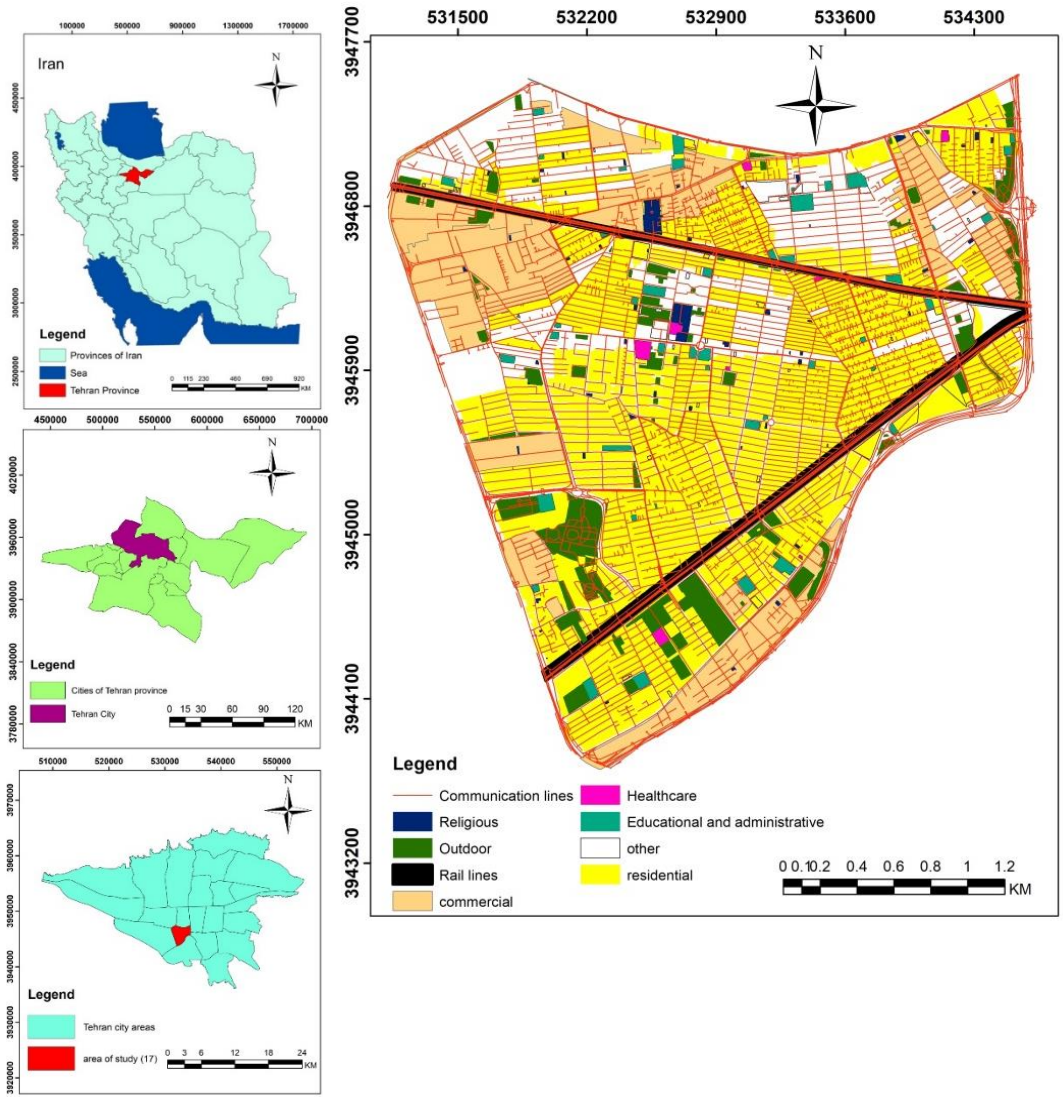

Figure 1. Geographical location of district 17 of Tehran city

3. METHODOLOGY

The purpose of this research is to measure the vulnerability of the urban fabric of the 17th district of Tehran in the face of land subsidence, which was realized in the form of an analytical model in four steps (Figure 2). In the first step, identification and classification of vulnerability indicators of the urban fabric was done based on three physical and demographic criteria, accessibility and proximity to high risk centers by reviewing the latest research. In the second step, using a questionnaire tool and a survey of 30 experts and people knowledgeable about the research topic, the priorities of the vulnerability of the urban fabric in the face of land subsidence were determined. In the third step, the analytical model was defined based on the ANP network analysis method, and the weight of each of the sub-criteria and criteria was obtained using Super Decision software. Also, specific weights obtained from ANP modeling were applied to the spatial layers of the region. In the fourth step, these weights were applied to each of the layers related to the criteria in the ArcGIS software environment, and along with that, the layers were combined. Finally, the final urban tissue vulnerability map was obtained as a raster in the geographic information system. The process of conducting research using the combined Delphi method and network analysis (ANP) has been proposed by researchers in different ways. The basis of this research is a combination of Fowles, 1978 and Cheng Eddie, 2007 and Saaty, 2005. The basis of the Delphi method is that the opinion of the experts of each scientific field is the most correct opinion regarding the prediction of the future; Therefore, unlike survey research methods, the credibility of the Delphi method does not depend on the number of participants in the research, but on the scientific credibility of the experts participating in the research. In this study, according to the use of paired comparisons questionnaire and network analysis method and the need to use the opinions of experts, 30 university professors, crisis and unforeseen events organization, environmental organization and municipality who were highly familiar with land subsidence issues , were selected

as samples by a purposeful method of judgment. For this purpose, a Delphi questionnaire and finally a pairwise comparison questionnaire were designed and distributed among experts.

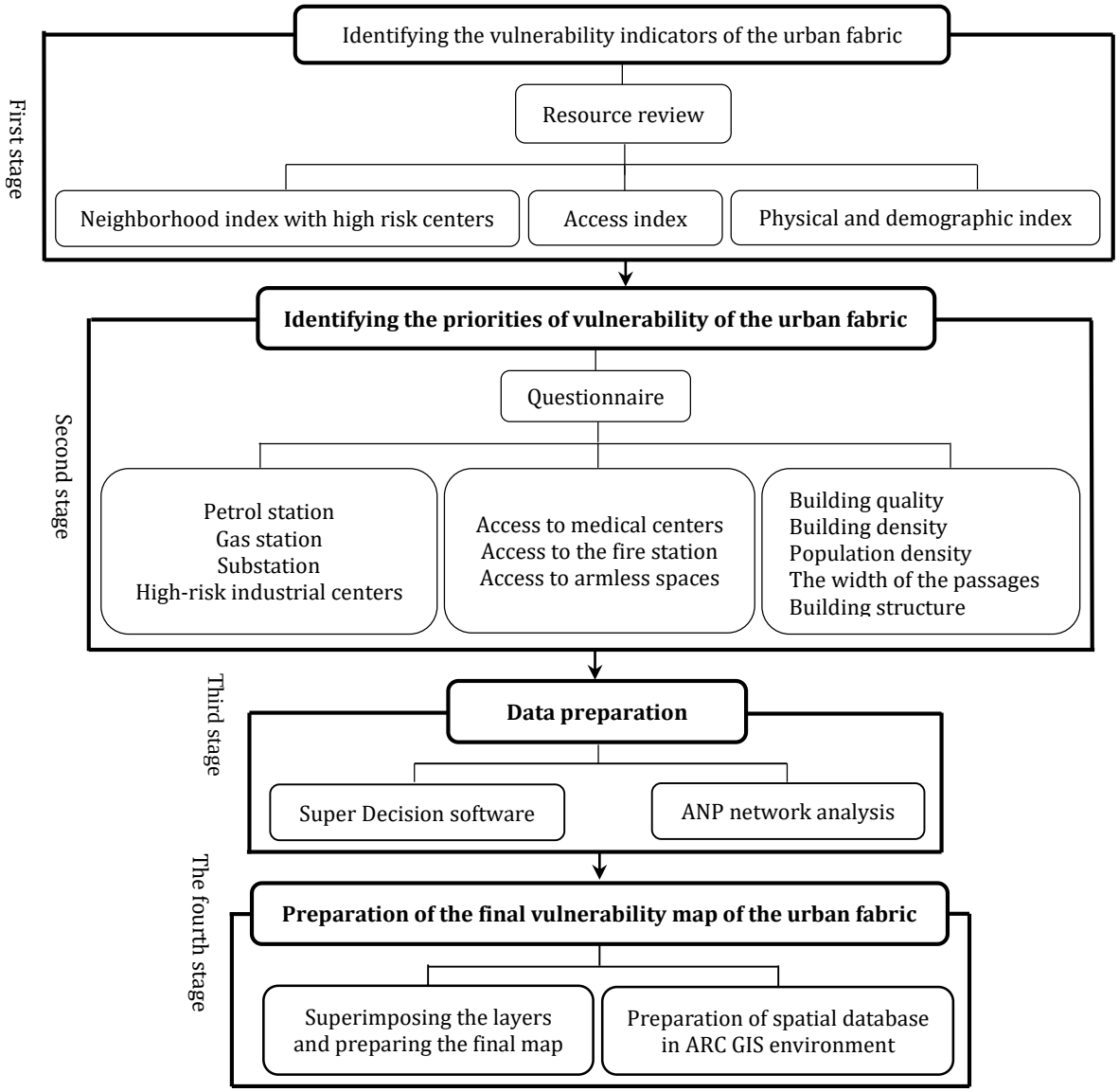

Figure 2. Analytical model for assessing the vulnerability of the urban fabric of the 17th district of Tehran in the face of land subsidence

3.1. Introducing the Criteria and Indicators for Measuring the Vulnerability of the Urban Fabric

Examining the opinions of experts in this study indicated that among the indicators considered for physical and demographic criteria, five basic indicators are 1. quality of buildings, 2. building density, 3. population density, 4. width of roads and 5. The skeleton of the building has been determined. Also, among the indicators considered for the access criteria, three basic indicators have been determined: 1. Access to medical centers, 2. Access to the fire station, and 3. Access to open and empty spaces. On the other hand, among the indicators considered for the criterion of proximity to high risk centers, four basic indicators 1. proximity to gas stations, 2. proximity to gas pumps, 3. proximity to electric substations, and 4. proximity to high-risk industrial centers were determined. (Table 3). In order to measure the level of vulnerability and within the framework of the proposed criteria, the determined indicators need to be conceptualized in order to make a quantitative judgment about measuring the level of vulnerability:

3.1.1. Quality of the building

The higher the strength of the building and the more durable materials it is made of, the less vulnerable it will be (Ahdanjadrosheni et al., 2014; Tavakoli & Akbarpour, 2010; Siyami et al., 2013). The quality of buildings and their construction is one of the factors affecting the resistance of urban

buildings against the pressures. From this point of view, urban buildings can be divided into three categories: newly built, renovated and demolished (Farzamshad & Iraqizadeh, 2011; MohammadiDeh-Ceshmeh, 2012; Ebrahimian-Qajari et al., 2013).

3.1.2. Building density

It is an important indicator that increases the probability of destruction and vulnerability. By dividing the city into a grid of 250x250 meters, the grids with the number of buildings up to 75 buildings will be low vulnerability, 75-150 buildings in each grid will be medium vulnerability and 150-300 buildings will be high vulnerability (Siyami et al., 2013; Ebrahimian-Qajari et al., 2013).

Table 3. The criteria and indicators for assessing the vulnerability of the urban fabric

Criterion	Indicator	The degree of vulnerability			Source
		Low	**Mediocre**	**High**	
Physical and demographic	Building quality	Newly built	Restoration	Destructive	Tavakoli & Akbarpour, 2010 Farzamshad & Iraqizadeh, 2011 MohammadiDeh-Ceshmeh, 2012 Siyami et al., 2013 Ebrahimian-Qajari et al., 2013 Ahadanjadroshani et al., 2014
	Building density	0-75	75-150	150-300	Siyami et al., 2013 Ebrahimian-Qajari et al., 2013
	population density	Less than 100 people per hectare	100-200 people per hectare	More than 200 people per hectare	Peacock et al., 1997 Enarson & Morrow, 1998 Tierney, 2006 Habibi et al., 2008
	The width of the passages	More than 14 meters	9-14 meters	Dead end, 6-9 meters, under 6 meters	Habibi et al., 2008 Azizi & Barnafar, 2011 Siyami et al., 2013 Ebrahimian-Qajari et al., 2013 Alikhani et al., 2017
	The skeleton of the building	Concrete	Metallic	Other	Okada & Takai, 2000 Hatami-Nejad et al., 2009 Firouzi et al., 2013 Ebrahimian-Qajari et al., 2013
Access	Access to medical centers	Less than 250 meters	200-500 meters	More than 500 meters	Azizi & Barnafar, 2011 Farzamshad & Iraqizadeh, 2011 Siyami et al., 2013
	Access to the fire brigade	Less than 750 meters	750-1500 meters	More than 1500 meters	Siyami et al., 2013
	Access to open, empty spaces	Less than 250 meters	250-500 meters	More than 500 meters	Siyami et al., 2013
Adjacent to high risk centers	Petrol station	More than 150 meters	75-150 meters	Less than 75 meters	Azizi & Barnafar, 2011 Siyami et al., 2013
	Gas station	More than 100 meters	50-100 meters	Less than 50 meters	
	Electricity substation	More than 100 meters	50-100 meters	Less than 50 meters	
	Industrial centers	More than 400 meters	200-400 meters	Less than 200 meters	Research processes

3.1.3. Population density

Population density is generally considered as a factor that aggravates the vulnerability of urban tissues (Habibi et al., 2008). Obviously, with the increase in population density, vulnerability also increases (Peacock et al., 1997; Enarson & Morrow, 1998; Tierney, 2006).

3.1.4. Width of roads

The smaller the width of the road, the more likely it is to be vulnerable, because with the collapse of the debris in the roads, it becomes difficult to provide assistance. Also, the greater the width of the roads, the less the possibility of passing traffic (Habibi et al., 2008; Azizi & Barnafar, 2011; Ebrahimian-Qajari et al., 2013).

3.1.5. Building skeleton

The resistance of all types of buildings can be defined by the intensity of the incoming loads, and the vulnerability of the building is one of the main factors affecting human casualties. Therefore, analysis of building safety against accidents is a very important issue (Okada & Takai, 2000). Metal and reinforced concrete skeletons have less vulnerability than other materials, brick and stone skeletons have medium vulnerability and wooden, cement block, clay and mud skeletons have high vulnerability (Hatami-Nejad et al., 2009; Firouzi et al., 2013; Ebrahimian-Qajari et al., 2013).

3.1.6. Access to medical centers

Access to medical centers speeds up rescue operations and service delivery. In this way, by moving away from medical centers, the possibility of vulnerability increases (Azizi & Barnafar, 2011; Farzamshad & Iraqizadeh, 2011; Siyami et al., 2013).

3.1.7. Access to the fire station

Proper access to relief centers can reduce the damage caused by land subsidence (Siyami et al., 2013).

3.1.8. Access to open and empty spaces

Appropriate distribution of places that have the ability to temporarily accommodate people, reduces damage during and after an accident. These spaces include green spaces, open spaces and indoor sports halls in cities (Siyami et al., 2013).

3.1.9. Adjacent to petrol stations, gas stations and industrial centers

At the city level, fuel storage tanks, gas stations and centers that have the potential to release a lot of energy can be considered as harmful uses (Azizi & Barnafar, 2011; Siyami et al., 2013).

3.2. Hierarchical Analysis

Analytic Network Process (ANP) is a multi-criteria decision-making method that is very similar to Analytical Hierarchy Process (AHP) and in better words, it is an extended form of Analytical Hierarchy Process. The main difference between the network and hierarchical analysis methods is in the structure of the model definition and the relationship between its elements. This relationship in the hierarchical analysis method is only independent, while in the ANP method, this relationship can be both independent and dependent. This feature causes dependencies and feedbacks between criteria and sub-criteria to be systematically checked (Chung & Lee, 2005). The network analysis method considers the complex relationships between decision elements by replacing the hierarchical structure with a network structure. For this reason, in recent years, the use of ANP has increased in most fields (Zebardast, 2011). In the process of network analysis, as in the process of hierarchical analysis, the comparative spectrum of 1-9 is used. This scale of comparison enables the decision maker to intuitively unite knowledge and experience and determine how many times one element is dominant over another element in terms of criteria. The decision maker has the possibility to express his preference in the form of each pair of elements verbally, equal importance, relatively more important, more important, very important, absolutely important. In the next step, these descriptive preferences are translated into numerical values of 3, 1, 5, 7, 9 respectively. Values 4, 2, 6, 8 are also used as median values in comparison between two consecutive judgments. The reverse of these numbers is used for the other side of judgments.

As mentioned earlier, in order to measure the vulnerability of the urban fabric of the 17th district of Tehran in the face of land subsidence, after determining the indicators using the Delphi method and preparing information layers, the ANP method was applied to the data. Then, the weight of each of the sub-criteria and criteria was determined and entered into the Super Decision software (Tables 4 and 5).

Table 4. The matrix of pairwise comparisons and the weight of the main criteria

Criteria	Physical and demographic	Access	Adjacent to high risk centers	Final weight
Physical and demographic	1	7	8	0/757
Access	1/7	1	6	0/188
Adjacent to high risk centers	1/8	1/6	1	0/055

Table 5. Calculated threshold super matrix for measuring urban tissue vulnerability

		Physical and demographic criteria					Access criteria			Neighborhood criteria with high risk markers			
		Building quality	Building density	Population density	The width of the passages	The skeleton of the building	Access to medical centers	Access to the fire station	Access to open space	Petrol station	gas station	Substation	High-risk industrial centers
Physical and demographic criteria	Building quality	0/214	0/214	0/214	0/214	0/214	0/214	0/214	0/214	0/214	0/214	0/214	0/214
	Building density	0/241	0/241	0/241	0/241	0/241	0/241	0/241	0/241	0/241	0/241	0/241	0/241
	Population density	0/123	0/123	0/123	0/123	0/123	0/123	0/123	0/123	0/123	0/123	0/123	0/123
	The width of the passages	0/119	0/119	0/119	0/119	0/119	0/119	0/119	0/119	0/119	0/119	0/119	0/119
	The skeleton of the building	0/126	0/126	0/126	0/126	0/126	0/126	0/126	0/126	0/126	0/126	0/126	0/126
ccess criteria	Access to medical centers	0/051	0/051	0/051	0/051	0/051	0/051	0/051	0/051	0/051	0/051	0/051	0/051
	Access to the fire station	0/021	0/021	0/021	0/021	0/021	0/021	0/021	0/021	0/021	0/021	0/021	0/021
	Access to open space	0/044	0/044	0/044	0/044	0/044	0/044	0/044	0/044	0/044	0/044	0/044	0/044
Neighborhood criteria with high risk markers	Petrol station	0/016	0/016	0/016	0/016	0/016	0/016	0/016	0/016	0/016	0/016	0/016	0/016
	gas station	0/019	0/019	0/019	0/019	0/019	0/019	0/019	0/019	0/019	0/019	0/019	0/019
	Substation	0/011	0/011	0/011	0/011	0/011	0/011	0/011	0/011	0/011	0/011	0/011	0/011
	High-risk industrial centers	0/015	0/015	0/015	0/015	0/015	0/015	0/015	0/015	0/015	0/015	0/015	0/015

The weight obtained from ANP modeling was applied to the input layers. In the end, the final map to determine the vulnerability of residential use was obtained in the form of a grid. By examining the vulnerability assessment model, it was found that vulnerability criteria and indicators do not have the same importance. Meanwhile, the physical and demographic criterion with a weight of 0.757 has the highest value in measuring vulnerability. Also, among the analyzed indices, the building density index with a weight of 0.241, the building quality index with a weight of 0.214, the building skeleton index with a weight of 0.126, the population density index with a weight of 0.123 and the road width index with a weight of 0.119 respectively has the highest value in measuring the level of vulnerability from the point of view of experts and people aware of the issue of land subsidence.

4. RESULTS

There are 5 CNG stations in the studied area and according to the standard distance of 50 meters, about 4.19 hectares (0.54%) of the built-up lands are in the radius of high vulnerability (Figure 3).

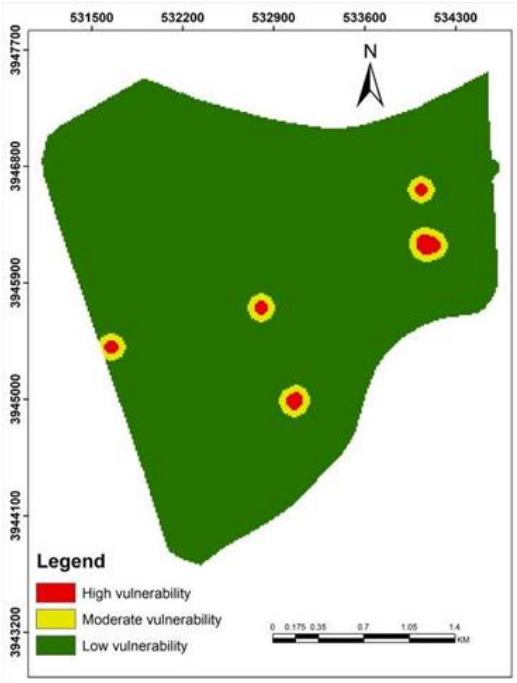

Figure 3. Vulnerability map due to CNG explosion

There are 3 petrol stations in the studied area, and according to the existing standard, the built structure that is less than 75 meters from the gas station has a high vulnerability, and according to this,

about 3.5 hectares (0.68 percent) of the total built-up land area of the region are in the high vulnerability range (Figure 4).

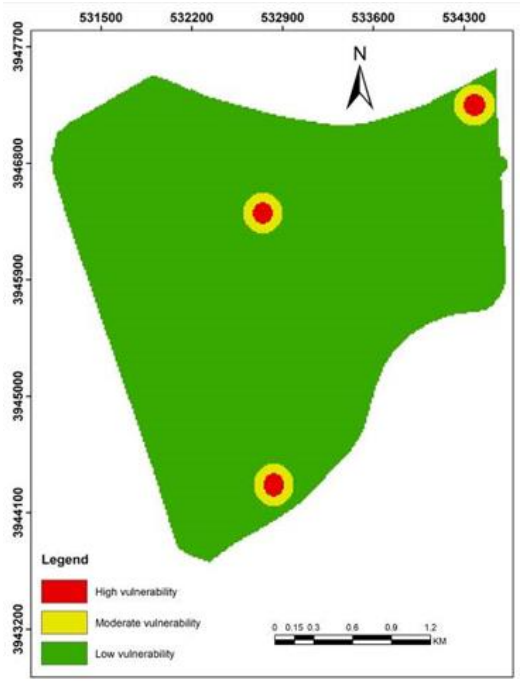

Figure 4. Vulnerability map due to petrol station explosion

There are 6 high-risk industrial centers in region 17, which according to the standards of the Ministry of Energy and Industry, about 12.57 hectares (1.62 percent) of the total built-up land area of the region are in the high vulnerability range (Figure 5).

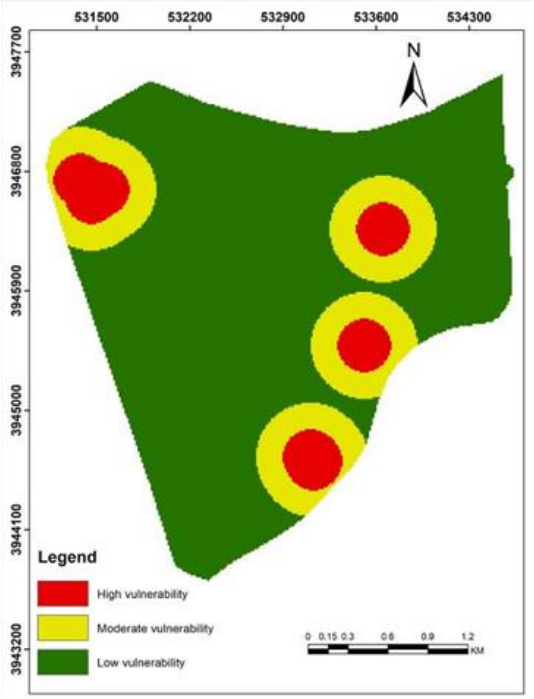

Figure 5. Vulnerability map according to the distance from high-risk industrial centers

Also, there are 79 electricity substations in the study area, which according to the 50 meter distance standard, about 62.6 hectares (8.09%) of the total built-up land area of the region is in the radius of high vulnerability (Figure 6).

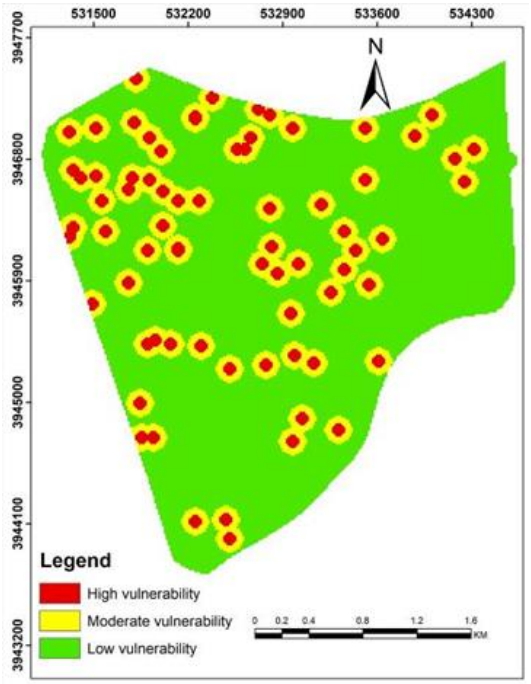

Figure 6. Vulnerability map due to the explosion of electric substations

In total, by analyzing the criteria indicators of proximity to high risk centers, it was determined that out of the total area of built-up lands in Region 17 (774 hectares), about 85 hectares (11 percent) of built-up lands are in the danger radius with high vulnerability. Based on the index of access to medical centers, a total of 262 hectares (32%) of the total area of Region 17 are outside the radius of effective access (with a distance of more than 500 meters) from medical centers (Figure 7).

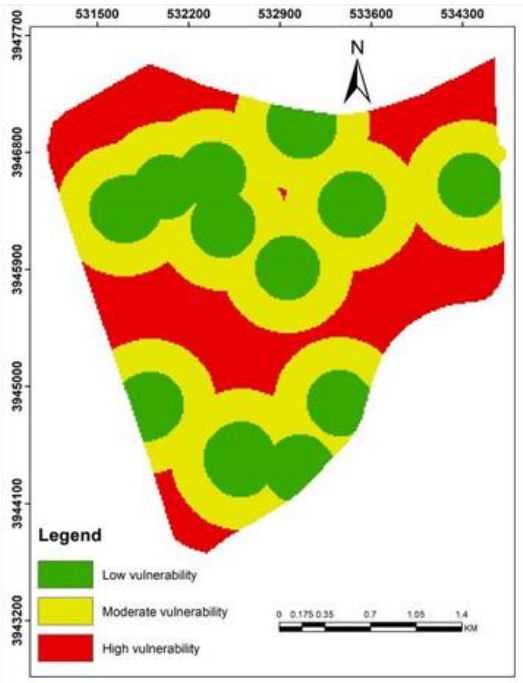

Figure 7. Vulnerability map according to access to medical centers

There have been 2 fire stations in region 17, which are located in about 114 hectares (14 percent) of the total built-up area of the region outside the effective access radius (with a distance of more than 1500 meters) from the fire station (Figure 8).

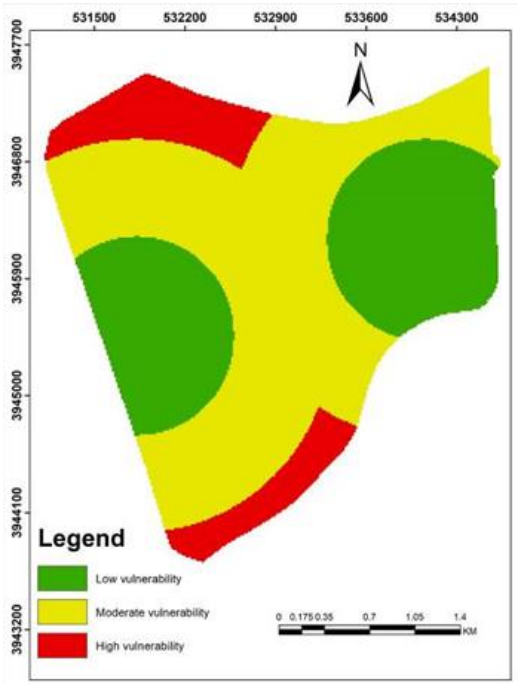

Figure 8. Vulnerability map according to access to the fire station

Access to open and empty places is another indicator that can be effective in reducing human injuries during and after a crisis. Examining this index in the studied area shows that in region 17, about 62 hectares (7.5 percent) of the entire area are outside the radius of effective access (with a distance of more than 500 meters) of open and empty spaces (Figure 9).

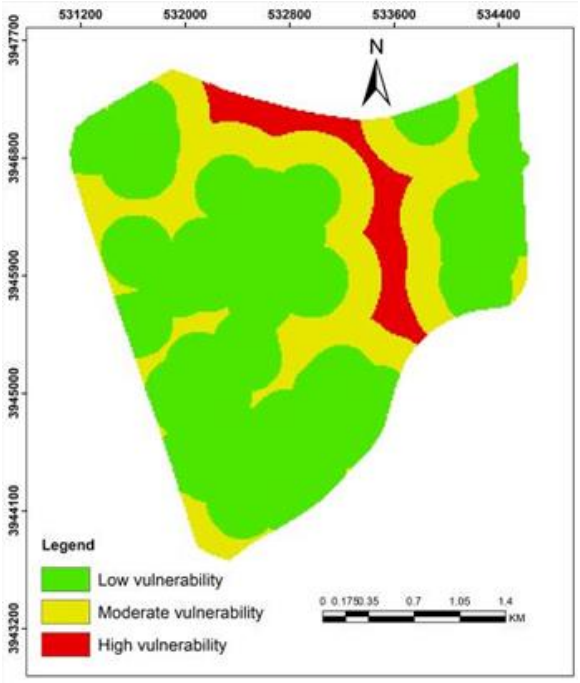

Figure 9. Vulnerability map according to access to armless spaces

By examining the building quality index in region 17, it was found that 491.2 hectares (63.4 percent) of the total built-up land have dilapidated buildings (high vulnerability) (Figure 10).

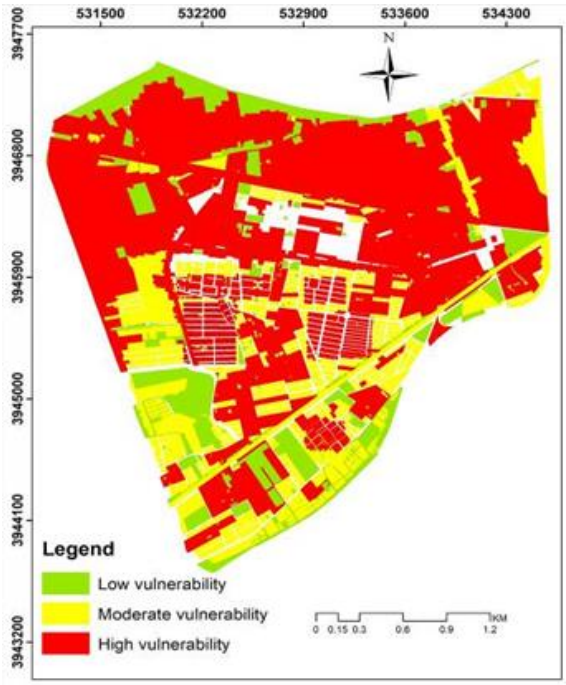

Figure 10. Vulnerability map according to building quality

The above percentages show that the vast majority of existing buildings in area 17 have a worn texture and in case of land subsidence in this area, we will witness a human disaster.

In terms of building density index, district 17 has a high building density and has a high percentage of vulnerability. Of the total area of built-up land in Region 17, about 464 hectares (60%) have high density, 52 hectares (7%) have medium density and 258 hectares (34%) have low density (Figure 11).

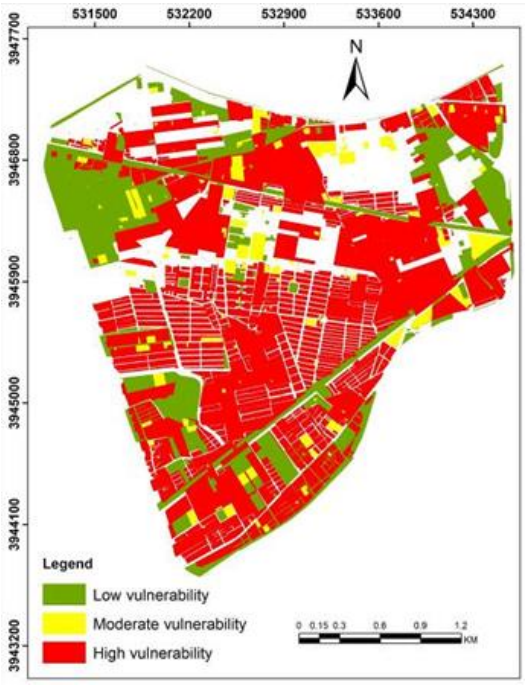

Figure 11. Vulnerability map according to building density

The road width index is an important index that will play a very important role in the event of a disaster in an area. Surveys showed that of the total area of built-up land in Region 17, 269 hectares (35%) have low vulnerability, 185 hectares (24%) have medium vulnerability, and 321 hectares (42%) have high vulnerability. The above survey shows that more than 66% of the studied area has narrow passages and no access hierarchy, and in case of land subsidence, many problems will be created for residents to escape from the danger area (Figure 12).

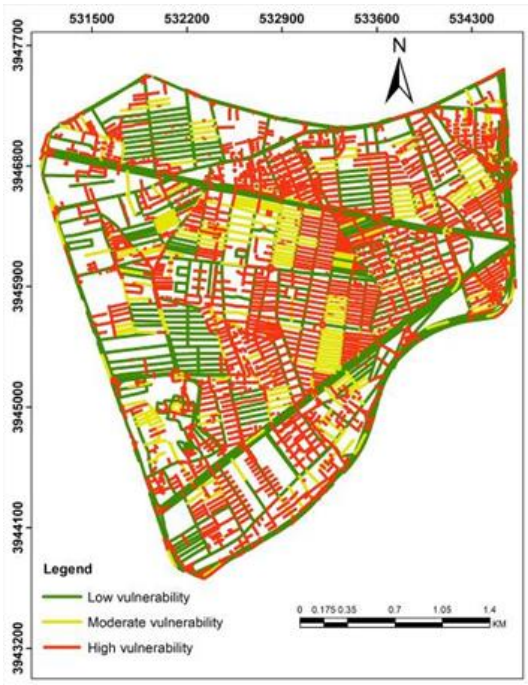

Figure 12. Vulnerability map according to the width of the roads

The building skeleton is another important indicator that can be effective in reducing human injuries during a crisis. Examining this index in the studied area shows that about 364 hectares (47%) of the constructed buildings have concrete skeletons, 145 hectares (19%) of the constructed buildings have iron and brick skeletons, and 267 hectares (35%) of the existing buildings have an unsustainable and weak skeleton and are highly vulnerable (Figure 13).

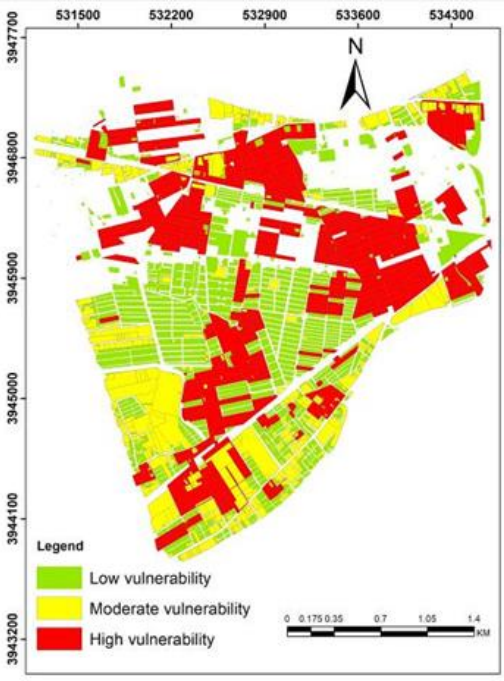

Figure 13. Vulnerability map according to the type of skeleton of buildings

The most influential indicator for measuring the vulnerability of urban tissue in the face of land subsidence is population density. In region 17, the population density is 668 people per hectare, and more than 161,047 people (58%) of the total residents of this region are at high risk in case of land subsidence. Excessive population density has greatly increased the vulnerability of region 17 and this region has the potential of a human and environmental disaster in case of land subsidence (Figure 14).

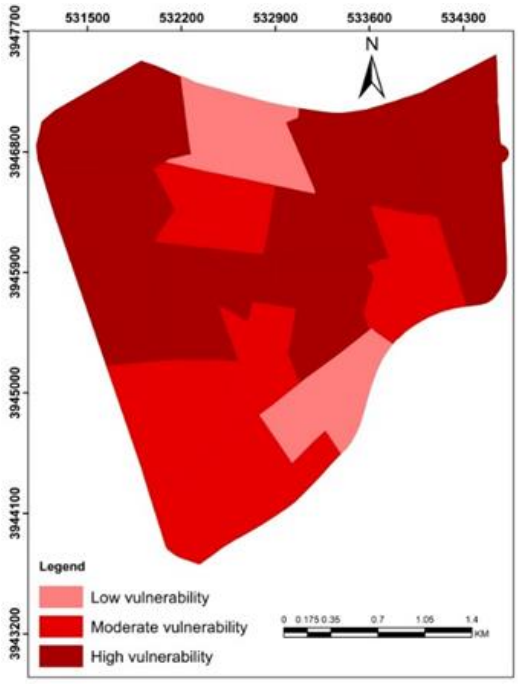

Figure 14. Vulnerability map according to population density

4.1. Combining the Layers and Preparing the Final Vulnerability Map of the 17th District of Tehran

By overlapping the vulnerability layers with area 17, the vulnerability status of this area was determined in three levels: low, medium and high. The investigations of this research showed that a high percentage of the built-up lands in the 17th region have characteristics such as worn texture, buildings with low structural strength, very low construction quality of buildings and high density of buildings and population and are prone to high vulnerability. Based on this, from the total area of region 17 (824 hectares), about 166.8 hectares (20.2%) are in the low vulnerability range, 92.5 hectares (11.2%) are in the medium vulnerability range and 564.5 hectare (68.5 percent) is in the range of high vulnerability in case of land subsidence (Figure 15). In total, 657 hectares (80 percent) of the built-up lands in Region 17 are under the influence of land subsidence.

Figure 15. Vulnerability map of the urban fabric of the 17th district of Tehran in the face of land subsidence

5. CONCLUSION

The phenomenon of land subsidence affects the structure, texture and components of a city, but many studies have not been done on the effect of this phenomenon on the urban fabric. In particular, this research has used ANP network analysis and GIS software to assess the vulnerability of the urban fabric of the 17th district of Tehran in the face of land subsidence. The high population and building density, existence of dilapidated texture, buildings with low structural strength, very low construction quality of buildings, small width of passages and irregular texture and lack of access hierarchy, and the study area is involved with three earthquake faults makes it important to measure the vulnerability of the urban fabric of the 17th region in the face of land subsidence. In this research, the most effective criteria and indicators for measuring the vulnerability of urban fabric under the influence of land subsidence were introduced using the Delphi method and the ANP method. According to the analysis done in ArcGIS software, regarding the studied area, the following can be mentioned as the main issues in region 17:

- In terms of the criterion of being adjacent to high risk centers, about 85 hectares (11%) of the total built-up land area is in the danger radius with high vulnerability.
- In terms of the index of access to medical centers, about 262 hectares (32%) of the total area of the region are outside the radius of effective access.
- In terms of access index to the fire station, about 114 hectares (14%) of the total area of the region are outside the radius of effective access.
- In terms of the index of access to open and empty spaces, about 62 hectares (7.5%) of the total area

of the region are outside the radius of effective access.
- In terms of building density index, this area has a high building density and has a high percentage of vulnerability.
- In terms of road width index, 506 hectares (66 percent) of the total built-up land area of the region is highly vulnerable. This area has narrow passages and no access hierarchy, and in case of land subsidence, many problems will be created for residents to escape from the danger zone.
- According to the building skeleton index, 267 hectares (35%) of the built buildings have weak and weak skeletons and are highly vulnerable. Also, most of the concrete and metal structures are old and have low construction quality.
- In terms of the population density index, more than 161,047 people (58%) of the residents of this region are exposed to high vulnerability.
- In terms of building quality index, more than 491 hectares (63%) of the existing buildings have worn texture and have a high percentage of vulnerability.

By overlapping the layers of vulnerability with the 17th district of Tehran, the vulnerability status of the region was determined in three levels: low, medium and high. The results of this research showed that a high percentage of built-up land in this region has characteristics such as high population and construction density, the presence of worn-out texture, buildings with low structural strength, very low construction quality of buildings, small width of roads and irregular texture. Based on this, land subsidence has exposed 657 hectares (80 percent) of the lands of the 17th district of Tehran to high vulnerability. Considering the importance of the issue of land subsidence and the need for the country's crisis management authorities to address this issue, the following executive-operational solutions are suggested to prevent the possibility of a crisis:

- Injection of double frames to places with subsidence using jet grouting or micropile methods;
- The use of geosynthetics under surface foundations in order to reduce the impact of subsidence on the structure;
- Injecting and pumping water inside the ground in order to reduce the subsidence rate;
- Using flexible foundations during new constructions in areas prone to subsidence; and
- Prohibition of construction in areas with severe subsidence.

Author contributions

The authors contributed equally to the article.

Conflicts of Interest

The authors declare no conflict of interest.

Research and publication ethics statement

In the study, the authos declare that there is no violation of research and publication ethics and that the study does not require ethics committee approval.

REFERENCES

Abedini, M., Aghyari, L. & Asghari, S. (2022). Evaluating and Zoning of Subsidence Risk Using MABAC and ANP Adaptive Algorithm (Case Study: Ardabil Plain). *Journal of Geography and Environmental Hazards*, 11(4), 43-68. (in Persian) https://geoeh.um.ac.ir/article_42545.html

Ahadanjadroshani, M., Roustaei, S. & Kamlifar, M. J. (2014). Assessing the Vulnerability of the Urban Road Network Against Earthquakes with a Crisis Management Approach (Case Study: Zone 1 of Tabriz City). *Sepehr Geographic Information Quarterly*, 24(95). (In Persian) https://www.sid.ir/paper/253205/fa

Ahsan, M. N. & Warner, J. (2014). The socioeconomic vulnerability index: A pragmatic approach for assessing climate change led risks-A case study in the south-western coastal Bangladesh. *Int J of Disaster Risk Reduction,* 8, 32-49. https://doi.org/10.1016/j.ijdrr.2013.12.009

Alikhani, A., Barezgarbfaroui, A. & Noorahi, H. (2017). Presenting a Comprehensive Evaluation Model of the Vulnerability of Urban Areas by Separating the Constituent Layers of the City with a Passive Defense Approach. *Crisis Management Quarterly,* 16, 33-46. (In Persian) https://magiran.com/p2103514

Amelung, F., Galloway, D. L., Bell, J. W., Zebker, H. A. & Laczniak, R. J. (1999). Sensing the Ups and Downs of Las Vegas: InSAR Reveals Structural Control of Land Subsidence and Aquifer-System Deformation. *Geology,* 27(6), 483-486. https://doi.org/10.1130/0091-7613(1999)027<0483:STUADO>2.3.CO;2

Asgari, A., Parhizkar, A. & Qadiri, M. A. (2002). The Application of Urban Planning Methods (Land Use) in Reducing the Vulnerability of Earthquake Hazards (Case Study: 17th District of Tehran). *Geographical Research,* 17(4), 63-78. (In Persian) https://sid.ir/paper/417141/fa

Asghari Saraskanroud, S., Pirouzi, A. & Aghayari, L. (2022). Land Subsidence Risk Zoning in Sarab Plain, Using MARCOS and CODAS Multi-Criteria Analysis Algorithms. *Journal of Geography and Environmental Hazards,* 11(4), 179-172. (In Persian) https://geoeh.um.ac.ir/article_43420.html

Azadnejad, S., Maghsoudi, Y. & Perissin, D. (2020). Evaluation of Polar Metric Capabilities of Dual

Polarized Sentinel-1 and TerraSAR-X Data to Improve the PSInSAR Algorithm Using Amplitude Dispersion Index Optimization. *Int J Appl Earth Obs Geoinf,* 84, 101950. https://doi.org/10.1016/j.jag.2019.101950

Azarm, Z., Mehrabi, H. & Nadi, S. (2022). Investigating the Correlation Between Subsidence and Groundwater Level Changes Using Radar Interferometric Time Series Analysis (Study Area: Isfahan). *Journal of Geography and Environmental Hazards,* 11(4), 173-192. (In Persian) https://geoeh.um.ac.ir/article_42372.html

Azizi, M. M. & Barnafar, M. (2011). The optimal process of urban planning in air attacks from the point of view of passive defense (case study: district 11, Tehran). *Urban Studies Quarterly,* 1(1), 10-22. (In Persian) https://www.sid.ir/paper/468589/fa

Azizzadeh, M., Enayati, B., Farzaneh, M. & Azizzadeh, B. (2016). District 17; The most vulnerable urban area of Tehran in times of crisis (earthquake). *The First National Conference on the Development of Health, Safety and Environment in the Field of Urban Recreational, Sports, Religious and Cultural Places*, Tehran, Iran. https://civilica.com/doc/584796

Babaee, S., Masoumi, Z. & Mousavi, Z. (2020). Land Subsidence From Interferometric SAR and Groundwater Patterns in the Qazvin Plain, Iran. *Int J Remote Sens,* 41, 4780-4798. (In Persian) https://doi.org/10.1080/01431161.2020.1724345

Baer, G., Schattner, U., Wachs, D., Sandwell, D., Wdowinski, S. & Frydman, S. (2002). The Lowest Place on Earth is Subsiding-An InSAR (Interferometric Synthetic Aperture Radar) Perspective. *Geol. Soc. Am. Bull,* 114, 12-23. DOI:10.1130/0016-7606(2002)114<0012:TLPOEI>2.0.CO;2

Baum, R. L., Galloway, D. L. & Harp, E. L. (2008). Landslide and Land Subsidence Hazards to Pipelines. *U.S. Geological Survey,* Open-File Report 2008-1164, 192. https://pubs.usgs.gov/of/2008/1164/index.html

Bott, L. M., Schone, T., Illigner, J., Haghighi, M. H., Gisevius, K. & Braun, B. (2021). Land Subsidence in Jakarta and Semarang Bay-The Relationship Between Physical Processes, Risk Perception, and Household Adaptation. *Ocean and Coastal Management,* 211. https://doi.org/10.1016/j.ocecoaman.2021.105775

Brown, S. & Nicholls, R. J. (2015). Subsidence and human influences in mega deltas: The case of the Ganges-Brahmaputra-Meghna. *Science of the Total Environment,* 527-528, 362-374. https://doi.org/10.1016/j.scitotenv.2015.04.124

Castañeda, C., Gutiérrez, F., Manunta, M. & Galve, J. P. (2009). DInSAR Measurements of Ground Deformation by Sinkholes, Mining Subsidence, and Landslides, Ebro River, Spain. *Earth Surf. Process. Landf,* 34(11), 1562-1574. DOI:10.1002/esp.1848

Casu, F. (2009). The small baseline subset technique: performance assessment and new developments for surface deformation analysis of very extended areas. *Ph.D. Thesis*, University of Cagliari, Cagliari, Italy. [Google Scholar]

Chaussard, E., Amelung, F., Abidin, H. & Hong, S. (2013). Sinking Cities in Indonesia: ALOS PALSAR Detects Rapid Subsidence Due to Groundwater and Gas Extraction. *Remote Sensing of Environment,* 128, 150-161. DOI: 10.1016/j.rse.2012.10.015

Chen, B., Gong, H., Chen, Y., Li, X., Zhou, C., Lei, K., Zhu, L., Duan, L. & Zhao, X. (2020). Land Subsidence and its Relation with Groundwater Aquifers in Beijing Plain of China. *Science of the Total Environment,* 735, 139111. https://doi.org/10.1016/j.scitotenv.2020.139111

Cheng Eddie, W. L. & Li, H. (2007). Application of ANP in process models: An example of strategic partnering. *Building and Environment, ELSEVIR*, 42: 278–287. doi:10.1016/j.buildenv.2005.07.031

Chung, S. H. & Lee, W. L. (2005). Analytic network process approach for mix planning. *International Journal of Production Economics*, 18(96): 15-36. https://doi.org/10.1016/j.ijpe.2004.02.006

Closson, D., Karaki, N. A., Klinger, Y. & Hussein, M. J. (2005). Subsidence and Sinkhole Hazard Assessment in the Southern Dead Sea Area, Jordan. *Pure Appl. Geophys,* 162, 221-248. [Google Scholar] [CrossRef]

Corapcioglu, M. Y. (1984). Land Subsidence-A State-of-the-Art Review. *Fundamentals of Transport Phenomena in Porous Media,* 369-444. [Google Scholar]

Corbau, C., Simeoni, U., Zoccarato, C., Mantovani, G. & Teatini, P. (2019). Coupling Land Use Evolution and Subsidence in the Po Delta, Italy: Revising the Past Occurrence and Prospecting the Future Management Challenges. *Sci. Total Environ,* 654, 1196-1208. https://doi.org/10.1016/j.scitotenv.2018.11.104

Country Mapping Organization. (2018). Tehran Subsidence Atlas (Radar Data Processing From 2017 to 2019). https://fa.ncc.gov.ir/fa/news/1461

Dehghani, M., Valadan Zoej, M., Entezam, I. & Saatchi, S. (2009). InSAR Monitoring of Progressive Land Subsidence in Neyshabour, Northeast Iran. *Geophys J Int,* 178(1), 47-56. https://doi.org/10.1111/j.1365-246X.2009.04135.x

Du, Z., Ge, L., Ng, A., Zhu, Q., Yang, X. & Li, L. (2018). Correlating the Subsidence Pattern and Land Use in Bandung, Indonesia with Both Sentinel-1/2 and ALOS-2 Satellite Images. *Int. J. Appl. Earth Obs. Geoinf,* 67, 54-68. https://doi.org/10.1016/j.jag.2018.01.001

Ebrahimian-Qajari, Y., Al-Sheikh, A. A., Moderi, M., Hasnawi, R. & Abbasi, M. (2013). Vulnerability Modeling of Urban Buildings Using Delphi Methods and Hierarchical Analysis in GIS Environment. *Sepehr Geographic Information Quarterly,* 23(91), 5-20. (In Persian) https://www.sid.ir/paper/253169/fa

Enarson, E. & Morrow, B. H. (1998). *The Gendered Terrain of Disaster*. Westport, CT: Praeger.

Ezquerro, P., Soldato, M. D., Solari, L., Tomás, R., Raspini, F., Ceccatelli, M., Fernández-Merodo, J. A., Casagli, N. & Herrera, G. (2020). Vulnerability Assessment of Buildings due to Land Subsidence Using InSAR Data in the Ancient Historical City of Pistoia (Italy). *Sensors,* 20, 2749. DOI:10.3390/s20102749

Fares, A. & Rana, A. (2005). The Utility of synthetic aperture radar (SAR) interferometry in monitoring sinkhole subsidence: subsidence of the Devil's Throat sinkhole area (Nevada, USA). *10th Multidisciplinary Conference on Sinkholes and the Engineering and Environmental Impacts of Karst, San Antonio,* TX, USA, 541-547. https://ascelibrary.org/doi/abs/10.1061/40796%28177%2957

Farzamshad, M. & Iraqizadeh, M. (2011). *Basics of safe city planning and design from the point of view of passive defense*. Alam Afarin Publishing House, Tehran. (In Persian) https://www.gisoom.com/book/1936523/

Firouzi, M. A., MohammadiDeh-Chashma, M., Nazarpurdzaki, R. & Shojayan, A. (2013). Measuring the Structural Vulnerability of Hospitals From the Point of View of Passive Defense with the Fuzzy Hierarchy Model. *Space Planning and Design Quarterly,* 20(1), 149-177. (In Persian) https://www.sid.ir/paper/515003/fa

Fowles, J. (1978). Handbook of futures research. *Greenwood Press: Connecticut*. ISBN: 570555869

Galloway, D. & Burbey, T. (2011). Review: regional land subsidence accompanying groundwater extraction. *Hydrogeol. J,* 19, 1459-1486. https://doi.org/10.1007/s10040-011-0775-5

Ganjaian, H., Asadi, M., Manbari, F. & Ebrahimi, A. (2022). Analyzing the State of Subsidence in the Urban Area of Hamedan Using Radar and Satellite Images. *Journal of Geography and Environmental Hazards,* 11(4), 236-221. (In Persian) https://geoeh.um.ac.ir/article_42183.html

García, G. H., Ezquerro, P., Tomás, R., Pizarro, M. B., Vinielles, J. L., … (2021). Mapping the Global Threat of Land Subsidence. *Science,* 371(6524), 34-36. DOI: 10.1126/science.abb8549

Guzy, A. & Malinowska, A. A. (2020). State of the art and recent advancements in the modelling of land subsidence induced by groundwater withdrawal. *Water*, 12(7), 2051. https://doi.org/10.3390/w12072051

Habibi, K., Pourahmad, A., Meshkini, A., Askari, A. & Nazari Adli, S. (2008). Determining Effective Building Factors in the Vulnerability of the Ancient Urban Fabric of Zanjan Using GIS and LOGIC FUZZY. *Fine Arts,* 33, 27-32. (In Persian) https://www.sid.ir/paper/5630/fa

Hatami-Nejad, H., Fathi, H. & Eshghabadi, F. (2009). Assessing the Level of Seismic Vulnerability in the City, Sample Studied: District 10 of Tehran Municipality. *Human Geography Research,* 68, 1-20. (In Persian) https://www.sid.ir/paper/139105/fa

Hosseinzadeh, S. R., Akbari, I., Javanshiri, M. & Mohammadpoursangani, Z. (2022). Spatial Analysis of Land Surface Subsidence Using Radar Interferometry (Case Study: Central Plain of Qain City). *Journal of Geography and Environmental Hazards,* 11(4), 99-126. (In Persian) https://geoeh.um.ac.ir/article_42647.html

Hu, B., Chen, B., Na, J., Yai, J., Zhang, Z. & Du, X. (2022). Urban Surface Deformation Management: Assessing Dangerous Subsidence Areas through Regional Surface Deformation, Natural Factors, and Human Activities. *Sustainability,* 14(17), 10487. https://doi.org/10.3390/su141710487

Hussain, M. & Abed, B. 2019. Simulation and assessment of groundwater for domestic and irrigation uses. *Civil Engineering Journal*, 5(9), 1877-1892. https://doi.org/10.28991/cej-2019-03091379

IPCC. (2013). Summary for Policymakers. *In Climate Change 2013: The Physical Sciences Basis. Contribution of Working Group I to the Fifth Assesment Report of the Intergovernmental Panel on Climate Change; Stocker*, T. F., Qin, D., Plattner, G. K., Tignor, M., Allen, S.K., Boschung, J., Nauels, A., Xia, Y., Bex, V., Midgley, P.M., Eds.; Cambridge University Press: Cambridge, UK; New York, NY, USA.

Karashima, K., Ohgai, A. & Saito, Y. (2014). A GIS-Based Support Tool for Exploring Landuse

Policy Considering Future Depopulation and Urban Vulnerability to Natural Disasters-A Case Study of Toyohashi City, Japan. *Procedia Environmental Sciences,* 22, 148-155. DOI:10.1016/j.proenv.2014.11.015

Karimi, M., Ghanbari, A. A. & Amiri, S. (2012). Assessing the Vulnerability of Urban Settlements to the Phenomenon of Land Subsidence, A Case Study: District 18 of Tehran. *Spatial Planning,* 3(1), 55-37. (In Persian) https://www.sid.ir/paper/395139/fa

Karimzadeh, S. & Matsuoka, M. (2020). Remote sensing x-band SAR data for land subsidence and pavement monitoring. *Sensors,* 20(17), 4751. https://doi.org/10.3390/s20174751

Kim, H. & Marcouiller, D. W. (2015). *Urban vulnerability and resiliency to natural disasters: an integrative tourism planning perspective*. 1st Edition. Routledge. ISBN: 9781315572109

Liu, L., Jafarov, E. E., Schaefer, K. M., Jones, B. M., Zebker, H. A., Williams, C. A., Rogan, J. & Zhang, T. (2014). InSAR Detects Increase in Surface Subsidence Caused by an Arctic Tundra Fire. *Geophys. Res. Lett,* 41, 3906-3913. https://doi.org/10.1002/2014GL060533

Mahmoudpour, M., Khamehchiyan, M., Nikudel, M. R. & Ghassemi, M. R. (2016). Numerical Simulation and Prediction of Regional Land Subsidence Caused by Groundwater Exploitation in the Southwest Plain of Tehran, Iran. *Engineering Geology,* 201, 6-28. DOI:10.1080/22797254.2020.1759455

Mayoral, J. M., Tepacapa, S., Roman de la Sancha, A., El Mohtar, C. S. & Rivas, R. (2019). Ground Subsidence and Its Implication on Building Seismic Performance. *Soil Dynamics and Earthquake Engineering,* 126, 105766. https://doi.org/10.1016/j.soildyn.2019.105766

Mehrnour, S., Robati, M., Khairkhah-Zarkash, M. M., Farsad, F. & Bikpour, S. (2022). Land Subsidence Risk Zoning in Hashtgerd Plain Based on Multi-Criteria Integrated Decision-Making Approach: WOI-BWM. *Journal of Geography and Environmental Hazards,* 11(4), 148-127. (In Persian) https://geoeh.um.ac.ir/article_42619.html

MohammadiDeh-Ceshmeh, M. (2012). *Passive urban safety and defense*. Shahid Chamran University Press. Ahvaz. Iran. (In Persian) https://www.gisoom.com/book/11022222/

Motagh, M., Shamshiri, R., Haghighi, M., Wetzel, H., Akbari, B., Nahavandchi, H., Roessner, S. & Arabi, S. (2017). Quantifying Groundwater Exploitation Induced Subsidence in the Rafsanjan Plain, Southeastern Iran, Using InSAR Time-Series and in Situ Measurements. *Eng Geol*, 218, 134-151. https://doi.org/10.1016/j.enggeo.2017.01.011

Okada, S. & Takai, N. (2000). Classification of structural types and damage patterns of building for earthquake field investigation, *Twelfth World Conference on Earthquake Engineering. Balkema, Rotterdam*. https://doi.org/10.3130/AIJS.64.65_5

Orhan, O., Oliver-Cabrera, T., Wdowinski, S., Yalvac, S. & Yakar, M. (2021). Land Subsidence and Its Relations with Sinkhole Activity in Karapınar Region, Turkey: A Multi-Sensor InSAR Time Series Study. *Sensors,* 21(3),774. https://doi.org/10.3390/s21030774

Oruji, S., Ketabdar, M., Gregorian, K. & Motamed, R. (2019). Climate change resiliency of natural gas pipelines: Overview of land subsidence and associated issues in central California. *International Conference on Sustainable Infrastructure*. https://doi.org/10.1061/9780784482650.001

Osmanoğlu, B., Dixon, T. H., Wdowinski, S., Cabral-Cano, E. & Jiang, Y. (2011). Mexico City Subsidence Observed with Persistent Scatterer InSAR. *Int. J. Appl. Earth Obs. Geoinf,* 13(1), 1-12. https://doi.org/10.1016/j.jag.2010.05.009

Paine, J. G., Buckley, S., Collins, E. W., Wilson, C. R. & Kress, W. (2009). Assessing sinkhole potential at Wink and Daisetta using gravity and radar interferometry. In *Symposium on the Application of Geophysics to Engineering and Environmental Problems; Society of Exploration Geophysicists*: Tulsa, OK, USA. pp. 480-488. DOI:10.4133/1.3176733

Paton, D. & Fohnston, D. M. (2001). Disaster and communities: vulnerability, resilience and preparedness. *Disaster, Prevention and Management*, 10(4). DOI:10.1108/EUM0000000005930

Peacock, W. G., Gladwin, H. & Hearn Morrow, B. (1997). *Hurricane Andrew: ethnicity, gender and the sociology of disaster*. London: Routledge. ISBN: 9780203351628. https://doi.org/10.4324/9780203351628

Poland, J. F. (1984). *Guidebook to studies of land subsidence due to ground-water withdrawal*; UNESCO, International Hydrological Programme: Paris, France. https://wwwrcamnl.wr.usgs.gov/rgws/Unesco/

Qu, F., Zhang, Q., Lu, Z., Zhao, C., Yang, C. & Zhang, J. (2014). Land Subsidence and Ground Fissures in Xi'an, China 2005-2012 Revealed by Multi-Band InSAR Time-Series Analysis. *Remote Sens. Environ,* 155, 366-376. DOI:10.1016/j.rse.2014.09.008

Recchia, F. (2008). Immigration, Politics and Violence in Urban France: Between Fiction and Facts. *Information, Society and Justice,* 2(1), 47-61. DOI:10.3734/isj.2008.2105

Rezaei, M., Yazdani Noori, Z. & Dashti Barmaki, M. (2020). Land Subsidence Susceptibility Mapping Using Analytical Hierarchy Process (AHP) and Certain Factor (CF) Models at Neyshabur Plain, Iran. *Geocarto Int*, 37(5), 1-20. https://doi.org/10.1080/10106049.2020.1768596

Roustaei, S. & NajafVand, S. (2022). Monitoring the subsidence phenomenon of the plains based on the SNAP2STAMPS automatic algorithm using the radar interferometry (PSI) method (case study: Marand plain). *Journal of Geography and Environmental Hazards,* 11(4), 21-42. (In Persian) https://geoeh.um.ac.ir/article_41839.html

Saaty T. L. (2005), Theory and applications of the ANP: Decision making with benefits, opportunities, costs, and risks; *RWS Publications*. ISBN: 1888603062

Saqazadeh, N., Ghasemieh, H., Omidvar, I. & Maqsoudi, Y. (2022). Evaluating the Effectiveness of Two-Variable Models in Determining the Sensitivity of Subsidence of the Kashan Plain Aquifer. *Journal of Geography and Environmental Hazards,* 11(4), 69-98. (In Persian) https://geoeh.um.ac.ir/article_42364.html

Sennewald, C. A. & Baillie, C. (2015). *Effective security management: butterworth-heinemann*. ISBN-13: 978-0128027745

SharifiKia, M., Mal-Amiri, N. & Shayan, S. (2012). Measuring the Vulnerability of Urban Tissues Against the Risk of Land Subsidence (Case Study: A Part of Southern Tehran). *Journal of Geography and Environmental Hazards,* 2(5), 91-106. (In Persian) https://sid.ir/paper/226708/fa

Siyami, Q., Latifi, G., Taghinjad, K. & Zahedi Kalaki, I. (2013). Pathology of Urban Structure Defense Using Hierarchical Analysis of AHP and GIS; A Case Study of Gorgan City. *Study of Space Geography*, 3(10), 21-42. (In Persian) http://gps.gu.ac.ir/article_7382.html

Tavakoli, H. & Akbarpour, S. (2010). Building improvement considerations against progressive components. *The first conference on passive defense and resistant structures*. (In Persian) https://civilica.com/doc/126066

Tierney, K. (2006). *Social inequality, hazards, and disasters in on risk and disaster: lessons from Hurricane Katrina*. Edited by Daniels, R. J, Kettl, D. F, Kunreuther, H. Philadelphia: University of Pennsylvania Press. https://doi.org/10.9783/9780812205473

Tung, H. & Hu, J. C. (2012). Assessments of serious anthropogenic land subsidence in Yunlin county ofcentralTaiwanfrom1996to1999by persistent scatterers Insar. *Tectonophysics,* 578, 126-135. https://doi.org/10.1016/j.tecto.2012.08.009

Üstün, A., Tuşat, E., Yalvaç, S., Özkan, İ., … (2015). Land Subsidence in Konya Closed Basin and its Spatio-Temporal Detection by GPS and DInSAR. *Environ. Earth Sci*, 73, 6691-6703. DOI:10.1007/s12665-014-3890-5

Vousdoukas, M. I., Mentaschi, L., Voukouvalas, E., Verlaan, M. & Feyen, L. (2017). Extreme Sea Level Rise Along Europe's Coast. *Earth's Future*, 5(3), 304-323. https://doi.org/10.1002/2016EF000505

Website of District 17 of Tehran Municipality. (2020).

Wu, J. C., Shi, X. Q., Ye, S. S. J., Xue, Y. Q., Zhang, Y. & Yu, J. (2009). Numerical Simulation of the Land Subsidence Induced by Groundwater Overexploitation in Su-Xi-Chang Area, China. *Environ. Geol,* 57, 1409-1421. https://doi.org/10.1007/s00254-008-1419-5

Yalvac, S. (2020). Validating InSAR-SBAS Results by Means of Different GNSS Analysis Techniques in Medium-and High-Grade Deformation Areas. *Environ. Monit. Assess,* 192(2), 120. DOI:10.1007/s10661-019-8009-8

Yamani, M., Najafi, I. & Abedini, M. H. (2009). The Relationship Between Ground Subsidence and Groundwater Level Drop in Qarabalag Plain of Fars Province. *Journal of Geography,* 3(8-9), 9-27. (In Persian) https://www.sid.ir/paper/208007/fa

Zebardast, E. (2011). Application of Network Analysis Process (ANP) in Urban and Regional Planning. *Journal of Fine Arts*, 2(41), 73-96. https://jfaup.ut.ac.ir/article_22270.html

Zhang, L. (2019). Big Data, Knowledge Mapping for SustainableDevelopment: A WaterQualityIndex Case Study. *Emerging Science Journal,* 3(4). https://doi.org/10.28991/esj-2019-01187

Araştırma Makalesi/Research Article
https://doi.org/10.51489/tuzal.1300939

2023; 5(1); 50-58

Turkish Journal of Remote Sensing

Türkiye Uzaktan Algılama Dergisi

https://dergipark.org.tr/tr/pub/tuzal

e-ISSN 2687-4997

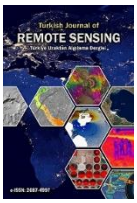

Göktürk-1 Uydu Görüntülerinden U-Net Modeli Kullanılarak Binaların Segmentasyonu

Duygu ARIKAN*[1], Ferruh YILDIZ[1]

[1]Konya Teknik Üniversitesi, Mühendislik ve Doğa Bilimleri Fakültesi, Harita Mühendisliği Bölümü, Konya, Türkiye

Anahtar Kelimeler:
Derin Öğrenme
U-Net mimarisi
Göktürk-1 Uydu Görüntüsü
Bina çıkarımı

ÖZ

Nüfus artışı, kentsel bölgelerde plansız yapılaşmanın ortaya çıkmasına yol açmaktadır. Bu durum dünya genelinde bir sorun haline gelmiştir. Bu alanların belirlenmesi ve tespit edilmesi, kentsel yönetim ve yeniden yapılanma planlaması için büyük öneme sahiptir. Ancak bu işlemler, arazide maliyetli ve zaman alıcı olabilmektedir. Uzaktan algılama görüntüleri kullanarak kentsel ve kırsal bölgelerde plansız yapılan binaları otomatik olarak tespit etmek ve karakterize etmek oldukça zordur. Son zamanlarda, derin öğrenme yöntemleri sayesinde karmaşık binaların tespiti mümkün hale gelmiştir. Bu çalışmada, Ankara'nın Etimesgut ilçesinden bir bölgenin bina çıkarımı işlemi, U-Net derin öğrenme mimarisi kullanılarak gerçekleştirilmiştir. İşlem için Inria Aerial Image Labeling adlı hazır bir veri seti kullanılmıştır. Eğitim işlemi için farklı sayıda görüntü (500, 1000, 2500, 5000) seçilmiştir. En iyi öğrenme sonucu, 0.5 m uzamsal çözünürlüğe sahip Göktürk-1 uydu görüntüleriyle test edilmiştir. Sonuçlara göre, U-Net modelinin bina segmentasyonunda Jaccard katsayısı 0.862, Dice benzerlik oranı 0.813 olarak bulunmuştur. Hazır veri seti kullanılarak U-Net modelinin derin öğrenme yöntemleri için kullanılabilir olduğu kanıtlanmıştır. Bu çalışma, kentsel alanlardaki binaların tespiti ve haritalanmasında derin öğrenme yöntemlerinin etkinliğini ve potansiyelini göstermiştir.

Segmentation of Buildings Using U-Net Model from Göktürk-1 Satellite Images

Keywords:
Deep Learning
U-Net Model
Gokturk-1 Satellite Image
Building Detection

ABSTRACT

The increase in population has led to unplanned urbanization in urban areas, becoming a global issue. The identification and detection of these areas are of great importance for urban management and redevelopment planning. However, these processes can be costly and time-consuming when conducted on-site. Automatic detection and characterization of unplanned buildings in urban and rural areas using remote sensing imagery is a challenging task. Recently, with the advancements in deep learning methods, the detection of complex buildings has become possible. In this study, the building extraction process of a region from the Etimesgut district of Ankara was performed using the U-Net deep learning architecture. The Inria Aerial Image Labeling dataset, a publicly available dataset, was used for the process. Different numbers of images (500, 1000, 2500, 5000) were selected for the training process. The best learning outcome was tested with Göktürk-1 satellite imagery with a spatial resolution of 0.5 m. According to the results, the U-Net model achieved a Jaccard coefficient of 0.862 and a Dice similarity coefficient of 0.813 for building segmentation.The effectiveness and potential of deep learning methods were demonstrated using the U-Net model with the available dataset. This study showcased the efficiency and potential of deep learning methods in the detection and mapping of buildings in urban areas.

Makale Bilgileri/Article Info

Geliş /Received: 23/05/2023
Kabul/Accepted: 23/06/2023
Yayınlanma/Published: 30/06/2023

Alıntı/Citation:

Arıkan, D. & Yıldız, F. (2023). Göktürk-1 Uydu Görüntülerinden U-Net Modeli Kullanılarak Binaların Segmentasyonu. Türkiye Uzaktan Algılama Dergisi , 5 (1) , 50-58 .

***Sorumlu Yazar/Corresponding Author:** Duygu Arıkan, darikan@ktun.edu.tr, +90 332 205 11 11

1. GİRİŞ

Son yirmi yılda insan nüfusu giderek artmakta ve şehirleşme söz konusu olmaktadır. Şehir planlamalarının yapılmasında, afet alanlarının tespit edilmesinde ya da zamansal olarak kentsel değişikliklerin izlenmesi gibi çalışmalarda binaların, yolların, arazi sınıflarının belirlenmesi önem arz etmektedir. Bina konumlarının, geometrik yapılarının belirlenmesi ve haritalanması birçok disiplin için altlık olarak kullanılmaktadır. Bozulan kentsel alanların yeniden yapılandırılması, plansız yerleşim alanlarının tespit edilmesi şehir planlamacıları ve belediye çalışmalarında gerekli olmaktadır (Kuffer vd., 2016; Mahabir vd., 2018; Wurm vd.,2019).

Örneğin; çalışma alanı olarak seçilen Ankara'nın bazı bölgelerinde yüksek katlı binalar, bazı kısımlarında tek katlı bahçeli yapılar bulunurken, bazı kısımlarında da gece kondu mahalleleri bulunmaktadır. Bu durum şehrin fiziksel ve görsel algısını bozmaktadır. Bu tarz yapıların belirlenmesi, kentsel ya da kırsal alanlardaki binaların tespiti, konumlandırılması, öznitelik bilgilerinin belirlenmesi ve sayısallaştırılması işlemi arazide yapılan saha çalışmalarına dayanmaktadır (Wurm vd., 2019). Kentsel bölgelerdeki bina yoğunluğunun fazla olması nedeniyle saha çalışmalarının süre bakımından yavaş olmasına buna bağlı olarak fazla bir maliyet ve emek gerektirmektedir. Bu sebepten, uydu görüntülerinin mekânsal çözünürlüğünün artması ile kentsel alanlarda bina gibi yapıların, ulaşım hatlarının otomatik olarak algılanmasına yönelik çalışmalar uzaktan algılama ile yapılabilmektedir. Bu teknoloji sayesinde düşük maliyet ile büyük alanlara ait bilgiler kısa süre içerisinde elde edilebilir. Ayrıca yapılan işin sürekli güncel olması da sağlanmış olur (Pan vd., 2020; Wurm vd., 2019). Fakat, görüntü üzerinde bulunan meydanlar, yollar gibi detaylar renk (spektral) ve şekil itibariyle bina özelliklerine benzemektedir. Bu karmaşık arka plan nesneleri binayı tespit etmede zorluk haline getirmektedir.

Bu nedenle kentsel alanlardaki binaların tespit edilmesi ve uzaktan algılama tekniğinden yararlanılarak harita üretim işlemi önem arz etmekle birlikte literatürde uzun bir geçmişe sahiptir. Yüksek yapılı binalar ya da bölgedeki bina miktarının yoğunlaştığı kısımlarda, geleneksel görüntü segmentasyon ya da sınıflandırma yöntemlerinin süre yönünden yeterli olmadığı tespit edilmiştir. Bina segmentasyonda, araştırmacılar piksel tabanlı özellik tanımlayıcıları tasarlamışlardı. Örneğin; Tuermer vd. (2013), çalışmada kentsel bölgelerdeki nesneleri tespit etmek amacıyla eğim histogramını (HOG-Histogram of oriented Gradients) kullanmışlardır. Zhang, vd. (2011) çalışmada ise, bina çıkarım işlemi için renk, doku ve şekil özellikleri birleştirilerek daha iyi sınıflandırma performansına ulaşabilmeyi hedeflemişlerdir. Klasik yöntemlere ek olarak, son zamanlarda, bu alanda yapılan çalışmalarda makine öğrenmesi ve derin öğrenme yöntemleri popülerlik kazanmıştır. Mitra vd. (2004) uydu görüntüleri kullanılarak yapılacak denetimli piksel sınıflandırması çalışmalarında gerekli olan etiketli verinin azlığı problemini çözmek amacıyla makine öğrenmesi algoritması olan destek vektör makinesini kullanmışlardır. Pal (2005), arazi sınıflarını tespit etmek amacıyla rastgele orman algoritmasını kullanmışlardır. Yapılan çalışmalarda geleneksel makine öğrenme algoritmalarının, çözümleyemediği ve eksik kaldığı kısımlar olduğu anlaşılmıştır. Etiketli veriyi oluşturmak için manuel bir işlem adımı olması dezavantaj olarak görülmektedir. Ayrıca bu çalışmalarda kullanılan donanımın da iyi olması gerekmektedir. Çünkü verilerin ya da görüntülerin işlenmesi süre bakımından önem arz etmektedir. Bu nedenle, GPU hesaplama hızındaki artış, Google Colab GPU kullanımının belirli sınırlamalar dahilinde ücretsiz kullanılması araştırmacıları derin öğrenme algoritma yöntemlerine yönlendirmiştir. Derin öğrenme algoritmalarından biri olan evrişimli sinir ağları (ESA) özellikle bina çıkarımı, yol çıkarımı gibi nesne çıkarımında başarılı bir şekilde kullanılmaktadır (Kattenborn vd., 2021; X. Li vd., 2023; Pan vd., 2020; Wurm vd., 2019). İlk olarak sağlık alanındaki görüntülerde, daha sonra yapılan çalışmalarda otonom araçlarda, arttırılmış gerçeklik çalışmalarında, arazi sınıflarının belirlenmesi gibi çalışmalarda ESA tercih edilmektedir (Sariturk & Seker, 2022). Yöntemde ağ eğitimi için girdi verilerine ait etiketlenmiş veriler arasında ilişkiler kurulmaktadır. Ağ eğitimi kullanılan bilgisayarın performansına göre değişkenlik göstermekte ve dezavantaj olarak görülmektedir (Zhu vd., 2017). Bu sebepten ötürü farklı ağ mimarileri oluşturulmuştur ve bunlardan bir tanesi de U-Net mimarisidir. Görüntü segmentasyonu için tasarlanmış ve tam evrişimli olan bu mimarinin yapısı kodlayıcı (sol taraf)-kod çözücü (sağ taraf) iki ana kısımdan oluşmaktadır. Simetrik yapısından dolayı ismini buradan almıştır (Hou, vd., 2021; Ronneberger vd., 2015).

Kentsel alandaki çalışmalarda U-Net algoritması kullanılarak birden çok çalışma bulunmaktadır. Temeldeki amaç kentsel alanlardaki bina çıkarımı olsa da kullanılan materyal-metot farklı olabilmektedir. Çeşitli uydu görüntüleri, havadan alınan görüntüler ya da hava lidar teknolojisinden yararlanılabilmektedir. Örneğin; L. Li vd. (2019), yaptıkları çalışmada Sentinel-1 SAR uydu görüntüsünü kullanırken, Abdollahi ve Pradhan (2021) ve Wu vd. (2018) hava görüntülerini kullanarak sınıflandırma işlemini gerçekleştirmişlerdir. Ayrıca U-Net ve diğer derin öğrenme algoritmalarını geliştirmek amacıyla kullanıcılara ücretsiz sunulan veriler de bulunmaktadır. Massachusetts (Mnih, 2013), Inria (Maggiori, vd., 2017) ve WHU bina veri kümeleri (Ji, Wei, & Lu, 2018) mevcut ve kullanıcılara açıktır.

Sinir ağlarının ve uydu verilerinin çeşitlilik kazanması, erişim imkanının kolay olması nedeniyle bu çalışmada, Inria Aerial Image Labeling Dataset

kullanılmıştır. Binaların segmentasyon işlemi U-Net mimarisi ile gerçekleştirilmiştir. Bu model kullanılırken eğitim verisinin ve epok sayısının sonuçlara olan etkisi irdelenmiştir. Ek olarak, en iyi optimizasyon sonucuyla, Göktürk-1 uydu görüntüsünden yararlanılarak bina segmentasyonu işlemi gerçekleştirilmiştir. Çalışmada mimarinin oluşturulması ve eğitilmesi, test işlemleri MSI diz üstü bilgisayarında gerçekleştirilmiştir. Bu çalışmanın literatüre katkısı U-Net mimarisi kullanılarak ilk kez Göktürk-1 uydu görüntüsünden bina tespiti çalışması gerçekleştirilmiştir. Yapılan bu çalışma 3 ana kısımdan oluşmaktadır. Birinci bölümünde, kullanılan veri seti, U-Net mimari ve çeşitli optimizasyon yöntemlerinin açıklanması, İkinci bölümünde farklı sayıda kullanılan veriler ile epok sayısının sonuçları ve Göktürk uydu görüntüsünde test edilmesi, son bölümde ise sonuçlar ve tartışma kısmıdır.

2. YÖNTEM

2.1. Veri Seti

Çalışmada eğitim verisi olarak "Inria Aerial Image Labelling Dataset (Etiketli Hava Görüntüsünün Veri Kümesi)" kullanılmıştır. Bu veri seti içerisinde bölgeler yoğun nüfuslu bölgeler (Austin, Chicago gibi) ve kırsal kasaba (Avusturya Tyrol) olacak şekilde farklı alanları içermektedir (Maggiori vd., 2017). Bu sayede farklı lokasyonlarda bulunan, farklı bina türlerinin bulunduğu görüntülerinin kullanılması modellemenin gücünü arttırmaktadır. Kullanılan görüntüler ve maskeler 5000 × 5000 piksel boyutunda olup, her biri 1500 m × 1500 m'lik bir alanı kaplamaktadırlar. Ayrıca birbirleriyle örtüşmeyecek şekilde ayarlanmış ve görüntülerin mekansal çözünürlüğü 0,3 m'dir. Çalışma kapsamında eğitim ve test amaçlı kullanılan görüntüler 3 bantlı (kırmızı, yeşil ve mavi) ve tek bantlı maskelenmiş görüntülerdir.

Çalışmanın son kısmında Inria veri setinde eğitilmiş modellerden en yüksek doğruluklu model alınarak, Göktürk-1 uydusunda test edilmiş ve sonuçları incelenmiştir. Bu uydu 2018 yılında fırlatışmış olup, RGB'de 0.5 m, pankromatikte de 2 m konumsal çözünürlüğe sahiptir. Uydu görüntüsü Ankara iline aittir. Şehir, Türkiye'nin başkenti olup, kentsel bölgelerde yoğun yapıların yer aldığı, bazı kısımlarında ise gece kondu mahallerinin bulunduğu bölgeler incelenmiştir. Çoğu makalede kullanılan görseller temel olarak üç kanaldan (Kırmızı, Yeşil ve Mavi) oluşur. Bu nedenle çalışmamızda hem örnek veri setinde hem de Göktürk-1 uydu görüntüsünden RGB görüntüler kullanılmıştır. Çalışmanın iş akış diyagramı Şekil1'de sunulmuştur. Derin öğrenme ağı eğitim ve modellemesi aşamaları, dört çekirdekli Intel Core i7 işlemci, NVIDIA GTX 850M GPU ve 32GB hafızaya sahip MSI dizüstü bilgisayarda yapılmıştır.

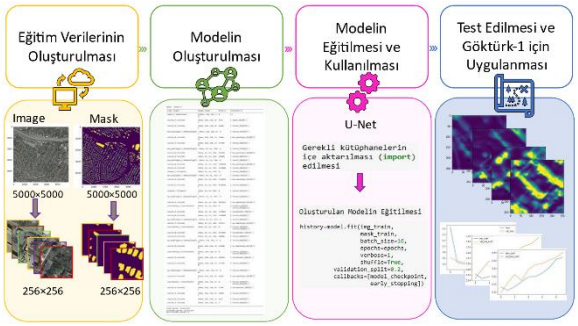

Şekil 1. İş – akış diyagramı

2.2. U-Net Mimarisi

Çalışmada U-Net mimarisi kullanılmıştır. Bu mimari yapı, Ronneberger ve diğerleri tarafından geliştirilmiş olan tekrarlayan evrişimli bloklardan oluşan bir sinir ağı mimarisidir (Ronneberger vd., 2015b; Sariturk & Seker, 2022). U-Net mimarisi daha çok segmentasyon, sınıflandırma ve görüntüler üzerinde çalışmalar yapmak amaçlı geliştirilmiş bir görüntü segmentasyon algoritmasıdır (Yan vd., 2022). Şekil 2'de yapılan çalışmadaki katman adımları verilmiştir ve modelin 'U' harfi şeklinde olduğu açıkça görülmektedir. Kod oluşturucu kısımda eğitim verilerinden özelliklerin çıkartılması sağlanır ve bir kodlayıcı blok dizi aracılığıyla giriş görüntülerinin soyut bir temsilini öğrenir. Her bir kod oluşturucu (enkoder) kısımda ReLU aktivasyon fonksiyonu tarafından takip edilen 3x3 evrişim ağından oluşmaktadır. RELU fonksiyonu eğitim verilerinin genelleştirilmesine yardımcı olurken, aynı zamanda ağında doğrusal olmamasına imkân vermektedir. Bu işlemlerden sonra özellik haritalarının ya da görsellerin boyutlarının yarıya indirildiği 2x2 maksimum havuzlama kısmı gelir. Kod çözümleyici blok kısmı 2x2 evrişim ağı ile başlar ve kodlayıcı bloğun atlamalı bağlantı özellik haritasıyla birleştirilir. Bundan sonraki her bir adımda evrişimin ReLU aktivasyon kodu tarafından takip edildiği 3x3 evrişim ağı kullanılır (Atlan, vd., 2020).

Kod çözücü kısımda ise eğitilen verilerin maskeleri oluşturulur. Bu kısım 2x2 devrik evrişim ağ ile başlar. Sonrasında kod oluşturucu bloktaki özellik haritasıyla birleştirilir. Bundan sonra, her bir evrişimin bir ReLU aktivasyon fonksiyonu tarafından takip edildiği iki 3x3 evrişim kullanılır. Son kod çözücünün çıkışı, sigmoid aktivasyonu ile 1x1 evrişimden geçer. Sigmoid aktivasyon işlevi, piksel bazında sınıflandırmayı temsil eden segmentasyon maskesini verir. Oluşturulan model Şekil. 2'de sunulmuştur.

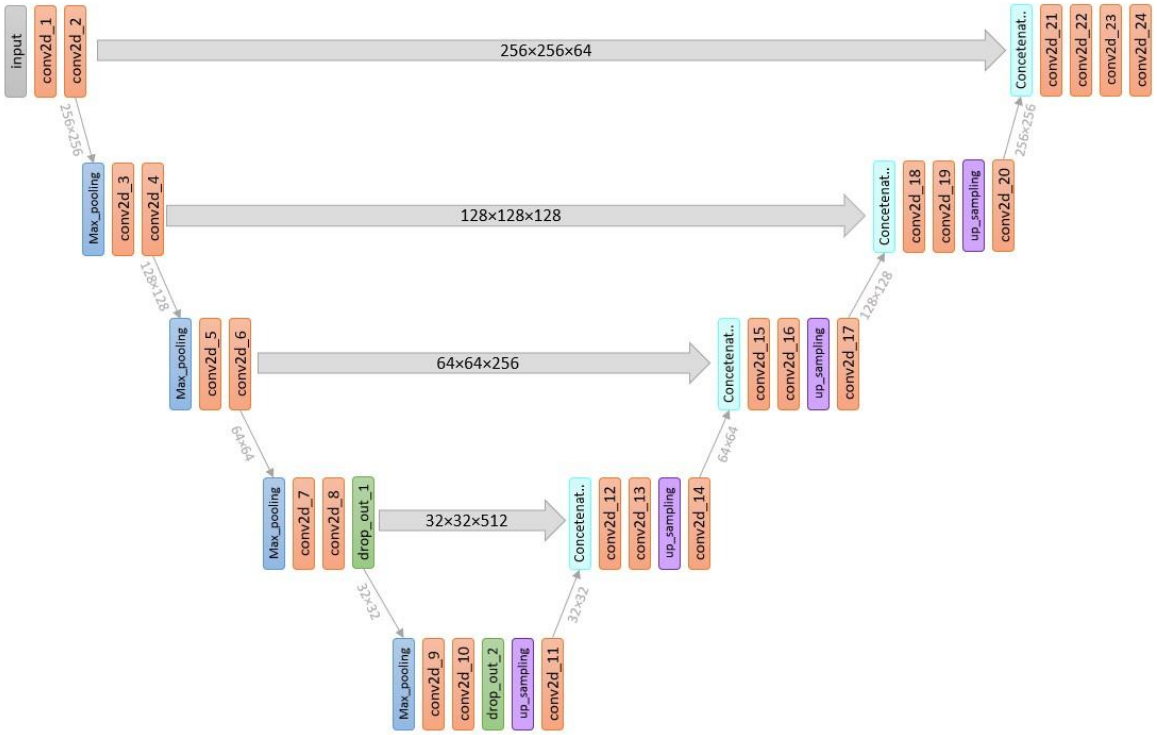

Şekil 2. Çalışma da kullanılan U-Net Modelinin Katmanları

2.3. Optimize Edilen Parametreler

Yapay zekâ uygulamalarında, veri setinin aynı anda işlenmesi ve öğrenme durumu için model eğitiminde optimizasyon seçenekleri vardır. Bunlar; epok sayısı, batch size ve aktivasyon fonksiyonları olarak ifade edilen optimizasyon yöntemleri bulunmaktadır. İfade edilen seçeneklerden herhangi bir parametrenin değiştirilmesi modelin başarı performansını etkilemektedir (Öz, 2021).

Batch size genellikle epok sayısı ile karıştırılan iki farklı kavramdır. Batch size öğrenme işlemi sırasında her iterasyon için hesap işleminin yapılmasını ifade ederken, epok sayısı da bir öğrenme için gerçekleştirilecek işlemdir. Batch size birden fazla girdi verisinin parçalar halinde işlenmesini ifade etmektedir. Böylelikle öğrenme işlemi gerçekleştirilirken her bir iterasyon işleminde ağırlık değerleri güncellenmekte ve hata oranları minimum seviyeye indirgenmektedir. Kısacası batch size verilerin her bir adımda işlenme miktarını belirtirken, epok sayısı tam bir eğitim veri setinin kaç kez işleneceğini belirtir. Örneğin; 2500'lük bir eğitim veri setinin batch size değeri 5 seçildiğinde, bu veri seti 500'lük gruplara bölünür. 1 epoğu tamamlamak için de 5 adet batch size işleminin yapılması gerekmektedir.

Bu parametrelerin sabit bir değer seçilmesi gibi bir durum söz konusu değildir. Modelin performansı aynı zamanda eğitim verisinin boyutlarına ve öğrenme hızına göre değişkenlik göstermektedir. Batch size değerinin 1 seçilmemesi tavsiye edilir. Çünkü, modelin genelleştirme yeteneklerini sınırlandırmaktadır (Öz, 2021).

Aktivasyon fonksiyonları, sinir ağlarında bir nöronun tetiklenip tetiklenmeyeceğine karar vermek amacıyla girdi verilerinin ve ağırlıklarının toplamını hesaplamak için kullanılan bir işlev görevindedir (Nwankpa, vd., 2018). Bu nedenle aktivasyon fonksiyonlarının seçimi ve kullanılması derin öğrenme algoritmalarında önemli bir yere sahiptir (Ramachandran, vd., 2017). Çünkü, algoritma içerisinde çok fazla katman (girdi, gizli ve çıkış) ve ağırlıklar tanımlanmaktadır. Ağ içerisindeki her bir katmana aktivasyon işlemi uygulanır ki, daha sonrasında bu katman bir başka katman için giriş katmanı olarak kullanılabilsin.

Derin öğrenme algoritmalarında görüntü, video, ses gibi karmaşık yapıdaki bilgeleri aktivasyon fonksiyonları sayesinde anlamlı özellikleri çıkartabilmektedir. Eğer bu fonksiyonlar kullanılmazsa, sinir ağı sınırlı öğrenme gücüne sahip tek dereceli bir polinom fonksiyonu işlemi yürütecektir. Fakat, girdi verileri sadece doğrusal yapıda olmadığı için, bu durum da ağın iyi eğitilememesini ifade eder. Bu nedenle doğrusal olmayan durumlarında öğrenilebilmesi için aktivasyon fonksiyonlarından yararlanılmaktadır. Yapay sinir ağlarında sıkça kullanılan aktivasyonlar, sigmoid, tanh, relu ve Leaky ReLu olarak ifade edilebilir. Aktivasyon fonksiyonları ve matematiksel modelleri Şekil 3'te sunulmuştur. Literatürde lojistik fonksiyon ya da ezici fonksiyon olarak da bilinen (logistic function or squashing function) sigmoid fonksiyonu karar vermeye yönelik olasılıksal bir yaklaşım olup, [0-1] aralığında değer almaktadır (Nwankpa vd., 2018). Eğer sürekli türevi alınabiliyorsa, bu fonksiyon girdi verisini öğrenmeye başladığı anlamına gelmektedir. Derin öğrenme

mimarilerinde daha çok çıktı katmanında yer almaktadır (Nwankpa vd., 2018). Tanh fonksiyonu sigmoid fonksiyonuna yapı olarak çok benzemektedir. Fakat tanh fonksiyonunda değer aralığı [-1,1] ve orijin etrafında simetriktir (Nwankpa vd., 2018). Bu fonksiyonun en önemli problemi uç noktalarda türevi sıfıra yaklaşmaktadır. Bu yüzden modeldeki katman sayısına bakılarak bu fonksiyon seçimi gerçekleştirilir. Eğer model çok katmanlı bir ağdan oluşuyorsa sigmoid ve tanh fonksiyonlarınının kullanılmaması tercih edilir. Daha çok evrişimli sinir ağlarında tercih edilen ReLu fonksiyonu tanh ve sigmoid fonksiyonuna göre daha verimli ve hızlı çalışmaktadır (Ramachandran vd., 2017; Zeiler vd., 2013). Bu neden ara katmanlarda bu fonksiyon tercih edilmektedir. Tanh fonksiyonunun tersine ReLu fonksiyonu çok katmanlı sinir ağlarında tercih edilmektedir. Fakat, ReLu fonksiyonu da geri yayılım sırasında pozitif olduğu durumda aktif işlem gerçekleşirken, negatif olduğu durumda sadece sıfır olması dezavantajı olarak karşımıza çıkmaktadır (Madhu, vd., 2023). Leaky (sızıntı) ReLu ise, ReLu fonksiyonundaki sınırlamayı kaldırmak amaçlı geliştirmiş olup, sıfır olmayan bir gradyana sahiptir (Maas, vd., 2013).

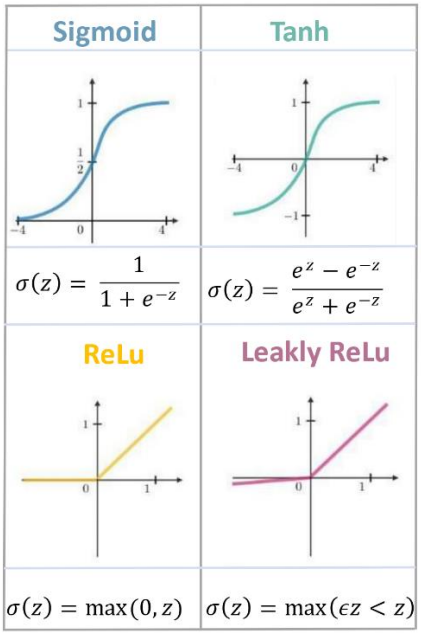

Şekil 3. Aktivasyon fonksiyonları ve matematiksel modelleri (Nwankpa vd., 2018)

2.4. Metrikler

Uydu görüntüleri kullanılarak segmentasyon işlemlerinde metriklerin hesaplanması gerekmektedir. Çünkü yöntemin performansının nicel olarak değerlendirilmesi gerekmektedir. Bunun için doğruluk, kesinlik, F-ölçüsü, Jaccard indeksi (IoU), Dice benzerlik katsayısı metriklerinden yararlanılmaktadır. Bu çalışma kapsamında görüntü segmentasyonunda yaygın olarak tercih edilen doğruluk ölçütü Dice benzerlik ve Jaccard katsayıları kullanılmıştır.

Dice Benzerlik katsayısı, maskelenmiş görüntü ile tahmin edilen görüntü arasındaki çakışma derecesini ifade eder. 0 ve 1 arasında değer almaktadır (Ataş, 2023). 1'e yakın olması durumunda model sınıflandırmasının iyi olduğunu ifade ederken, 0'a yakın olması durumunda tam tersi durum geçerlidir (Zhang et al., 2019). Matematiksel formülü Eşitlik 1'de verilmiştir.

$$DBK = \frac{2|X \cap Y|}{(|X|+|Y|)} \quad (1)$$

Jaccard katsayısı ise, benzerlik ölçmek için kullanılan bir istatiksel yöntemdir (Zhang et al., 2019). İki kümenin kesişimlerinin birleşimlerine oranı olarak ifade edilmektedir (Ataş, 2023). Doğruluk değeri 0 ve 1 arasındadır. Matematiksel formülü Eşitlik 2'de verilmiştir.

$$J(X,Y) = \frac{|X \cap Y|}{|X \cup Y|} \quad (2)$$

Eşitliklerde kullanılan X maskelenmiş görüntüleri ve Y ise model sonucunda tahmin edilen görüntüyü ifade etmektedir.

U-Net mimarisi ve yapılan tüm segmentasyon işlemleri için Python programlama dili kullanılmıştır. Python, açık erişim tabanlı olup, kullanımı kolay, nesne yönelimli ve etkileşimi yüksek bir programlama dilidir. İçerisinde bulunan kütüphaneler vasıtasıyla, birçok işlemi doğrudan gerçekleştirilebilir (Bayraktar, 2018). Bu çalışmada kodlama işlemi yapılırken farklı kütüphanelerden yararlanılmıştır. Bunlar; numpy, os, cv2, h5py, matplotlib, keras ve tensorflowdur.

İşlemlerdeki hesaplama maliyetini azaltmak ve veri kümesinin boyutunu artırmak amacıyla 5000 × 5000 piksellik görüntüler ve etiketlenmiş görüntülerin boyutu 256 × 256 piksel olacak şekilde yeniden boyutlandırıldı. Toplamda 20.090 görüntü bulunmaktadır. Fakat çalışmada kullanılan görüntülerin sayısı Tablo 1'de sunularak, dört kısımda ele alınmıştır. 1. Kısım da görüntüler eğitilirken yaklaşık %50'si eğitim, %25'i test ve %25'i de doğrulama verisi olarak kullanılmıştır. Sonraki kısımlarda test ve doğrulma sayıları aynı tutulmuş, fakat eğitim verisindeki görüntü sayıları arttırılmıştır. Sırasıyla 1000,2500 ve 5000 olarak seçilmiştir. Çalışmada farklı eğitim ve test verilerinin sonuca katkısı incelenmiş olup, çalışmada kullanılan görüntülerin sayıları tabloda verilmiştir.

Tablo 1. Modelde kullanılan eğitim, test ve doğrulama verilerinin sayısı

	Eğitim Verisi	Test Verisi	Doğrulama Verisi
1.Kısım	500	250	250
2. Kısım	1000	250	250
3. Kısım	2500	250	250
4. Kısım	5000	250	250

3. BULGULAR

Farklı sayıdaki her bir eğitim verisi için model çalıştırılmış ve Şekil 4'te sunulmuştur. Çok fazla görüntü olduğu ve sonuçları görsel olarak ifade edebilmek için, test verisi içerisinden bina yoğunluğun fazla olduğu alanlardan, hiç olmayacak şekilde 4 adet görüntü seçilmiştir ve model sonunda öğrenme durumları verilmiştir. Şekil 4'te 1 numaralı görüntü de bina bulunmamaktadır, 2 ve 3 numaralı görüntüde küçük iki bina vardır. 4 numaralı görüntüde ise karmaşık bir bina görüntüsü yer almaktadır. 2 numaralı görüntü de ayrıca otoparkın bulunması spektral ve dokusal olarak binaya benzemektedir. Bundan dolayı model sonucunda doğruluğu test etmek amacıyla özellikle seçilmiştir.

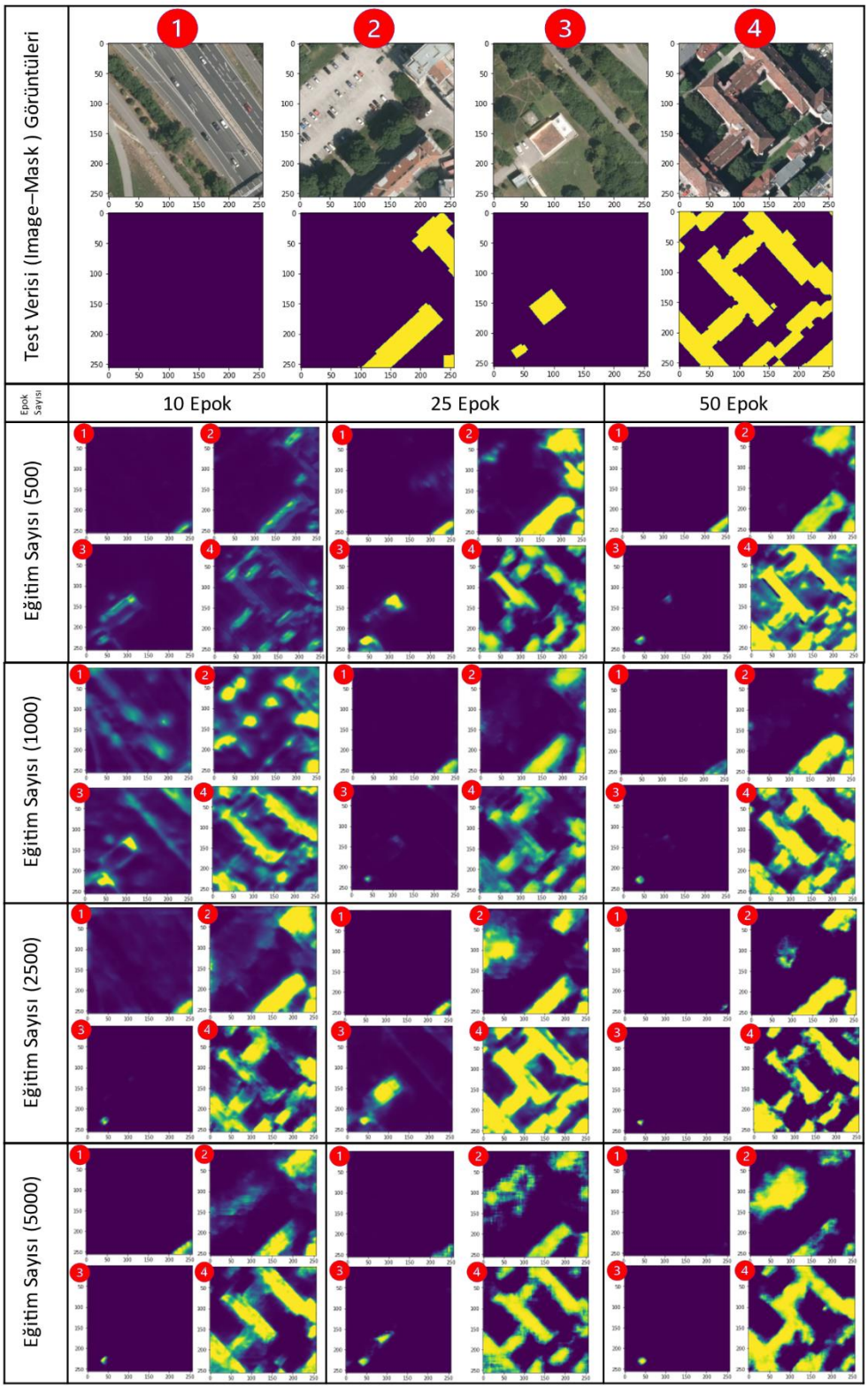

Şekil 4. Öğrenme sonucunda elde edilen görüntüler

Çalışma da epok sayısındaki miktarının sonuca olan etkisi incelenmiştir. Epok sayısı arttıkça eğitim ve doğrulamanın doğruluğu artarken, kayıp oranında azalmalar olduğu tespit edilmiştir. Çalışmada eğitim sayısı 500 ve epok sayısı 10 iken, öğrenme durumu neredeyse olmamıştır. Fakat epok sayısı arttıkça binaların bulunduğu kısımlar belirginleşmeye başlamıştır. Sadece öğrenme işlemi yeterli olmamıştır. Bu nedenle çalışmada eğitim verisinin miktarı arttırılmıştır. Eğitim sayısı 1000 ve epok sayısı 10 olduğunda 1 numaralı görüntü de bina olmamasına rağmen, yol ağlarının rengini bina olarak algılamış, aynı şekilde 2 numaralı görüntüde otopark kısmını ve bazı araçlar, 3 numaralı görüntü de ise yol ağı bina olarak algılanmıştır. 10 epok için tüm eğitim verileri incelendiğinde eğitim sayısı 5000 olan modelin sonucu diğerlerine göre daha iyi olduğu anlaşılmaktadır.

Doğruluk artışı ve kayıp düşüşü başlangıçta hızlı bir şekilde değişime uğrarken, ardından olarak sabit hale geldi. 10 epokluk eğitimde 4. epoktan sonra, 25 epokluk eğitimde 11. epoktan sonra ve 50 epokluk eğitimde 21. epoktan sonra doğruluk artışı ve kayıp miktarındaki değişimler azalmaya başlamıştır.

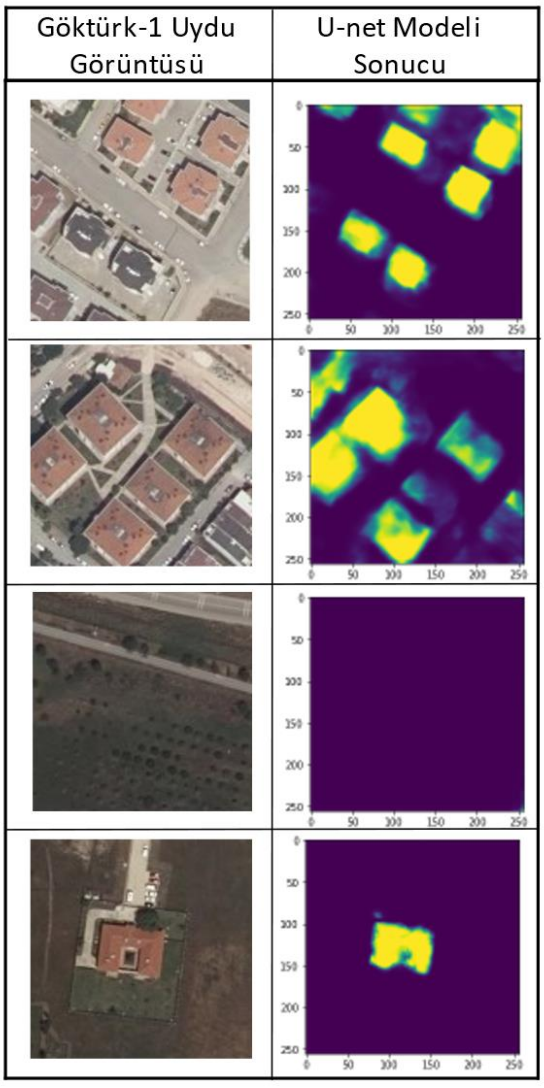

Şekil 5. U-Net modeli sonucu Göktürk-1 görüntülerinden bina çıkarımı

Eğitim verisi 2500 ve epok sayısı 25 için Göktürk-1 verilerinden U-Net modeli kullanılarak bina çıkarımı gerçekleştirilmiştir. U-Net modelinin bina segmentasyonu için Jaccard katsayısı için 0.862 iken, Dice benzerlik oranı 0.813 çıkmıştır. Her iki doğruluk ölçütü de benzer sonuçlar verdiği görülmüştür. Maskelenmiş görüntüler ve tahmin edilen görüntülerin %81 oranında doğru eşlendiği tespit edilmiştir. Bundan dolayı aynı model Göktürk için de uyarlanmış ve test edilmiştir. Şekil 5' te sonuçları verilmiştir.

4. SONUÇLAR

Kentsel bölgelerde otomatik olarak bina çıkarım işlemi uzun ve zahmetli olmaktadır. Bu nedenle son zamanlar uydu görüntüsünden nesne çıkarımı için kullanılan birçok yapay zekâ teknolojisi kullanılmıştır. Derin öğrenme yöntemleri diğer tekniklere göre nispeten yeni olmasına rağmen kullanılan mimariler hızlı bir şekilde geliştirilmektedir.

Yapılan bu çalışmada hazır veri seti kullanılarak, eğitim modellemesi gerçekleştirilmiş olup Göktürk-1 uydu görüntüleri test amacıyla kullanılmıştır. Sonuç olarak, ağ modeli, binaları tespit etmede iyi performans göstermiştir. Göktürk-1'den tahmin edilen görüntüler, kentsel ortamları sınıflandırmada oldukça iyi performans gösterdiği görülmüştür. Şekil 5'te görüldüğü üzere, çoğu binanın doğru bir şekilde ayrıldığı görülmektedir. Buda, hazır veri setinden yararlanılarak Göktürk-1 uydu görüntüsünün ve U-Net ağının yüksek yoğunluklu kentsel alanlarda bu tür binaları ayırt etme yeteneğini göstermektedir. Ayrıca, modelde eğitim ve epok sayısının, sonuçlara olan etkisi de ele alınmış olup değerlerin artması sonuçlara olumlu katkı sağlamıştır. Fakat bir modeli eğitmek için şu kadar veri veya epokta yapılması gerektiğini söylemek zordur. Çünkü, kullanılan ağ mimarisinde eğitim verisinin miktarına, kullanılan görüntülerin çözünürlüğüne bağlı olarak duyarlılık analizin yapılması gerekmektedir. Yeterli miktarda veri yoksa eğer, veri arttırma yöntemleri uygulanabilir. Tüm bunlar sonuçların farklı olmasında etkendir. Süreç bakımından ele alındığında geleneksel yöntemlere göre daha az manuel müdahale gerektirmektedir. Bu sebepten ötürü, derin öğrenme yöntemleri kullanılarak uydu görüntülerinden, nesne çıkarımı gerçekleştirmek daha kolay olmaktadır. Çalışma doğrultusunda sonuçların iyi ve doğru olması da umut vericidir. Binaların otomatik olarak belirlenmesi, özellikle kentsel bölgelerde yapılan çalışmalarda altlık olarak kullanılmasını sağlar.

Bilgilendirme/Teşekkür

Bu araştırma Duygu ARIKAN'ın "Yüksek Çözünürlüklü Uydu Görüntülerinden Arazi Sınıflarının Derin Öğrenme Yöntemiyle Belirlenmesi" başlıklı tez çalışmasından

gerçekleştirilmiştir. Ayrıca, yazarlar Göktürk-1 uydu görüntülerinin teminini sağlayan Harita Genel Müdürlüğü'ne ve makalenin değerlendirme sürecine zaman ayırarak katkı sunan hakemlere teşekkür eder.

Araştırmacıların katkı oranı beyan özeti

D. Arıkan: Veri temini, Veri analizi, Araştırma, Modelleme, Makale yazımı;
F. Yıldız: Makalenin dil bilgisi kontrolü.

Çıkar çatışması beyanı

Makale ile ilgili olarak, herhangi bir kurum, kuruluş, kişi ile mali çıkar çatışması yoktur ve yazarlar arasında çıkar çatışması bulunmamaktadır.

Araştırma ve yayın etiği beyanı

Yapılan çalışmada yazarlar, araştırma ve yayın etiğine aykırı bir durum olmadığını ve çalışmanın etik kurul izni gerektirmediğini beyan etmektedir.

KAYNAKÇA

Abdollahi, A., & Pradhan, B. (2021). Integrating semantic edges and segmentation information for building extraction from aerial images using UNet. Machine Learning with Applications, 6, 100194.

Atlan, F., Hançer, E., & Pençe, İ. (2020). U-Net ile Çekirdek Segmentasyonunda Hiper Parametre Optimizasyonu Etkisinin Değerlendirilmesi. Avrupa Bilim ve Teknoloji Dergisi, 60-69.

Ataş, İ. (2023). Performance Evaluation of Jaccard-Dice Coefficient on Building Segmentation from High Resolution Satellite Images. Balkan Journal of Electrical and Computer Engineering, 11(1), 100-106.

Bayraktar, U. (2018). Derin Öğrenme Tabanlı Kanserli Hücre Tespiti. no. December, 2019.

Hou, Y., Liu, Z., Zhang, T., & Li, Y. (2021). C-UNet: Complement UNet for remote sensing road extraction. Sensors, 21(6), 2153.

Ji, S., Wei, S., & Lu, M. (2018). Fully convolutional networks for multisource building extraction from an open aerial and satellite imagery data set. IEEE Transactions on Geoscience and Remote Sensing, 57(1), 574-586.

Kattenborn, T., Leitloff, J., Schiefer, F., & Hinz, S. (2021). Review on Convolutional Neural Networks (CNN) in vegetation remote sensing. ISPRS Journal of photogrammetry and remote sensing, 173, 24-49.

Kuffer, M., Pfeffer, K., & Sliuzas, R. (2016). Slums from space—15 years of slum mapping using remote sensing. Remote Sensing, 8(6), 455.

Li, L., Wang, C., Zhang, H., & Zhang, B. (2019). Residual UNet for urban building change detection with Sentinel-1 SAR data. Paper presented at the IGARSS 2019-2019 IEEE International Geoscience and Remote Sensing Symposium.

Li, X., Zhang, G., Cui, H., Hou, S., Chen, Y., Li, Z., . . . Wang, H. (2023). Progressive fusion learning: A multimodal joint segmentation framework for building extraction from optical and SAR images. ISPRS Journal of photogrammetry and remote sensing, 195, 178-191.

Maas, A. L., Hannun, A. Y., & Ng, A. Y. (2013). Rectifier nonlinearities improve neural network acoustic models. Paper presented at the Proc. icml.

Madhu, G., Kautish, S., Alnowibet, K. A., Zawbaa, H. M., & Mohamed, A. W. (2023). NIPUNA: A Novel Optimizer Activation Function for Deep Neural Networks. Axioms, 12(3), 246.

Maggiori, E., Tarabalka, Y., Charpiat, G., & Alliez, P. (2017). Can semantic labeling methods generalize to any city? the inria aerial image labeling benchmark. Paper presented at the 2017 IEEE International Geoscience and Remote Sensing Symposium (IGARSS).

Mahabir, R., Croitoru, A., Crooks, A. T., Agouris, P., & Stefanidis, A. (2018). A critical review of high and very high-resolution remote sensing approaches for detecting and mapping slums: Trends, challenges and emerging opportunities. Urban Science, 2(1), 8.

Mitra, P., Shankar, B. U., & Pal, S. K. (2004). Segmentation of multispectral remote sensing images using active support vector machines. Pattern recognition letters, 25(9), 1067-1074.

Mnih, V. (2013). Machine learning for aerial image labeling: University of Toronto (Canada).

Nwankpa, C., Ijomah, W., Gachagan, A., & Marshall, S. (2018). Activation functions: Comparison of trends in practice and research for deep learning. arXiv preprint arXiv:1811.03378.

Oliphant, T. E. (2006). A guide to NumPy (Vol. 1): Trelgol Publishing USA.

Öz, M. (2021). Eye segmentation using deep neural networks.

Pal, M. (2005). Random forest classifier for remote sensing classification. International journal of remote sensing, 26(1), 217-222.

Pan, Z., Xu, J., Guo, Y., Hu, Y., & Wang, G. (2020). Deep learning segmentation and classification for urban village using a worldview satellite image based on U-Net. Remote Sensing, 12(10), 1574.

Ramachandran, P., Zoph, B., & Le, Q. V. (2017). Searching for activation functions. arXiv preprint arXiv:1710.05941.

Ronneberger, O., Fischer, P., & Brox, T. (2015a). U-net: Convolutional networks for biomedical image segmentation. Paper presented at the Medical Image Computing and Computer-Assisted Intervention–MICCAI 2015: 18th International Conference, Munich, Germany, October 5-9, 2015, Proceedings, Part III 18.

Ronneberger, O., Fischer, P., & Brox, T. (2015b). U-net: Convolutional networks for biomedical image segmentation. Paper presented at the International Conference on Medical image computing and computer-assisted intervention.

Sariturk, B., & Seker, D. Z. (2022). Comparison of Residual and Dense Neural Network Approaches for Building Extraction from High-Resolution Aerial Images. Advances in Space Research.

Tuermer, S., Kurz, F., Reinartz, P., & Stilla, U. (2013). Airborne vehicle detection in dense urban areas using HoG features and disparity maps. IEEE Journal of selected topics in applied earth observations and remote sensing, 6(6), 2327-2337.

Wu, G., Shao, X., Guo, Z., Chen, Q., Yuan, W., Shi, X., . . . Shibasaki, R. (2018). Automatic building segmentation of aerial imagery using multi-constraint fully convolutional networks. Remote Sensing, 10(3), 407.

Wurm, M., Stark, T., Zhu, X. X., Weigand, M., & Taubenböck, H. (2019). Semantic segmentation of slums in satellite images using transfer learning on fully convolutional neural networks. ISPRS Journal of photogrammetry and remote sensing, 150, 59-69.

Yan, X., Tang, H., Sun, S., Ma, H., Kong, D., & Xie, X. (2022). After-unet: Axial fusion transformer unet for medical image segmentation. Paper presented at the Proceedings of the IEEE/CVF Winter Conference on Applications of Computer Vision.

Zeiler, M. D., Ranzato, M., Monga, R., Mao, M., Yang, K., Le, Q. V., . . . Dean, J. (2013). On rectified linear units for speech processing. Paper presented at the 2013 IEEE International Conference on Acoustics, Speech and Signal Processing.

Zhang, L., Zhang, L., Tao, D., & Huang, X. (2011). On combining multiple features for hyperspectral remote sensing image classification. IEEE Transactions on Geoscience and Remote Sensing, 50(3), 879-893.

Zhang, J., Du, J., Liu, H., Hou, X., Zhao, Y., & Ding, M. (2019). LU-NET: An improved U-Net for ventricular segmentation. IEEE Access, 7, 92539-92546.

Zhu, X. X., Tuia, D., Mou, L., Xia, G.-S., Zhang, L., Xu, F., & Fraundorfer, F. (2017). Deep learning in remote sensing: A comprehensive review and list of resources. IEEE geoscience and remote sensing magazine, 5(4), 8-36.